

**UNIVERSITY OF CALIFORNIA**

**Santa Barbara**

**The Impact of Morphology on the Performance of Green-Solvent Processed Organic  
Electronic Devices**

A dissertation submitted in partial satisfaction of the  
requirements for the degree Doctor of Philosophy  
in Chemistry

by

Mark Alan Burgers

Committee in charge:

Professor Martin Moskovits, Chair

Professor Mattanjah S. de Vries

Professor Steven K. Buratto

Professor Daniel Little

December 2016

The dissertation of Mark Alan Burgers is approved.

---

Mattanjah S. de Vries

---

Steven K. Buratto

---

R. Daniel Little

---

Martin Moskovits, Committee Chair

August 2016

The Impact of Morphology on the Performance of Green-Solvent Processed Organic

Electronic Devices

Copyright © 2016

by

Mark Alan Burgers

## ACKNOWLEDGEMENTS

First I would like to thank my mother, Bonita Yoder, and my father, Peter Burgers, for providing me with continued advice and inspiration to drive forward and pursue my dreams. I would like to thank my beautiful fiancée, Hengjing Yan, for taking care of me, cooking for me during the writing of my dissertation, and guiding me through one of the hardest times in my life and having confidence in me even when I didn't have any in myself. I would like to thank my older brother and best friend, Alex Burgers, for his continued support, confidence, and advice. I would like to thank my committee members for giving me immeasurable support and providing me with both academic and life support, I would not have succeeded without you. I would finally like to thank my colleagues and coworkers for all of the useful discussion, and collaborations.

# Mark A. Burgers

Department of Chemistry and Biochemistry

Center for Polymers and Organic Solids

University of California, Santa Barbara

93101-9510

mburgers@chem.ucsb.edu

mbug718@gmail.com

(314) 497-9072

---

## EDUCATION

**Ph.D. University of California** (GPA: 3.9), Santa Barbara, CA 2011-Current

**Materials Chemistry**, Advisors: Professor Martin Moskovits, Professor Gui Bazan

*Dissertation: Impact of morphology on performance of green-solvent processed organic electronic devices*

**B.Sc. Saint Louis University** (GPA: 3.4), Saint Louis, MO 2006-2010

**Chemistry, Mathematics** (Minor), Advisors: Professor Steven Buckner, Professor Paul Jelliss

*Marcus thesis award: Environmental factors on long-term stability of capped aluminum nanoparticles*

## TECHNICAL SKILLS

- **Device Fabrication:** Organic Light Emitting Diodes (OLEDs), Organic Photovoltaics (OPVs), Organic Field Effect Transistors (OFETs), Single Carrier Diodes, Cleanroom Techniques
- **Analytical Methods:** Silica Gel Chromatography, Size Exclusion Chromatography (SEC), Gel Permeation Chromatography (GPC), High Performance Liquid Chromatography (HPLC), Volumetric Analysis
- **Materials Characterization:** Atomic Force Microscopy (AFM), Transmission Electron Microscopy (TEM), X-ray diffraction, Secondary Ion Mass Spectrometry (SIMS), Mass Spectrometry
- **Spectroscopy:** UV-Vis, Photoluminescence, X-ray Photoelectron Spectroscopy (XPS), Ultraviolet Photoelectron Spectroscopy (UPS), Transient Absorption
- **Electrochemistry:** Cyclic Voltammetry (CV), Differential Pulse Voltammetry (DPV)

## RESEARCH EXPERIENCE

**Graduate Student Researcher**, University of California Santa Barbara, CA 2011-Current

- Designed a non-fullerene based all small molecule solar cell processable from environmentally friendly solvents and displayed control on crystallization through GIWAXS and TEM.
- Discovered the use of green solvent processing for series of molecular semiconductors.
- Fabricated small molecule/polymer solar cells and investigated processing condition effects on efficiency, morphology, and charge carrier transport.
- Investigated the use of conjugated polyelectrolyte cathode interlayers to improve efficiency in small molecule based organic solar cells.

**Laboratory Manager**, Saint Louis University, MO. 2010-2011

- Coordinated with a moving company to pack up and move an entire lab and resume normal operations in the span of two weeks.
- Rebuilt a Nitrogen dye laser and in charge of maintenance on gloveboxes, UV-Vis-NIR, Fluorimeter, ATR-IR.
- Synthesized TiO<sub>2</sub> nanowires of different lengths and diameters and characterized by TEM measurements.

**Undergraduate Researcher**, Saint Louis University, MO. 2007-2010

- Investigated the impact post treatment conditions had on long-term air stability of aluminum nanoparticles by monitoring hydrogen production.
- Demonstrated that different capping and passivation materials led to control on crystallite size through p-XRD measurements.
- Investigated the quenching properties of PbS quantum dots and displayed control on quantum dot size by TEM.

## JOURNAL PUBLICATIONS

1. **M. A. Burgers**, S. Holliday, M. Ford, X. Liu, I. McCulloch, G. C. Bazan, High efficiency all small molecule solar cells processed from environmentally friendly solvents. 2016 *Manuscript*.

2. **M. A. Burgers**, X. Liu, J. Yuan, C. McDowell, G. C. Bazan, Towards green-solvent processing of organic solar cells. 2016 *Submitted*.
3. H. K. Lee, V. V. Brus, C. M. Proctor, X. Liu, **M. A. Burgers**, T.-Q. Nguyen, G. C. Bazan, Balance between light absorption and recombination losses in solution-processed small molecule solar cells with normal or inverted structures. 2016 *Submitted*.
4. X. Liu, **M. A. Burgers**, B. B.-Y. Hsu, J. E. Coughlin, L. A. Perez, A. J. Heeger, G. C. Bazan, Molecular orientation within thin films of isomorphous molecular semiconductors. **RSC Advances**, 2015, 5, 89144-89148
5. M. Abdelsamie, N. D. Treat, K. Zhao, C. McDowell, **M. A. Burgers**, R. Li, D.-M. Smilgies, N. Stinglen, G. C. Bazan, A. Amassian, Toward additive-free small-molecule organic solar cells: roles of the donor crystallization pathway and dynamics. **Advanced Materials**, 2015, DOI:10.1002/adma.201503395
6. X. Chen, X. Liu, **M. A. Burgers**, Y. Huang, G. C. Bazan, Green-solvent-processed molecular solar cells. **Angewandte Chemie**, 2014, 126, 14606-14609 (Inside Cover)
7. D. W. Hammerstroem, **M. A. Burgers**, S. W. Chung, E. A. Gulianst, C. E. Bunker, K. M. Wentz, S. E. Hayes, S. W. Buckner, P. A. Jelliss, Aluminum nanoparticles capped by polymerization of alkyl-substituted epoxides: ratio-dependent stability and particle size. **Inorganic Chemistry**, 2011, 50, 5054-5059
8. S. W. Chung, E. A. Gulians, C. E. Bunker, D. W. Hammerstroem, Y. Deng, **M. A. Burgers**, P. A. Jelliss, S. W. Buckner, Capping and passivation of aluminum nanoparticles using alkyl-substituted epoxides. **Langmuir**, 2009, 25, 8883-8887

## CONFERENCE PRESENTATIONS

1. “Impact of Green Solvent Processing on Morphology”, University of California Symposium for the Chemical Sciences, Lake Arrowhead, CA
2. “Green Solvent Processed Molecular Solar Cells”, University of California Santa Barbara – South China University of Technology Joint Workshop, Guangzhou, China
3. “Environmentally friendly light harvesting solar cell research at the center for polymers and organic solids”, University of California Santa Barbara Year of Light Symposium, Santa Barbara, CA

4. "Organic solar cells processed from green solvents", 12<sup>th</sup> international symposium on functional  $\pi$ -electron systems, Seattle, WA (1<sup>st</sup> place poster)
5. "Organically Capped Aluminum Nanoparticles", NanoFrontiers Gateway to Economic Development in Missouri, St. Louis, MO
6. "Capping and passivation of aluminum nanoparticles and the environmental effects on long-term air stability", Missouri Inorganic Day, Saint Louis, MO
7. "Capping and Passivation of Al Nanoparticles and the Environmental Effects on the Long-Term Air Stability", 40<sup>th</sup> Marcus Award Symposium, Department of Chemistry, Saint Louis University, St. Louis, MO
8. "Long-Term Air Stability of Organically-Capped Aluminum Nanoparticles", 239<sup>th</sup> National Meeting of the ACS, Division of Fuel Chemistry, San Francisco, CA
9. "Stability of Organically-Capped Aluminum Nanoparticles", 44<sup>th</sup> Annual Midwest Regional Meeting of the ACS, Iowa City, IA
10. "Synthesis and Characterization of Aluminum Nanoparticles Using Epoxides as Capping Agents", St. Louis ACS Section Undergraduate Research Symposium, St. Louis, MO

## **TEACHING EXPERIENCE**

### **Lead TA position**

Inorganic synthesis and physical characterization laboratory (Fall 2014, Fall 2015)

Advanced physical chemistry laboratory (Spring 2013, Spring 2015, Spring 2016)

Quantitative analytical and physical methods laboratory (Winter 2013, 2014, 2015)

### **Teaching Assistant**

Laboratory methods of organic chemistry B (Summer 2014)

Honors general chemistry lecture (Fall 2013)

Inorganic synthesis and physical characterization laboratory (Fall 2012)

General chemistry laboratory C (Spring (2012)

General chemistry laboratory B (Winter 2012, Spring 2014)

General chemistry laboratory A (Fall 2011)

## **SELECTED AWARDS**

- Undergraduate award from the analytical chemistry division of the ACS **2009**

- 40<sup>th</sup> annual Leopold Marcus award winner **2010**
- American institute of chemists outstanding senior chemistry award **2010**
- ACS Applied Materials and Interfaces Award for excellence in poster presentation and 12<sup>th</sup> International symposium on functional  $\pi$ -electron systems **2015**

## ABSTRACT

### The Impact of Morphology on the Performance of Green Solvent Processed Organic Electronic Devices

by

Mark Alan Burgers

Organic photovoltaics have received a large amount of attention in recent years due to their potential for relatively low cost fabrication, light weight and flexible devices, and because of their high solubility, inkjet printing and roll-to-roll processing. Thanks to the new development of novel materials and methods for controlling self-assembly, organic photovoltaics have achieved over 10% efficiencies. One issue that has received relatively little attention is the types of solvents used for processing, mainly their toxicity and sustainability. Recently we discovered the use of a green solvent, 2-MeTHF, from which to process the semiconducting layer. Here we further investigate the feasibility of using 2-MeTHF as a processing solvent for a wide array of molecular donors by device fabrication, electrical and morphological characterization. We also investigated the processing of two novel non-fullerene acceptors from 2-MeTHF, and characterized their morphologies and evaluated their efficiencies.

## TABLE OF CONTENTS

Chapter 1: Introduction and Background .....	1
1.1 Organic Semiconductors.....	1
1.2 Bulk Heterojunction (BHJ) Solar Cells .....	4
<i>1.2.1 Small Molecule Solar Cells</i> .....	7
1.3 Conjugated Polyelectrolytes (CPEs).....	15
1.4 Alternative Processing Solvents .....	17
<i>1.4.1 Green Solvent Processed Organic Electronics</i> .....	19
1.5 Non-Fullerene Acceptors.....	26
1.6 Conclusions.....	32
1.7 References.....	33
Chapter 2: Experimental Techniques.....	40
2.1 Overview.....	40
2.2 Solubility Testing.....	41
2.3 Atomic Force Microscopy (AFM).....	42
2.4 Grazing Incidence Wide Angle X-ray Scattering (GIWAXS) .....	44
2.5 UV/Vis Absorption.....	47
2.6 Solar Cell Fabrication .....	49
2.7 Solar Cell Characterization.....	51
2.8 Single Carrier Diodes for Space-Charge Limited Current (SCLC)	
Mobilities.....	54
2.10 References	

Chapter 3: Application of Conjugated Polyelectrolyte Interlayers in Small Molecule Solar Cells and the Impact of Methanol Treatments .....	59
3.1 Introduction.....	59
3.2 Results and Discussion .....	62
3.2.1 <i>Device Properties</i> .....	62
3.2.3 <i>Contact Angle Measurements</i> .....	63
3.2.4 <i>Surface Potential Measurements</i> .....	64
3.2.5 <i>Methanol Penetration Measurements</i> .....	67
3.3 Conclusions.....	69
3.4 Experimental.....	70
3.5 References.....	72
Chapter 4: Towards Green Solvent Processing of Organic Solar Cells .....	74
4.1 Introduction.....	74
4.2 Results and Discussion .....	78
4.2.1 <i>Solar Cell Performance</i> .....	79
4.2.3 <i>Charge Carrier Mobility</i> .....	81
4.2.4 <i>EQE and UV/Vis</i> .....	83
4.2.5 <i>Probing the Structural Order</i> .....	85
4.2.6 <i>Surface Morphology</i> .....	88
4.3 Conclusions.....	90
4.4 Experimental.....	92
4.5 References.....	95

Chapter 5: High Efficiency Non-Fullerene Based Small Molecule Organic Solar Cells Processed from Green Solvents.....	98
5.1 Introduction.....	98
5.2 Results and Discussion .....	101
5.2.1 <i>UV/Vis &amp; Energy Levels</i> .....	101
5.2.2 <i>Device Performances</i> .....	102
5.2.3 <i>Blend UV/Vis &amp; Photoluminescence Quenching</i> .....	104
5.2.4 <i>Structural Order</i> .....	105
5.2.5 <i>Charge Carrier Mobility</i> .....	107
5.3 Conclusions.....	109
5.4 Experimental.....	110
5.5 References.....	113
Chapter 6: Summary and Outlook .....	116

# Chapter 1: Introduction & Background

## 1.1 Organic Semiconductors

Organic semiconductors are an extremely interesting class of material that have recently garnered a large amount of academic and industrial attention due to their relatively low cost, inherent flexibility, and ease of device fabrication. While these properties are quite simple to understand the phenomenon by which polymers and small molecules are able to transport charge is more complex. The charge transporting properties of organic semiconductors stems from the nature of  $sp^2$  carbons to form pi-bonds. When many of these pi-bonds come together they form a pi-conjugated system. This delocalized nature allows for electronic communication across an entire molecule, and even across other, similarly delocalized, systems. With a wide variety of hetero-atoms and modular functional groups the optical, and electronic transport properties can be finely tuned using organic synthesis, leading to a near infinite amount of possible polymeric and molecular structures.

Due to the large amount of disorder, both morphologically and electronically, in bulk samples of organic semiconductors, the charge transport mechanism is quite different. Instead of fast transport through well-defined bands, organic semiconductors transport charges by a thermally activated hopping mechanism. Because of this performance limitation the goal of organic semiconductors was not to out-perform their inorganic counterparts, but rather to reduce production costs of devices, or afford new device properties (e.g., flexibility, transparency) that conventional semiconductors struggle to achieve. In the last decade organic semiconductors have made their way into the commercial market, most notably with organic light emitting diodes (OLEDs) being used for displays in both smartphones and televisions.

OLEDs,<sup>1</sup> organic photovoltaics (OPVs),<sup>2</sup> and organic field effect transistors (OFETs)<sup>3</sup> have all seen great improvement in the last few years. These performance increases are thanks to efforts in molecular design,<sup>4,5</sup> morphology control,<sup>6-8</sup> and device engineering.<sup>9,10</sup> The desired properties of the semiconductor used will vary depending on which type of device it will be used in, for example in OLEDs strong luminescence and high quantum yield are desired,<sup>11</sup> while a broad absorption profile and good charge carrier mobilities are desired for OPVs,<sup>12,13</sup> and a high charge carrier mobility leads to good transistor performance.<sup>14</sup> Since each organic optoelectronic device emphasizes different properties, the impact of different functional groups on the bulk properties has been an active area of study.

All Photovoltaics, organic and inorganic, are evaluated using the same equation for power conversion efficiency (PCE) shown in the equation below, and a typical JV curve is exhibited in figure 1.1 below indicating important characteristics.

$$PCE = \frac{J_{sc} V_{oc} FF}{P_{in}}$$

$J_{sc}$  stands for short circuit current, and represents the amount of charge carriers collected at the electrodes. This charge carrier generation is directly related to the total number of incident photons absorbed. The total number of absorbed photons can be controlled in a few different ways, such as increasing the film thickness and narrowing the bandgap.<sup>15</sup>  $V_{oc}$  stand for open circuit voltage, or the bias that needs to be applied in order to have zero current flowing through the device. The  $V_{oc}$  is proportional to the energy difference between the highest occupied molecular orbital (HOMO) of the donor material and the lowest unoccupied molecular orbital (LUMO) of the acceptor material. By tuning the energy levels of the donor and the acceptor, the  $V_{oc}$  can also be controlled.<sup>16</sup>  $FF$ , or fill factor, is a value

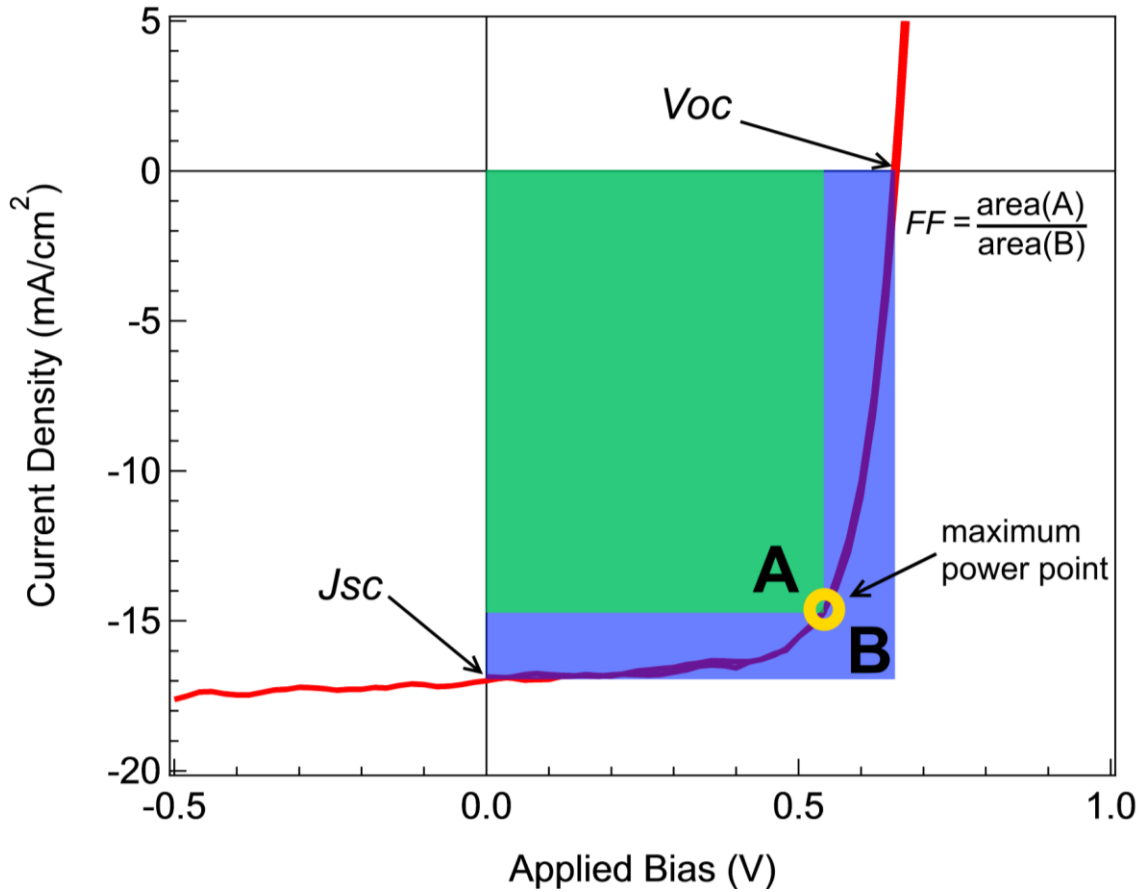


**Figure 1.1.** A typical current voltage (JV) curve of a photovoltaic. The short circuit current, open circuit voltage, and maximum power point are indicated. The method by which fill factor is calculated is also shown

that compares the amount of charge carriers collected, to the charge carriers generated. By improving the overall charge carrier mobility as well as ensuring a well-balanced electron and hole mobility *FF* can be improved.<sup>17,18</sup>

## 1.2 Bulk Heterojunction (BHJ) Solar Cells

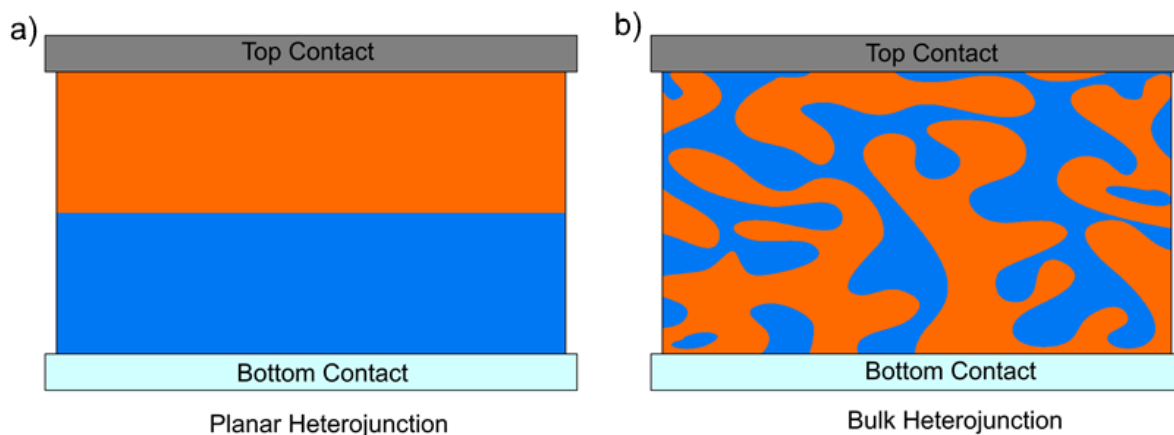


**Figure 2.2.** A cross-sectional representation of the morphologies of a) a Planar Heterojunction and b) a Bulk Heterojunction. The blue and orange colors represent donor and acceptor phases.

Due to the significantly lower dielectric constant of organic materials, compared to their inorganic counterparts, when an organic semiconductor absorbs light that excited electronic state (exciton) acts like an electron hole pair that struggle to create separate and mobile charge carriers. This strong coulombic attraction between the electron and hole can be screened by the dielectric field of the material, but in organics it is not enough to overcome the coulombic binding energy, and because of this a donor (p-type) and acceptor (n-type) heterojunction must be utilized to separate and transport charges. There are two different types of heterojunctions that are used in the study of OPVs: a planar heterojunction and a bulk heterojunction (Figure 1.2). A planar heterojunction, more commonly a bi-layer device has a very well defined interface between the donor and acceptor phase at which charge separation will occur. Since charges can only be separated at this interface, only the

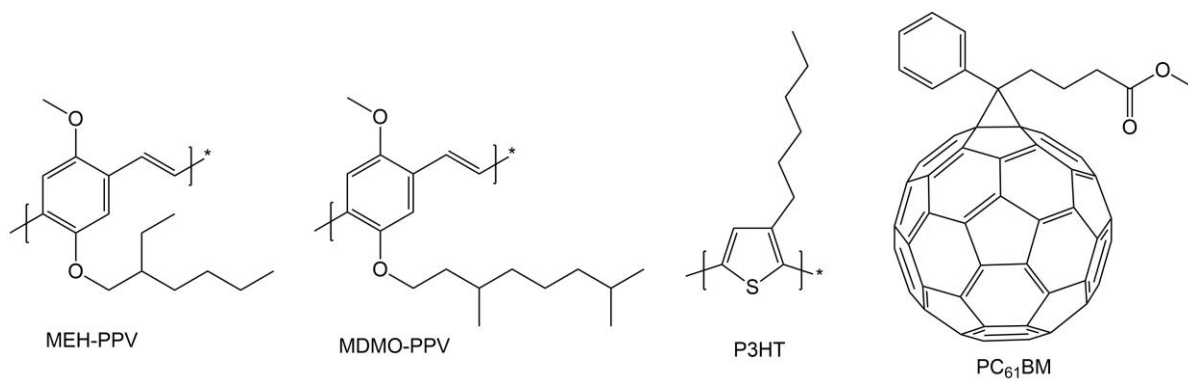


**Figure 1.2.** Chemical structures of some of the first, and widely used electron donor materials (Three on the left). On the far right is the soluble fullerene derivative, PC<sub>61</sub>BM, that is still considered to be the highest performing electron acceptor.

excitons that can physically diffuse to the interface will become separated. This means that the thickness of any absorbing layer must be within the range of the exciton diffusion length,  $\sim 15$  nm for most organic semiconductors.<sup>19,20</sup> This restriction on thickness greatly decreases the total amount of potential light that can be harvested for energy production.

Planar heterojunctions are most commonly made by thermal evaporation, or solution processing of a donor material, followed by thermal evaporation of the acceptor material, usually Fullerene (C<sub>60</sub>). By creating a more soluble fullerene derivative, Phenyl C<sub>61</sub> butyric acid methyl ester (PC<sub>61</sub>BM) shown in Figure 1.3, and solution processing together with the donor material an interpenetrating network of donor and acceptor phases can form.<sup>21</sup> This donor/acceptor network significantly increases the interfacial area between the two phases allowing for improved charge separation. With this network spanning the entirety of the film, the exciton diffusion length no longer becomes the limiting factor for film thickness. Controlling the morphology of these two phases is quite difficult, and has a major focus of research in the field of OPVs.<sup>2,22–24</sup> Controlling the phase separation between the donor and

**Table 1.1.** Comparison of bulk heterojunction solar cell performances using the older generation MDMO-PPV, and P3HT donor polymers, to the new generation of donor-acceptor polymers.

Donor	$J_{sc}$ [mA/cm <sup>2</sup> ]	$V_{oc}$ [mV]	FF [%]	PCE [%]
MDMO-PPV	5.25	820	61	2.5
P3HT	9.2	620	61	3.6
PCPDTBT	16.2	620	55	5.5

acceptor is a fine balance. If the phases become too large then excitons will decay before an interface is reached, geminate recombination, and if either phase is too small then a large amount of potential recombination sites will form and while charge separation will occur the system will greatly suffer from non-geminate recombination.<sup>25,26</sup>

The first conjugated polymers used for OPVs were poly p-phenylene vinylene (PPV) derivatives such as poly[2-methoxy-5-(2-ethylhexyloxy)-1,4-phenylenevinylene] (MEH-PPV),<sup>21</sup> poly[2-methoxy-5-(3',7'-dimethoxyloxy)-1,4-phenylenevinylene] (MDMO-PPV),<sup>27,28</sup> and poly[3-hexylthiophene] (P3HT)<sup>29</sup> shown in Figure 1.3. While these materials worked quite their wide bandgaps lead to an absorption profile that had a mismatch with the solar irradiance spectrum. To reconcile this mismatch, a narrower bandgap donor must be used; however, certain aspects must be taken into account. If the HOMO of the donor is raised then the  $V_{oc}$  of the system will suffer, and if the LUMO of the donor is lowered then the driving force for charge transfer between the donor and acceptor will be reduced. What had to be done was that the HOMO and LUMO must have been moved together to allow for a narrower bandgap, high  $V_{oc}$  from the deeper HOMO, and still have a strong driving force for charge separation with a shallower LUMO. By using what is called a push-pull structure

narrow bandgap materials with broad absorption have been obtained.<sup>30-32</sup> This push pull architecture was obtained by connecting electron donating groups, such as cyclopentadithiophene or carbazole, to an electron withdrawing moiety, such as benzothiadiazole derivatives, to form a repeated donor-acceptor sequence. This new donor-acceptor (D-A) polymer structure was able to significantly improve device performance when compared to the previously used MEH-PPV and P3HT donors as shown in table 1.1. The  $V_{oc}$  dropped for the D-A polymer, which was expected due to the raising of the HOMO to narrow the bandgap. The fill factor also dropped when using the D-A polymer, which is likely due to a slight decrease in charge separation caused by dropping of the LUMO. Both of these drawbacks when using the D-A polymer are counteracted by a significant increase in the  $J_{sc}$ , 3 times greater than MDMO-PPV and almost two times greater than P3HT, thanks to the increase in photon flux at the blue end of the visible spectrum. With the introduction of the D-A polymer an even larger number of potential donor polymer structures can be investigated.

### **1.2.1 Small Molecule Solar Cells**

Organic Solar cells have received a large amount of attention due to their ability to be solution processed, like an ink, which can allow for large area device fabricated by roll to roll processing. Conjugated polymers were initially used in these studies because of their favorable film forming properties; however, conjugated small molecules can also be processed in the same method as conjugated polymers. The field of conjugated small molecule donors received very little attention, but now small molecule based solar cells have achieved power conversion efficiencies that rival their polymeric counterparts.<sup>33</sup> Both polymers and small molecules do have their issues though. Polymers performance suffers

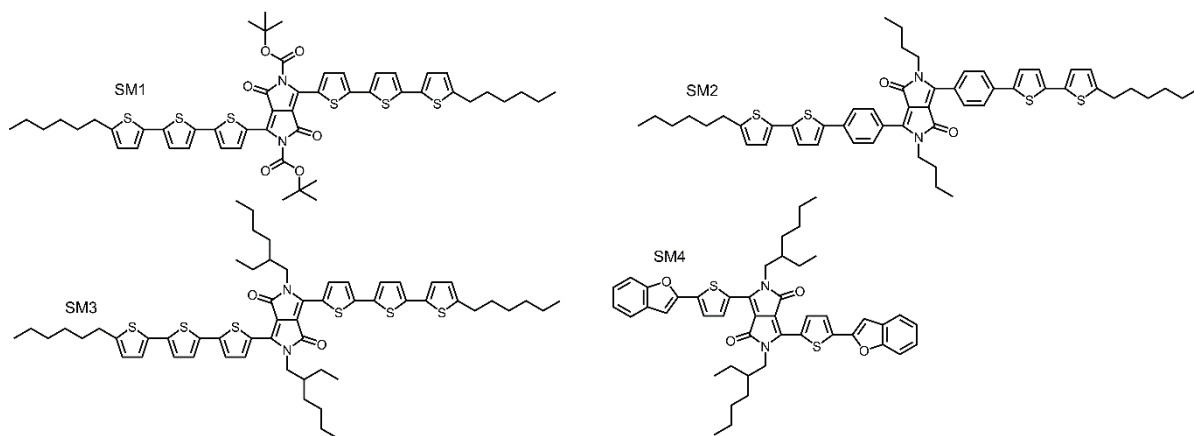


**Figure 1.3.** Structures of a few of the DPP based small molecule donors for organic solar cells synthesized in the Nguyen group.

greatly from batch-to-batch variability,<sup>34</sup> and optoelectronic properties can be heavily dependent on molecular weight and poly dispersity.<sup>35–37</sup> By switching to small molecule donors the impact of molecular weight on device performance can be detangled from the inherent optoelectronic properties of the structure, and the issue of batch-to-batch variability can be solved by using standard organic purification techniques such as column chromatography. Conjugated small molecules do have their drawbacks though, lower viscosity at the same concentration as a polymer making a higher solubility a necessity in order to achieve thick films, and much higher crystallinity leading to large degrees of phase separation.<sup>38</sup> With these issues facing small molecules, clever molecular design must be used to mitigate the problems facing the field. This section will briefly introduce two classes of small molecule donors: diketopyrrolopyrrole (DPP) core molecules, and modular donor-acceptor small molecules.

The majority of early small molecule donors comprised of oligothiophenes, and soluble acenes which all performed quite poor. In fact, the vast majority of these compounds

**Table 1.2.** Summarized J-V characteristics of SM1, SM2, SM3, and SM4. A series of DPP based small molecule donors synthesized by the Nguyen group.

Donor	Jsc [mA/cm <sup>2</sup> ]	Voc [mV]	FF [%]	PCE [%]
SM1	8.4	670	45	2.3
SM2	9.3	840	48	3.7
SM3	9.2	750	44	3.0
SM4	10.0	920	48	4.4

were never able to achieve efficiencies greater than 2%. By using the idea of a donor-acceptor structure the Nguyen group was able to synthesis several soluble small molecules with a DPP core and thiophene or benzofuran end groups (Figure 1.3).<sup>39-42</sup> DPP is a well-known material and is used in industrial inks and pigments due to its strong light absorption, stability, and ability to be synthesized on a large scale which makes them ideal candidates for organic photovoltaic materials.<sup>43,44</sup> SM1 was the first molecule that was investigated and achieved significant performance at the time; however, the morphology was unstable due to the alkoxy linkages on the DPP core,<sup>42</sup> these linkages were replaced with a hexyl (SM2)<sup>40</sup> and ethyl hexyl (SM3)<sup>41</sup> groups leading to much more stable morphologies and yielded devices that, at the time, were the highest performing small molecule based solar cells. Then by replacing the terthiophene end groups with a more electron withdrawing benzofuran (SM4) the band gap was widened, but the  $V_{oc}$  received significant improvement leading to an overall improvement in device performance.<sup>39</sup> The J-V characteristics for these four molecules are summarized in the table below. These new DPP based small molecules led to a massive breakthrough in the solution process small molecule solar cells, and opened the field to rapid improvement.

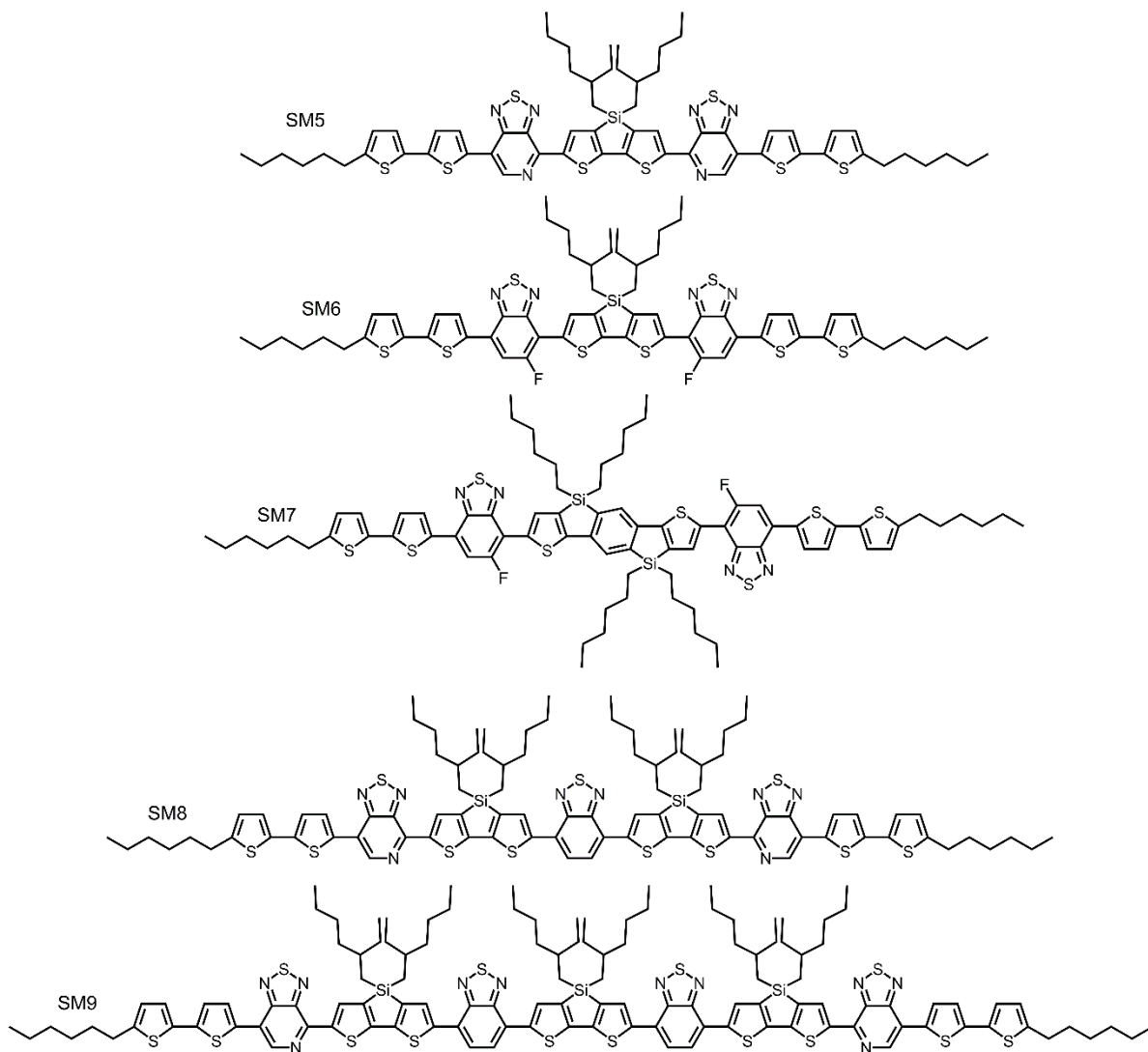


**Figure 1.4.** Chemical structures of several high performance molecular semiconductors that utilize the modular donor-acceptor architecture.

With the success of these DPP based small molecules, solution processed small molecules have been pushed to the forefront of organic photovoltaic research. With the understanding of how donor and acceptor moieties can impact the bandgap of a material, the Bazan group started work on making modular donor-acceptor molecule that would be able to achieve high performance. By implementing a  $D^1-A-D^2-A-D^1$  architecture extended

**Table 1.3** Summarized J-V characteristics of a few high performing molecular semiconductors utilizing a modular donor-acceptor architecture.

Donor	$J_{sc}$ [mA/cm <sup>2</sup> ]	$V_{oc}$ [mV]	FF [%]	PCE [%]
SM5	14.4	780	59	6.7
SM6	12.8	810	68	7.0
SM7	11.0	910	65	6.4
SM8	9.8	710	60	5.8
SM9	15.7	690	68	7.4

conjugation length, as well as favorable intramolecular charge transfers could be obtained. Using internal donors that differed from the external donors also allowed for the series of materials to take on a modular nature. The first molecule to implement this architecture (SM5) used a silolodithiophene (SDT or DTS) core, pyridylthiadiazole (PT) acceptor, and a bithiophene wing, shown in figure 1.5. Because of this new core and architecture, SM5 had astonishing success achieving power conversion efficiencies of 6.7%, thanks to a more red shifted and broader absorption profile, as well as greatly improve charge transport due to the improved crystallinity afforded by the silicon bridge head atom in the DTS.<sup>45</sup> SM5 had one major drawback though, the lone pair of electrons in the pyridyl nitrogen has a slightly basic nature and would be protonated by the acidic proton from the common anode buffer layer, poly[3,4-ethylenedioxythiophene]:polystyrene sulfonate (PEDOT:PSS), and in order to achieve optimal performance required the use of thermally evaporated molybdenum oxide.<sup>46</sup> By replacing the pyridyl nitrogen with a carbon fluorine bond, this protonation issue was solved, and devices could be fabricated using PEDOT:PSS,<sup>47</sup> and while the protonation issue was the main focus, the addition of a carbon fluoride bond also severed another

purpose, phase separation. The addition of fluorine to the material allowed for significant phase separation and promoted crystallinity, allowing for very efficient charge transport pathways to form and significantly improve the fill factor of the devices.<sup>48</sup> By utilizing the modular nature of SM6 the SDT core was exchanged for a silaindacenodithiophene (SIDT) core in order to synthesize SM7.<sup>49</sup> Since SIDT group was less electron rich than the DTS group, the result would be a blue shifted absorption, but more important, the HOMO would drop yielding a much higher  $V_{oc}$ , and this was in fact the case increasing the  $V_{oc}$  by 100 mV; however, because HOMO was dropped and the LUMO remained nearly the same, the bandgap widened and the improved current production brought about by narrower bandgaps was lost, resulting in a decrease in  $J_{sc}$  by nearly 2 mA/cm<sup>2</sup>. Interestingly, SM7 has significantly different packing properties to compared SM5, and SM6. The molecule appears to adopt a cross weave packing style, and has an out of plane molecular orientation, unlike the other two small molecules which exhibit an in plane orientation further highlighting the importance of understanding structure to property relationships.<sup>24,45,47,49</sup>

With the emergence of high performance small molecule solar cells an interesting correlation that molecular semiconductors had significantly different optimal processing conditions from conjugated polymers.<sup>50,51</sup> In order to better bridge the processing gap between conjugated small molecules and conjugated polymers. The Bazan group began working on developing a series of oligomeric small molecules of varying length.<sup>4,52</sup> These new molecular semiconductors expanded the molecular length of the well-studied SM5 using a D<sup>1</sup>-A<sup>1</sup>-D<sup>2</sup>-A<sup>2</sup>-D<sup>2</sup>-A<sup>1</sup>-D<sup>1</sup> (SM8) and a D<sup>1</sup>-A<sup>1</sup>-D<sup>2</sup>-A<sup>2</sup>-D<sup>2</sup>-A<sup>2</sup>-D<sup>2</sup>-A<sup>1</sup>-D<sup>1</sup> (SM9) architecture. As the molecular length increased the absorption was further red shifted and the thermal stability increased, exhibiting consistent mobilities at annealing temperatures

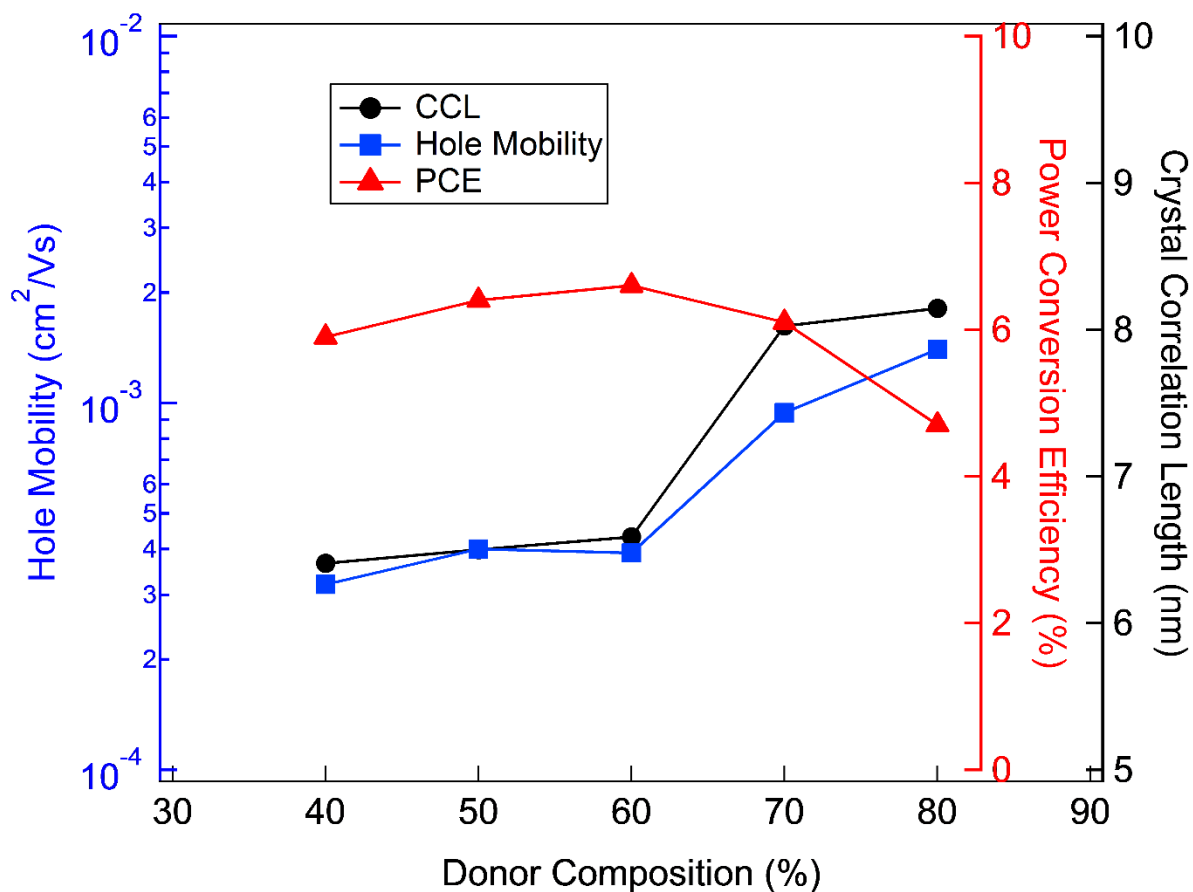


**Figure 1.5.** P-type Charge carrier mobility (Blue Squares) measured by space charge limited current methods, Power Conversion Efficiency (Red Triangles), and Crystalline Correlation Lengths (Black Circles) extracted from x-ray measurements of the X2:PC<sub>61</sub>BM system across a range of donor compositions (80%-60%).

greater than 200 °C, whereas SM5 saw a greater than two order of magnitude drop in mobility between 100 °C and 150 °C annealing. The most interesting property of these extended molecular length semiconductors is the processing conditions required to achieve an optimal performance. Where SM5 requires the use of high boiling point solvent additives to achieve 6.7% efficiency, SM8 and SM9 are rather unique in that no high boiling point solvent additives are necessary, and instead merely require simple thermal annealing at 100

°C to achieve efficiencies of 5.8% and 7.4% respectively. Even more interesting was that SM9 exhibited a rather robust morphology, and would yield devices with efficiencies as low as 4.7% and as high as 6.6% between the range of 40% to 80% donor composition.<sup>53</sup> SM9:PCBM was also able to exhibit efficient charge carrier mobility as well as consistent crystalline correlation lengths across the investigated range, which has also been observed for both SM6 and SM7; however, neither of these materials were capable of maintaining high efficiencies outside a rather narrow donor content range.<sup>54</sup> This class of extended molecular length semiconductors has received a large amount of attention recently<sup>55,56</sup> and has exhibited quite favorable properties, such as composition tolerant performance,<sup>4,52,53</sup> high thermal stability,<sup>57</sup> and interesting molecular orientations;<sup>58</sup> this class of materials is a continually growing field and shows a lot of promise.

### 1.3 Conjugated Polyelectrolytes (CPEs)

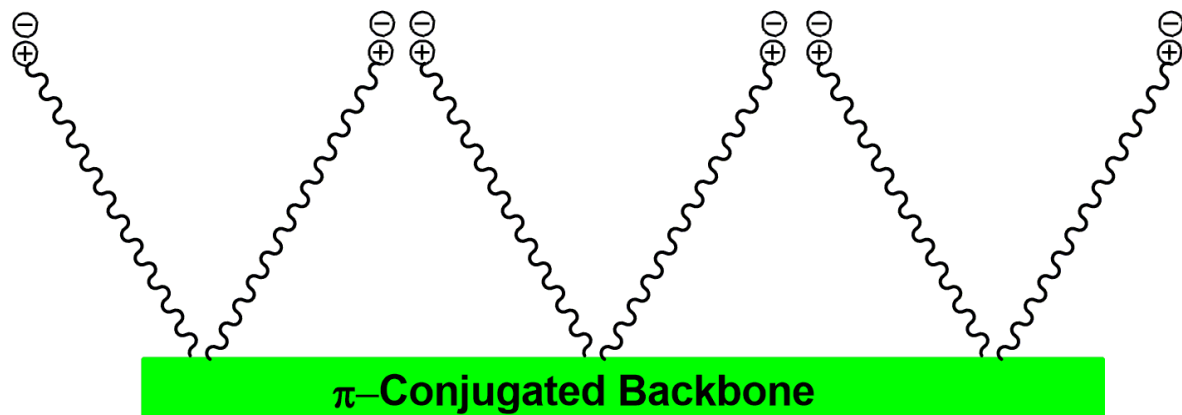
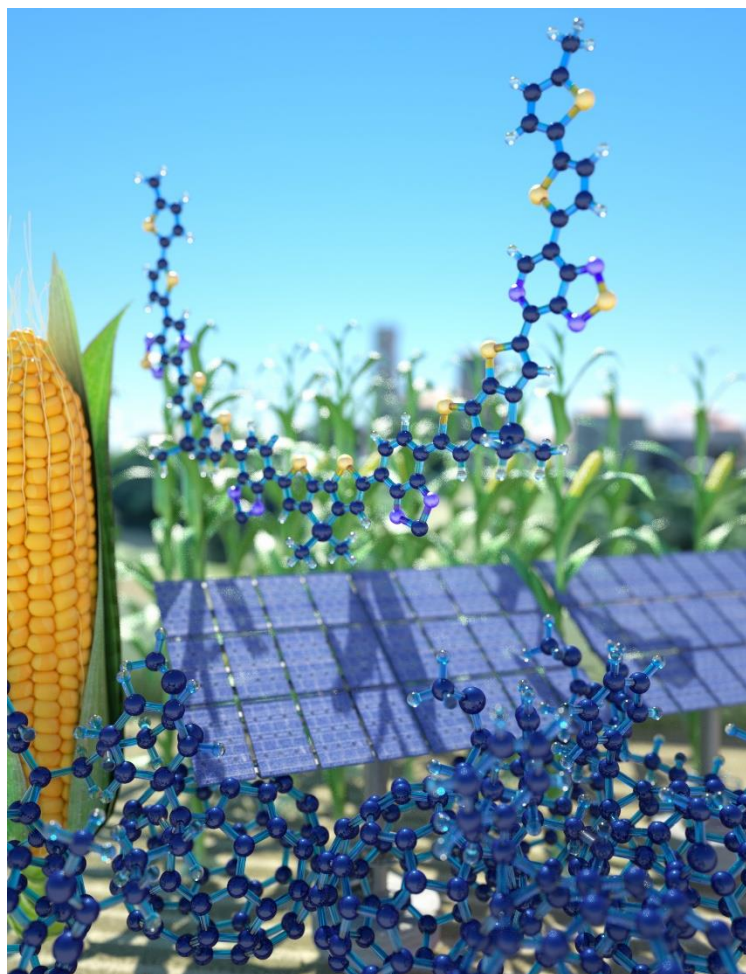


**Figure 1.6.** General structure of a conjugated polyelectrolyte (CPE). The ionic functionalities can be modified to impact the solubility in certain solvents, packing orientation, solution aggregation, and charge carrier type. The  $\pi$ -conjugated backbone can be chosen to control the absorption and emission properties, as well as the semiconducting/conducting properties.

Conjugated polyelectrolytes (CPEs) are polymers containing a  $\pi$ -conjugated backbone with ionically functionalized pendant groups allowing for solubility in polar media.<sup>59</sup> There has been a large number of applications for conjugated polyelectrolytes including biological and chemical sensors,<sup>60,61</sup> thermoelectric devices,<sup>62,63</sup> thin-film work-function modifiers.<sup>10,64</sup> The organic electronics field has taken full advantage of the work-function modifying capabilities of CPEs and have used them as interlayers in light-emitting transistors,<sup>65,66</sup> polymer light emitting diodes,<sup>67</sup> and photovoltaic devices.<sup>68–70</sup> The concept of work-function modification stems from the need to reduce injection barriers, particularly barriers to electron injection.

The majority of cathodes used in organic electronics are high work function metals such as Aluminum, Calcium, Barium, and Lithium Fluoride. All of these materials are quite unstable and reactive with oxygen, which becomes a major problem when considering long-term stability of these devices. To envision stable, large area devices, these high work-function metals must be removed from the devices, however as the work-function of the electrode is dropped the ohmic nature of the contact will decrease. In order to obtain an ohmic contact while using lower work-function metals the barrier to injection at the metal semiconductor interface must be decreased. When being used as a top contact interlayer, fabrication takes advantage of the solubility nature of a CPE. Thanks to its ionic functionality a CPE has solubility in highly polar/orthogonal processing solvents, allowing for the CPE to be spin coated on top of the active layer without disrupting the morphology below. While the film is forming, the nonpolar  $\pi$ -conjugated backbone will orient itself with the hydrophobic active layer, and the ionic pendant groups will protrude forming an interfacial dipole. Once the electrode is deposited on top of the layer, the interfacial dipole will interact with the metal causing a vacuum level shift, lowering the electron injection barrier allowing for lower work-function, and more chemically stable metals such as gold and silver to work as cathodes.<sup>64,71</sup>



#### 1.4 Alternative Processing Solvents

Recently there has been a movement in research towards technologies that have, as its core objectives renewable energy, sustainability, and environmental protection.<sup>72-74</sup> Solution processed organic electronics are a relevant case, with a promising vision of roll-to-roll processing of light weight flexible devices, reducing manufacturing and installation costs. More importantly, organic electronics focuses on the use of earth abundant elements such as carbon, sulfur, nitrogen, and oxygen, unlike their inorganic counterparts which use rarer and more toxic elements such as lead, tin, and ruthenium.<sup>75-77</sup> Organic electronics still have a major issue that goes against the concept of sustainability and environmental

protection, the solvents. The vast majority of high performance organic electronics are processed from halogenated and aromatic solvents, and use high boiling point halogenated solvent additives.<sup>2</sup> In order to move towards a more sustainable future for the field, this problem must be addressed.

There have been few reports of work in the field of alternative/non-halogenated solvents and they are a step in the right direction, however they still fall short of the goal of sustainability. Griffin et al. did work using a well know carbazole based polymer and compared the performances between processing with chlorobenzene and a binary solvent mixture of acetone and carbon disulfide.<sup>78</sup> They were able to achieve significant improvement in device performance by using the binary solvent mixture, increase from 5.5% to 6.6%, but despite their device improvements the use of such a harsh and dangerous chemical as CS<sub>2</sub> does not fall in line with the concept of sustainability.<sup>79</sup> Similarly, Fu et al. showed quite promising work using non-halogenated solvents, o-Xylene, p-Xylene, and 1,2,3,4-tetrahydronaphtalene (THN), for processing OFETs and compared the performances to processing from Dichlorobenzene (DCB).<sup>80</sup> The DCB base devices exhibited a mobility of 0.26 cm<sup>2</sup>/Vs, while the p-xylene, and THN processed devices exhibited a mobility of 0.31 cm<sup>2</sup>/Vs and 0.30 cm<sup>2</sup>/Vs respectively. Despite these improvements in device performance again the solvents used have very well documented toxicities and carcinogenic properties.<sup>81,82</sup> One of the most promising examples of using alternative solvents comes from work done by Sprau et al., focusing on the processing of a well know known conjugated polymer donor, PTB-7,<sup>25,83,84</sup> from alternative solvents.<sup>85</sup> They showed that device performance could be boosted by using anisole as the processing solvent in comparison to chlorobenzene or o-xylene; however, the devices also included the high

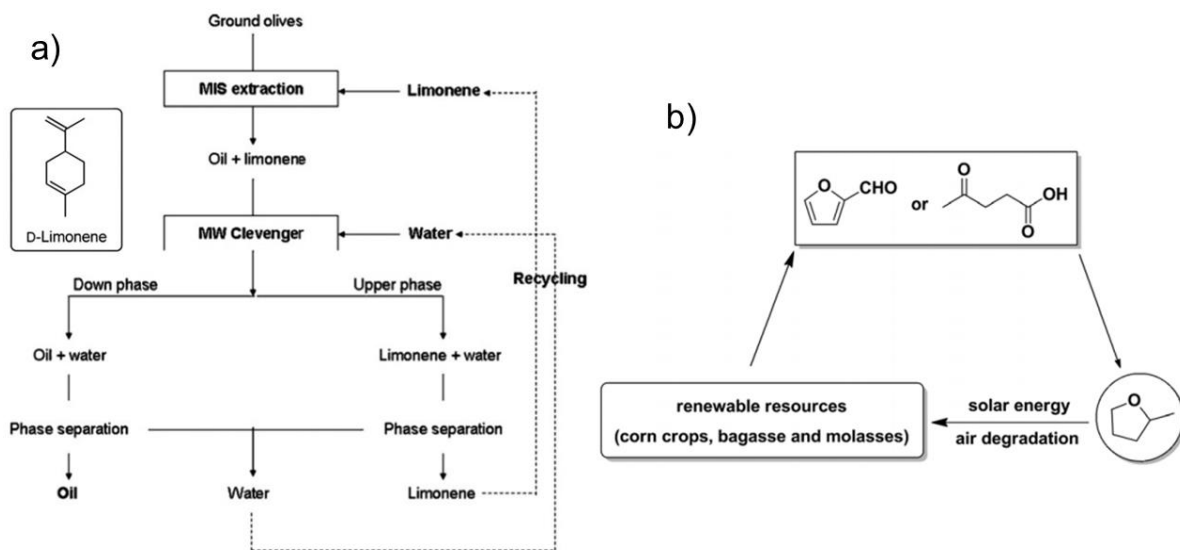


**Figure 1.7.** General reaction scheme for obtaining a) D-limonene and b) 2-MeTHF from their agricultural precursors. Reproduced from reference 86.

boiling point solvent diiodooctane.<sup>85</sup> The work done, is a step in the right direction, but do not fall under the idea of sustainability that organic electronics has at its core. In order to achieve this goal more sustainable, “green” solvents must be used.

### 1.4.1 Green Solvent Processed Organic Electronics

What makes a solvent a “green” solvent? For a solvent to be classified as a green solvent, it must have the following characteristics. It must be an environmentally friendly solvent or, preferably, biosolvent. It must have a low toxicity and have no carcinogenic properties. It must degrade to a naturally occurring or reusable product, and most importantly, it must be obtained from a renewable resource, such as agricultural waste.<sup>86</sup> A few solvents that fall under this category are D-Limonene, which is derived from the processing of olives,<sup>86</sup> 2-methyltetrahydrofuran (2-MeTHF), and cyclopentyl methyl ether

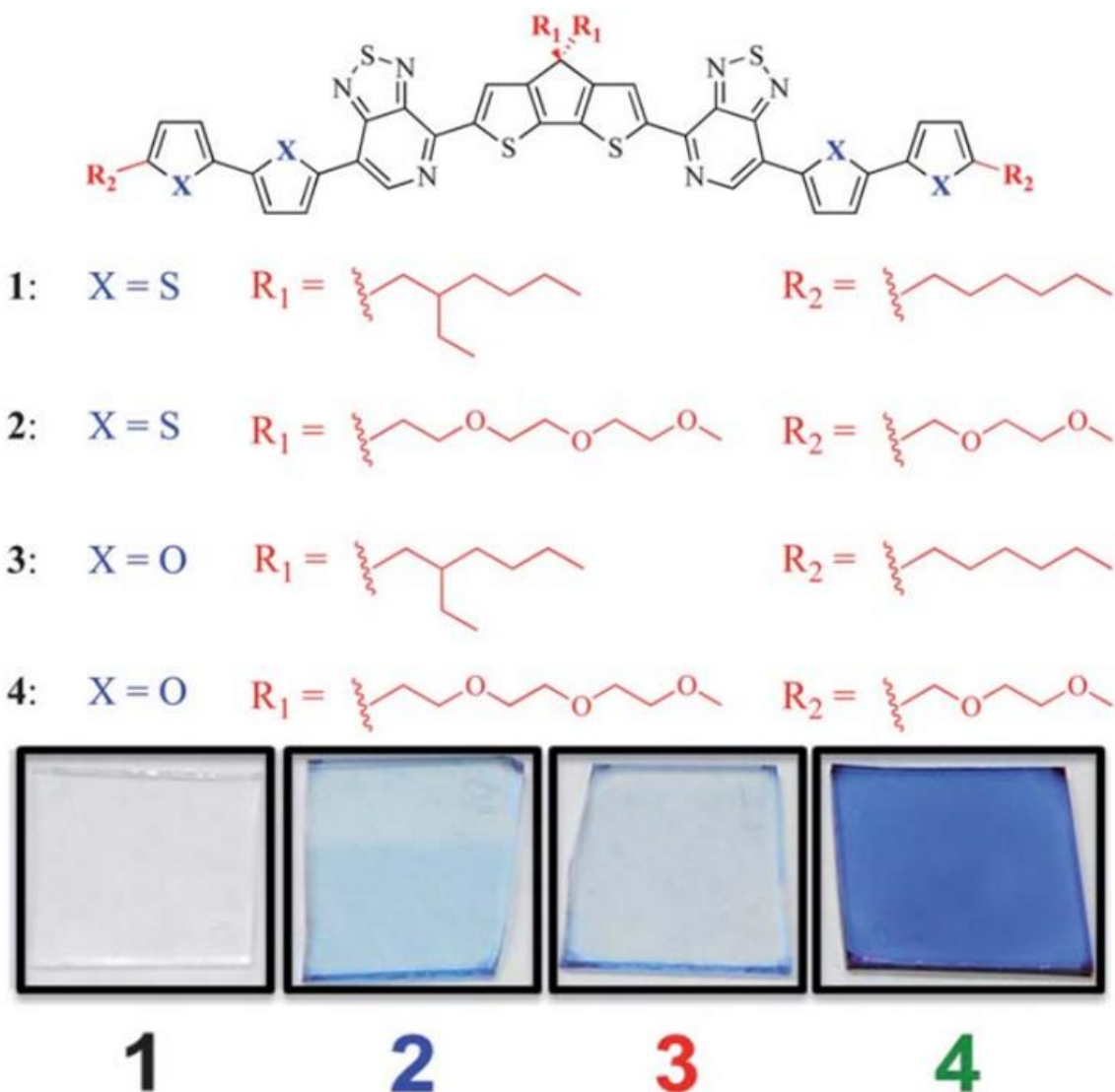


**Figure 1.8.** Structures used to study the impact of functional groups and heteroatoms on the solubility in ethyl acetate, and the films that were spun from the saturated solutions.

Reproduced from reference 89.

(CPME), both of which are derived from corn cobs.<sup>87,88</sup> figure 1.7 shows the general synthetic scheme for obtaining D-limonene and 2-MeTHF.<sup>86</sup>

The largest issue facing the processing of organic semiconductors from these alternative solvents is the solubility.<sup>89,90</sup> In order to improve the solubility in these more

polar media, Henson et al. compared the effect of using different heteroatoms, as well as pegilated side chains in a well-defined molecular chromophore (Figure 1.8). They found that when replacing the thiophenes with furans, there was a small improvement in solubility, ~2-4 mg/ml soluble, and when replacing the alkyl sidechains with ethylene glycol units led to similar solubility improvements. The largest improvement came from using both furans and the ethylene glycol sidechains, 15-18 mg/ml soluble. With the significant improvement of solubility, the impact of these new functional groups on the semiconducting nature was investigated through OFET measurements. It was found that the saturated mobility was on the order of  $10^{-5}$  cm<sup>2</sup>/Vs, which is significantly lower than semiconductors of similar structure. This decrease is likely due to the use of a carbon bridgehead atom instead of silicon, and the ethylene glycol chains absorbing water and disrupting both transport and crystallinity.<sup>4,45,91,92</sup>

The next reasonable step forward was to use these new molecules in a solar cell architecture, but fullerene derivatives have little to no solubility in ethyl acetate, so the green solvent 2-MeTHF was investigated next. The commonly used PC<sub>61</sub>BM has less than 1 mg/ml solubility in 2-MeTHF, but bis-PC<sub>61</sub>BM and PC<sub>61</sub>BC<sub>8</sub> have a solubility of 15 mg/ml and 9 mg/ml respectively.<sup>56</sup> When blending the newly soluble material from Henson et al.'s study, with the new fullerene derivatives there was little to no photovoltaic activity. Despite the lack of ethylene glycol solubilizing chains, and the bi furan building block, SM9 (figure 1.4) was discovered to be highly soluble, ~25 mg/ml, in 2-MeTHF and given its ability to form robust and composition tolerant morphologies, it seemed like the best choice to further study green solvent processing for OPVs.<sup>56</sup> Initial investigations revealed that the bis-PC<sub>61</sub>BM based devices performed significantly lower than the PC<sub>61</sub>BC<sub>8</sub> base devices making

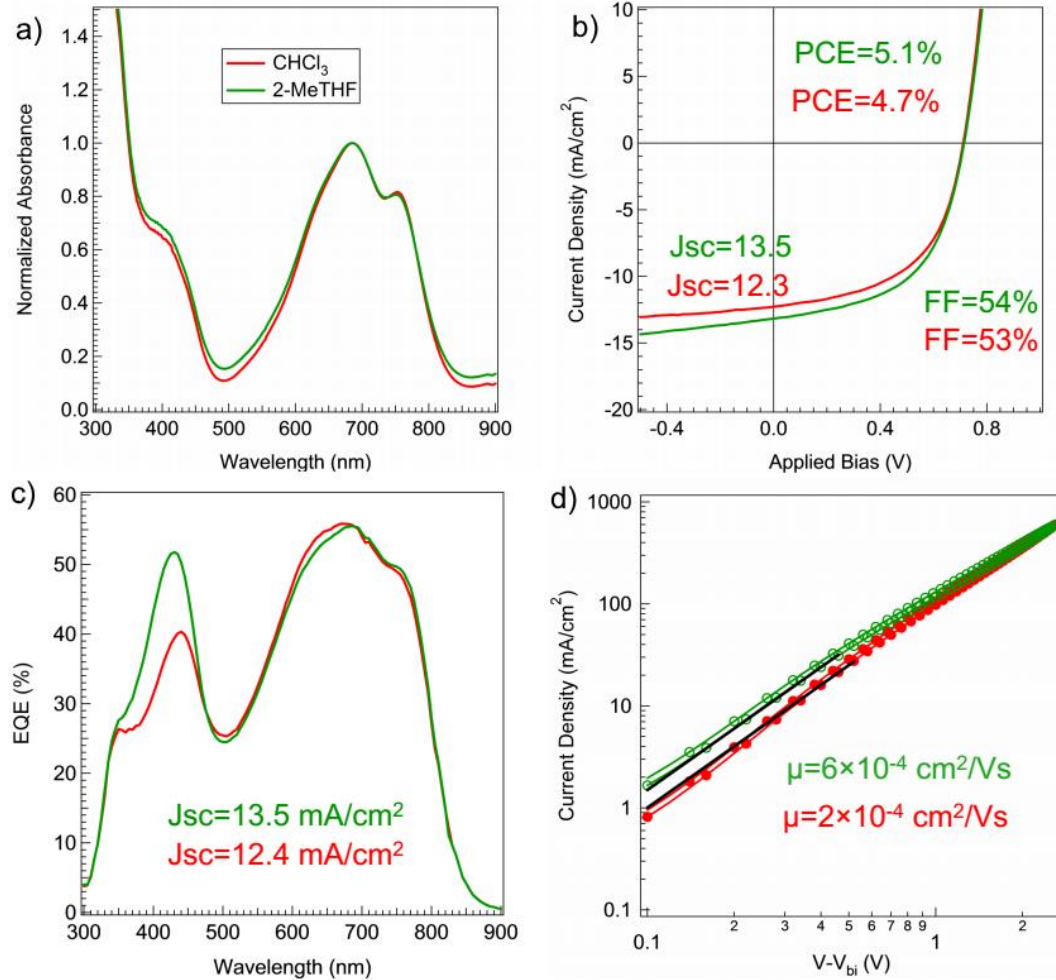
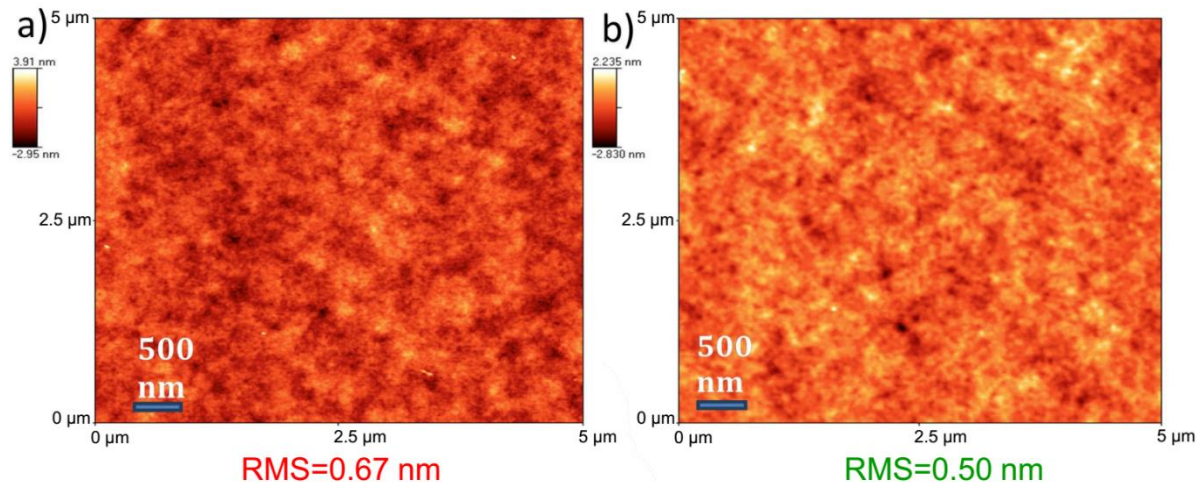


Figure 1.9. Optical and electronic measurements of SM9:PCBC8 system from 2-MeTHF (green) and  $\text{CHCl}_3$  (red). a) Normalized UV/Vis for SM9:PC<sub>61</sub>BC<sub>8</sub> from the two solvents. b) J-V curves with JV characteristics for highlighted in the plot. c) EQE for SM9:PC<sub>61</sub>BC<sub>8</sub> devices with the integrated values written out. d) Space charge limited current Hole mobility measurements of the SM9:PCBC8 systems. Reproduced from reference 56.

the SM9:PC<sub>61</sub>BC<sub>8</sub> system the focus of further investigation. The impact of processing from 2-MeTHF on both the morphology and the optoelectronic properties, was compared to chloroform processed devices, figure 1.9. While the UV/Vis had no overall change between



**Figure 1.10.** AFM measurements of the SM9:PC<sub>61</sub>BC<sub>8</sub> system processed from a) CHCl<sub>3</sub>, and b) 2-MeTHF. Figure reproduced from reference 56.

the 2-MeTHF processed films and the CHCl<sub>3</sub> processed films the electrical measurements all exhibited noticeable improvement when using 2-MeTHF. The power conversion efficiency improved by nearly half a percent, the collected current from the  $\pi$ - $\pi^*$  transition increases by 10% when processed from 2-MeTHF, and the charge carrier mobility has a 3 times increase when processing from 2-MeTHF. In order to understand why the 2-MeTHF processed devices yielded an improvement the morphology was characterized by AMF, figure 1.10. There is little to any visually discernable difference between the 2-MeTHF and CHCl<sub>3</sub> processed devices, but there is a little difference in the RMS roughness with the CHCl<sub>3</sub> processed devices being slightly rougher. In order to investigate the impact of processing solvent on structural order, 2D-grazing incidence wide angle x-ray scattering (GIWAXS) was done, figure 1.11. This measurement can easily probe the structural order and molecular orientation of the thin films using high energy x-rays. For both solvent systems, the SM9  $\pi$ - $\pi$  stacking is predominately in-plane and the alkyl stacking is

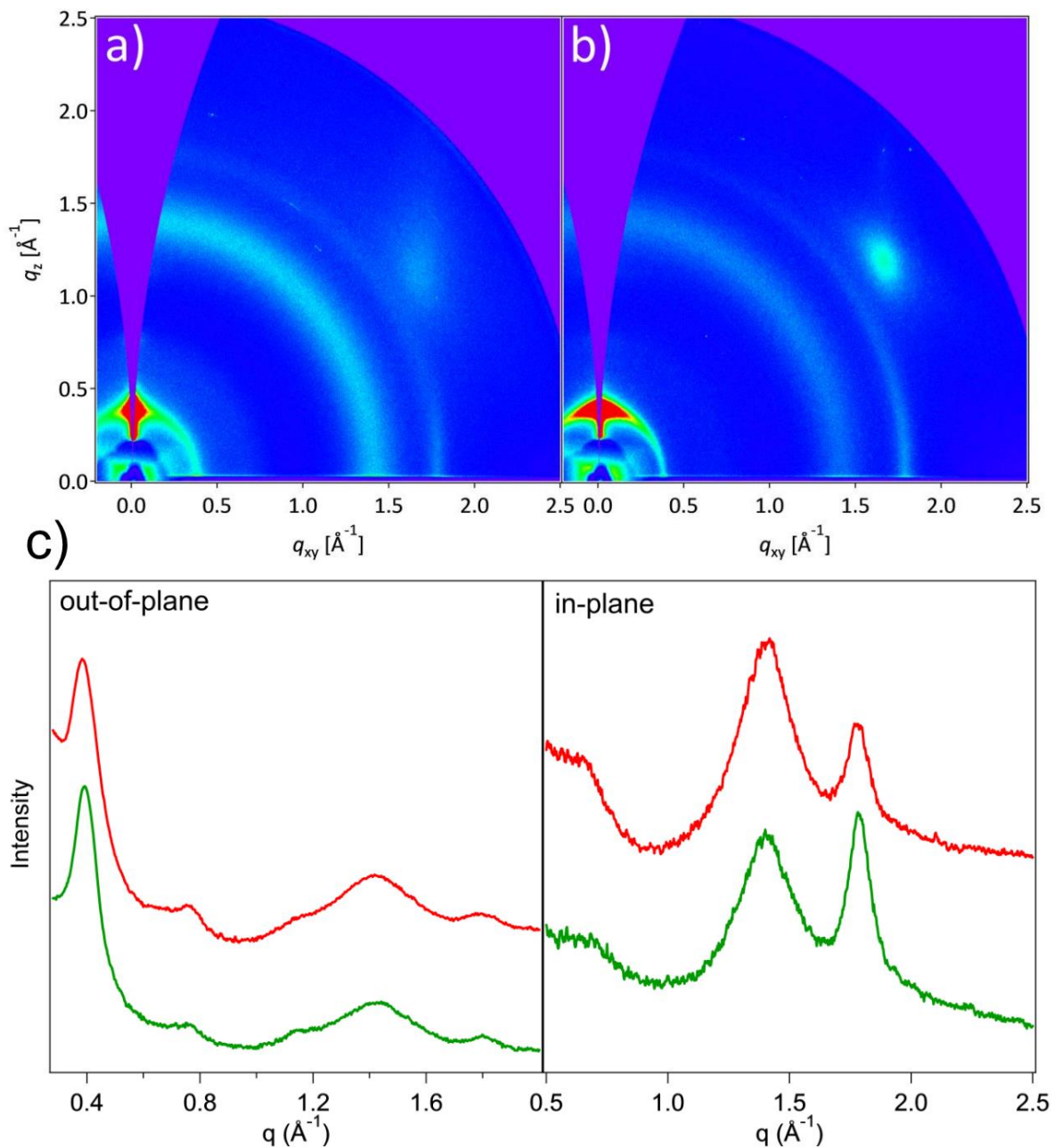


**Figure 1.11.** 2-D GIWAXS plots for a)  $\text{CHCl}_3$  processed and, b) 2-MeTHF processed films. C) line cuts from both the in-plane and out-of-plane directions for  $\text{CHCl}_3$  (red) and 2-MeTHF (green) processed films.

predominately out-of-plane. By taking in-plane and out-of-plane line cuts the crystalline correlation length, a measure of crystallite size and quality, for the  $\pi$ - $\pi$  stacking and the alkyl

stacking can be determined.<sup>93</sup> SM9 exhibited an alkyl/out-of-plane CCL of 11.9 nm and 12.4 nm for CHCl<sub>3</sub> and 2-MeTHF respectively, more importantly SM9 exhibited a  $\pi$ - $\pi$  CCL 6.2 nm and 6.8 nm for CHCl<sub>3</sub> and 2-MeTHF respectively. This increase in structural order when processing from 2-MeTHF is likely the cause of the device improvements. This new discovery completely opens up the field of green solvent processing and will hopefully usher in a new focus of sustainability.

## 1.5 Non-Fullerene Acceptors

Since the first BHJ organic solar cells were made fullerene derivatives, mostly PC<sub>61</sub>BM and PC<sub>71</sub>BM, have dominated the field as the best electron acceptors.<sup>21</sup> This is due to their highly delocalized LUMO allowing for accepting and transport of electrons in three dimensions, three reversible electrochemical reductions, high electron mobility, and their high propensity to aggregate forming both highly pure and mixed domains of the proper length for charge separation and transport. Despite these favorable properties, fullerene derivatives do have some rather significant drawbacks, weak absorption limiting the ability to harvest more light for energy production, limited optical and electronic tunability fixing the LUMO of the molecule leading to little control over  $V_{oc}$  enhancement, high synthetic costs, hard to purify, and morphological instability due to aggregation over time.

The main focus of materials design efforts in the OPV field had been on the development of high performance donors, that are more tailor-made towards fullerene based acceptors, and this has led to the development of solar cells exceeding 10% efficiencies. Designing and optimizing donors to account for the shortcomings of fullerenes, is a poor strategy and limits the other potential acceptors that can form optimal BHJ morphologies. A more modular approach to molecular design focuses on the development of non-fullerene acceptors (NFAs) to be used with the multitude of high performance polymers and small molecules. It is important to keep in mind that while some donors might perform well with PCBM, there might be factors in the optoelectronic properties, or self-assembly that will hinder the donor's performance with some NFAs which makes it important to investigate these properties before the fact and pick the right donor to match the acceptor.

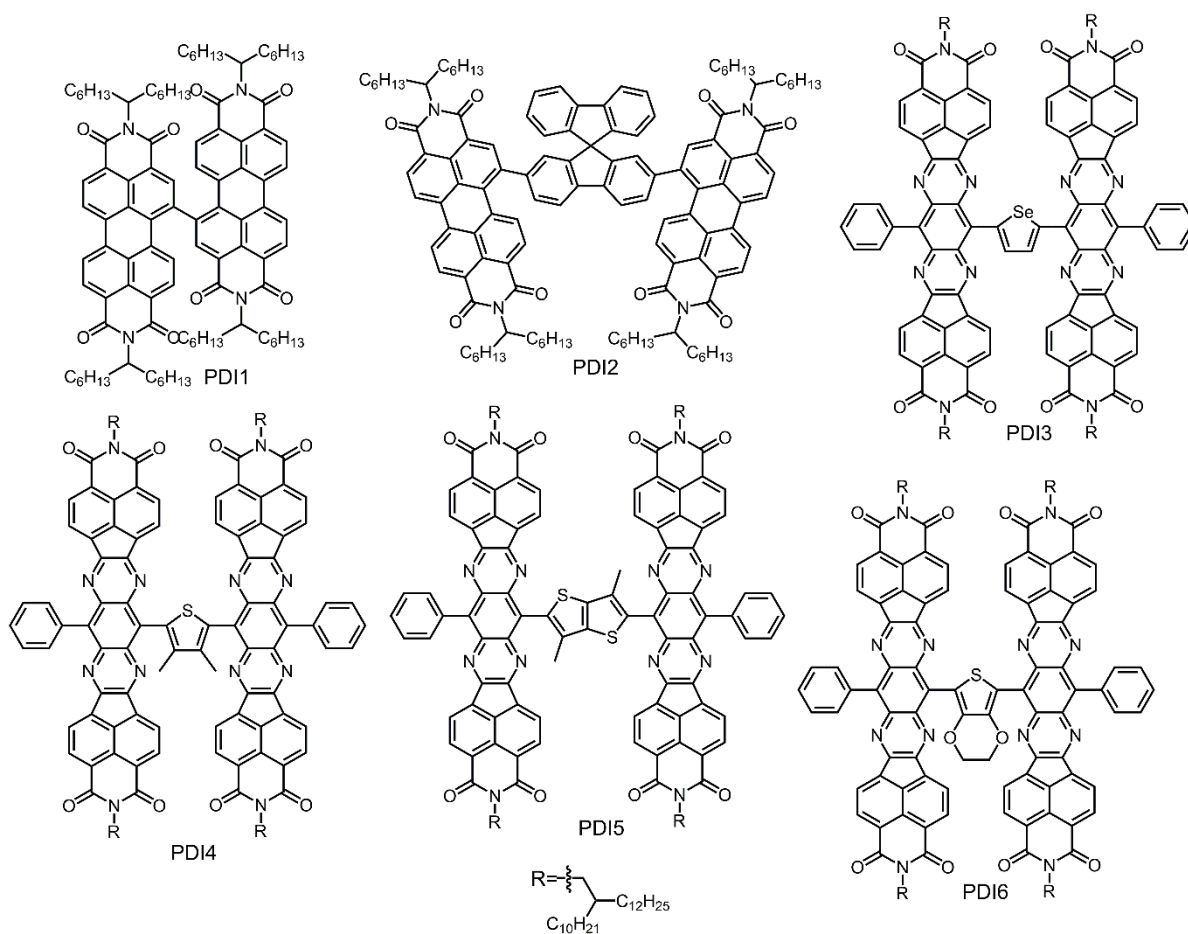


**Figure 1.12.** Several different PDI derivatives that highlight the clever molecular design in order to properly inhibit the acceptor crystallization. Structures reproduced from references 95, 96, 98.

Currently there are many different NFAs reported in the literature, each with their own interesting structure and falling into many different classes, but the scope of this review will only focus on two different types: perylene diimides (PDIs), and calamitic molecules (CMs). The vast majority of high performance NFAs reported in the literature are PDI derivatives due to their high electron mobilities and higher LUMO relative to PCBM.<sup>94-97</sup> PDIs tend to have very high crystallinity which leads to a large degree of phase separation

**Table 1.4.** J-V characteristic summary of the PDI based NFAs shown in figure 1.12.

Data from references 95, 96, 98.

<b>Acceptor</b>	<b><math>J_{sc}</math> [mA/cm<sup>2</sup>]</b>	<b><math>V_{oc}</math> [mV]</b>	<b><i>FF</i> [%]</b>	<b>PCE [%]</b>
PDI1	11.4	840	53	5.1
PDI2	10.7	980	57	6.0
PDI3	5.6	820	54	2.4
PDI4	12.1	920	56	6.2
PDI5	8.1	930	51	3.8
PDI6	15.5	910	60	8.4

during film formation. This strong driving force for crystallization has led to interesting molecular design methods to reduce the crystallinity leading to a larger donor-acceptor interfacial area, but not so much as to prevent the development of efficient electron transport pathways. These recent efforts in PDI molecular design have led to a wide array of PDI based NFAs achieving efficiencies upwards to 8.5%, figure 1.12 and table 1.4.<sup>95,96,98</sup> Li et al. found that by linking the PDI core a twist is introduced into the structure and this twist allows for reduced crystallinity of the PDI based molecules, and the degree of rotation between the two PDIs determines the degree of reduced crystallinity the NFA will have.<sup>96</sup> PDI3 exhibited a rotation of  $\sim 40^\circ$  and a power conversion efficiency of 2.4% with the main performance decrease coming from the  $J_{sc}$ . When the angle of rotation was increased from  $40^\circ$  to  $53^\circ$  in PDI5, there was an increase in device performance of nearly 1.5% attributed to significantly improved short circuit current. Subsequently further increase in the angle of rotation, from  $53^\circ$  to  $62^\circ$  yielded a performance increase of nearly 2.5%, again attributed to

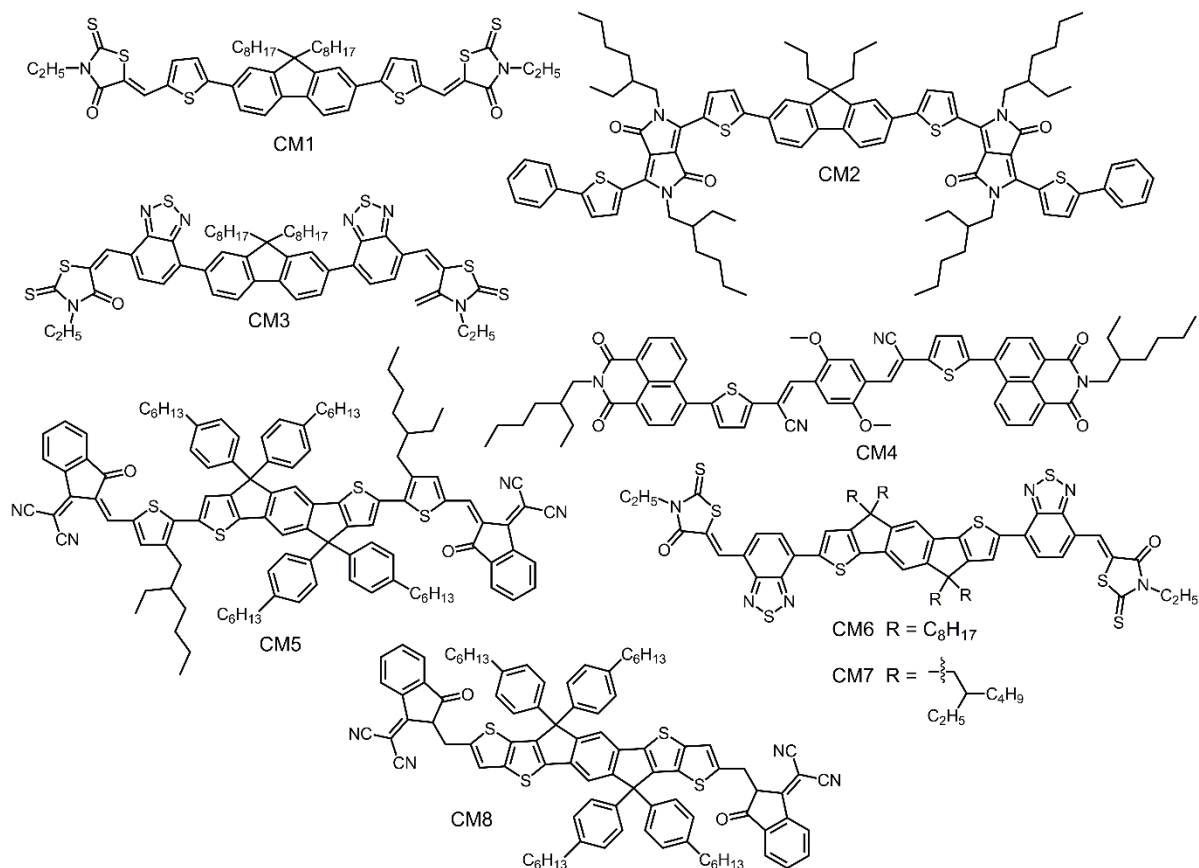


**Figure 1.13.** Calamitic non-fullerene acceptors with power conversion efficiencies ranging from 3% to nearly 7%. Reproduced from references 94, 99-104.

a massive increase in  $J_{sc}$ .<sup>96</sup> Finally, by increasing the twist angle to  $76^\circ$ , a massive improvement in  $J_{sc}$  and  $FF$  yielded a PCE of nearly 8.5%.<sup>95</sup>

These improvements in PDI based NFAs have led to a wide range of new structures to be developed in order to achieve higher and higher power conversion efficiencies, however they fail to address one major issue in the use of PDI derivatives, the limited optical tunability. Calamitic acceptors have begun to receive attention as another promising class of NFAs. By drawing on the donor-acceptor architecture of narrow bandgap polymers and small molecules, the absorption profile of these calamitic molecules (CMs) can be

**Table 1.5.** Summarized J-V characteristics from calamitic NFAs shown in figure 1.13.

Data from references 94, 99-104.

<b>Acceptor</b>	<b><math>J_{sc}</math> [mA/cm<sup>2</sup>]</b>	<b><math>V_{oc}</math> [mV]</b>	<b><math>FF</math> [%]</b>	<b>PCE [%]</b>
CM1	5.7	1030	52	3.1
CM2	5.4	1180	50	3.2
CM3	8.0	820	63	4.1
CM4	9.6	850	64	5.4
CM5	13.6	970	48	6.3
CM6	14.1	730	62	6.4
CM7	12.2	770	62	6.0
CM8	14.2	810	59	6.8

controlled and tuned to compliment the absorption of specific donors. Figure 1.13 and table 1.5 show the structures and device performance parameters of a few CMs with efficiencies ranging from 3% up to 6.8%.<sup>94,99-104</sup> While the optical and electronic properties are much more tunable compared to the PDI based molecules, they tend to suffer much more from a lower driving force for phase separation.<sup>94</sup> The first 3 CMs that are displayed exhibit this problem quite well, the core functional groups, fluorene or phenyl, tend to have a lower driving force for crystallization; however, once replaced by a more planar fused ring system, such as indacenodithiophene, can greatly improve crystallinity, and the use of polar functional groups, such as cyano, can lead to further improved phase separation and self-assembly thanks to dipole alignment. This method of self-assembly is most apparent when comparing CM5 to CM8. The main difference between these two materials is the replacement of an indacenodithiophene core with an indacenodithienothiophene core, yielding an increase in fill factor by 11%. This increase in fill factor hints at the

development of more efficient transport pathways brought about by more crystalline domains.

## 1.6 Conclusions

A great deal of attention has been given to organic photovoltaics in the past two decades developing new materials,<sup>21,45</sup> device engineering,<sup>105,106</sup> and operational understanding.<sup>107–109</sup> It has been shown that through careful design, the energy levels, charge carrier mobility, and degree of crystallinity can be controlled using careful molecular design,<sup>52</sup> and processing conditions.<sup>7</sup> By the introduction of donor-acceptor architecture optical bandgaps were narrowed allowing for increased photon flux and improved short circuit current and open circuit voltage.<sup>110</sup> This push-pull concept was then brought to the realm of small molecules where batch-to-batch variability and molecular weight dependences could be removed,<sup>45</sup> and presenting an idea of a modular architecture.<sup>47</sup> Using this modular architecture, molecular length could be controlled,<sup>52</sup> or solubility could be affected by functional group modification.<sup>89</sup>

Utilizing this idea of solubility modification, ethylene glycol chains were introduced to improve solubility in more polar solvents.<sup>89</sup> Despite improving solubility in polar solvents, they had rather poor device performance, but that study further led to the usage of green solvents for device processing.<sup>56</sup> This usage of green solvents for active layer processing started a push towards a more sustainable future of organic photovoltaics.

Finally, by clever molecular design, non-fullerene acceptor based devices have been able to achieve comparable performance to fullerenes derivatives.<sup>95</sup> Getting away from fullerenes allows for more control over the absorption profile, and energetics of the active layer blend. This also reduces the overall cost of devices, due to the costly synthesis of fullerenes and the inherent struggle to purify them. With this in mind perhaps the next step for organic photovoltaics is non-fullerene based devices processed from green solvents?

## 1.7 References

- (1) Zhang, Q.; Li, B.; Huang, S.; Nomura, H.; Tanaka, H.; Adachi, C. *Nat. Photonics* **2014**, 8 (4), 326.
- (2) Liu, Y.; Zhao, J.; Li, Z.; Mu, C.; Ma, W.; Hu, H.; Jiang, K.; Lin, H.; Ade, H.; Yan, H. *Nat. Commun.* **2014**, 5, 5293.
- (3) Wang, M.; Ford, M.; Phan, H.; Coughlin, J.; Nguyen, T.-Q.; Bazan, G. C. *Chem. Commun.* **2016**, 52 (15), 3207.
- (4) Liu, X.; Sun, Y.; Hsu, B. B. Y.; Lorbach, A.; Qi, L.; Heeger, A. J.; Bazan, G. C. *J. Am. Chem. Soc.* **2014**, 136 (15), 5697.
- (5) Hu, H.; Jiang, K.; Yang, G.; Liu, J.; Li, Z.; Lin, H.; Liu, Y.; Zhao, J.; Zhang, J.; Huang, F.; Qu, Y.; Ma, W.; Yan, H. *J. Am. Chem. Soc.* **2015**, 137 (44), 14149.
- (6) Lee, J. K.; Ma, W. L.; Brabec, C. J.; Yuen, J.; Moon, J. S.; Kim, J. Y.; Lee, K.; Bazan, G. C.; Heeger, A. J. *J. Am. Chem. Soc.* **2008**, 130 (11), 3619.
- (7) Peet, J.; Kim, J. Y.; Coates, N. E.; Ma, W. L.; Moses, D.; Heeger, A. J.; Bazan, G. C. *Nat. Mater.* **2007**, 6 (7), 497.
- (8) Treat, N. D.; Nekuda Malik, J. A.; Reid, O.; Yu, L.; Shuttle, C. G.; Rumbles, G.; Hawker, C. J.; Chabinyc, M. L.; Smith, P.; Stingelin, N. *Nat. Mater.* **2013**, *advance online publication*.
- (9) Nam, S.; Seo, J.; Woo, S.; Kim, W. H.; Kim, H.; Bradley, D. D. C.; Kim, Y. *Nat. Commun.* **2015**, 6, 8929.
- (10) Hoven, C. V.; Yang, R.; Garcia, A.; Crockett, V.; Heeger, A. J.; Bazan, G. C.; Nguyen, T.-Q. *Proc. Natl. Acad. Sci.* **2008**, 105 (35), 12730.
- (11) Hung, L. S.; Chen, C. H. *Mater. Sci. Eng. R Rep.* **2002**, 39 (5–6), 143.
- (12) Dennler, G.; Scharber, M. C.; Brabec, C. J. *Adv. Mater.* **2009**, 21 (13), 1323.
- (13) Andersson, L. M.; Müller, C.; Badada, B. H.; Zhang, F.; Würfel, U.; Inganäs, O. *J. Appl. Phys.* **2011**, 110 (2), 24509.
- (14) Braga, D.; Horowitz, G. *Adv. Mater.* **2009**, 21 (14–15), 1473.
- (15) Choi, H.; Ko, S.-J.; Kim, T.; Morin, P.-O.; Walker, B.; Lee, B. H.; Leclerc, M.; Kim, J. Y.; Heeger, A. J. *Adv. Mater.* **2015**, 27 (21), 3318.
- (16) Burke, T. M.; Sweetnam, S.; Vandewal, K.; McGehee, M. D. *Adv. Energy Mater.* **2015**, 5 (11), n/a.

- (17) Bartelt, J. A.; Lam, D.; Burke, T. M.; Sweetnam, S. M.; McGehee, M. D. *Adv. Energy Mater.* **2015**, n/a.
- (18) Proctor, C. M.; Love, J. A.; Nguyen, T.-Q. *Adv. Mater.* **2014**, *26* (34), 5957.
- (19) Mikhnenko, O. V.; Azimi, H.; Scharber, M.; Morana, M.; Blom, P. W. M.; Loi, M. A. *Energy Environ. Sci.* **2012**, *5* (5), 6960.
- (20) Lin, J. D. A.; Mikhnenko, O. V.; Chen, J.; Masri, Z.; Ruseckas, A.; Mikhailovsky, A.; Raab, R. P.; Liu, J.; Blom, P. W. M.; Loi, M. A.; García-Cervera, C. J.; Samuel, I. D. W.; Nguyen, T.-Q. *Mater. Horiz.* **2014**, *1* (2), 280.
- (21) Yu, G.; Gao, J.; Hummelen, J. C.; Wudl, F.; Heeger, A. J. *Science* **1995**, *270* (5243), 1789.
- (22) Hoppe, H.; Sariciftci, N. S. *J. Mater. Chem.* **2006**, *16* (1), 45.
- (23) Huang, W.; Gann, E.; Cheng, Y.-B.; McNeill, C. R. *ACS Appl. Mater. Interfaces* **2015**, *7* (25), 14026.
- (24) Love, J. A.; Proctor, C. M.; Liu, J.; Takacs, C. J.; Sharenko, A.; van der Poll, T. S.; Heeger, A. J.; Bazan, G. C.; Nguyen, T.-Q. *Adv. Funct. Mater.* **2013**, n/a.
- (25) Foertig, A.; Kniepert, J.; Gluecker, M.; Brenner, T.; Dyakonov, V.; Neher, D.; Deibel, C. *Adv. Funct. Mater.* **2013**, n/a.
- (26) Vithanage, D. A.; Wang, E.; Wang, Z.; Ma, F.; Inganäs, O.; Andersson, M. R.; Yartsev, A.; Sundström, V.; Pascher, T. *Adv. Energy Mater.* **2014**, n/a.
- (27) Mihailetchi, V. D.; Koster, L. J. A.; Hummelen, J. C.; Blom, P. W. M. *Phys. Rev. Lett.* **2004**, *93* (21), 216601.
- (28) Shaheen, S. E.; Brabec, C. J.; Sariciftci, N. S.; Padinger, F.; Fromherz, T.; Hummelen, J. C. *Appl. Phys. Lett.* **2001**, *78* (6), 841.
- (29) Chi, D.; Qu, S.; Wang, Z.; Wang, J. *J. Mater. Chem. C* **2014**, *2* (22), 4383.
- (30) Dhanabalan, A.; van Duren, J. K. J.; van Hal, P. A.; van Dongen, J. L. J.; Janssen, R. a. J. *Adv. Funct. Mater.* **2001**, *11* (4), 255.
- (31) Meier, H. *Angew. Chem. Int. Ed.* **2005**, *44* (17), 2482.
- (32) Campos, L. M.; Tontcheva, A.; Günes, S.; Sonmez, G.; Neugebauer, H.; Sariciftci, N. S.; Wudl, F. *Chem. Mater.* **2005**, *17* (16), 4031.
- (33) Zhang, Q.; Kan, B.; Liu, F.; Long, G.; Wan, X.; Chen, X.; Zuo, Y.; Ni, W.; Zhang, H.; Li, M.; Hu, Z.; Huang, F.; Cao, Y.; Liang, Z.; Zhang, M.; Russell, T. P.; Chen, Y. *Nat. Photonics* **2014**, advance online publication.

- (34) Lee, H. K. H.; Li, Z.; Constantinou, I.; So, F.; Tsang, S. W.; So, S. K. *Adv. Energy Mater.* **2014**, *4* (16), n/a.
- (35) Himmelberger, S.; Vandewal, K.; Fei, Z.; Heeney, M.; Salleo, A. *Macromolecules* **2014**, *47* (20), 7151.
- (36) Moet, D. J. D.; Lenes, M.; Kotlarski, J. D.; Veenstra, S. C.; Sweelssen, J.; Koetse, M. M.; de Boer, B.; Blom, P. W. M. *Org. Electron.* **2009**, *10* (7), 1275.
- (37) Müller, C.; Wang, E.; Andersson, L. M.; Tvingstedt, K.; Zhou, Y.; Andersson, M. R.; Inganäs, O. *Adv. Funct. Mater.* **2010**, *20* (13), 2124.
- (38) Coughlin, J. E.; Henson, Z. B.; Welch, G. C.; Bazan, G. C. *Acc. Chem. Res.* **2014**, *47* (1), 257.
- (39) Walker, B.; Tamayo, A. B.; Dang, X.-D.; Zalar, P.; Seo, J. H.; Garcia, A.; Tantiwiwat, M.; Nguyen, T.-Q. *Adv. Funct. Mater.* **2009**, *19* (19), 3063.
- (40) Walker, B.; Han, Xu; Kim, C.; Sellinger, A.; Nguyen, T.-Q. *ACS Appl. Mater. Interfaces* **2011**, *4* (1), 244.
- (41) Tamayo, A. B.; Dang, X.-D.; Walker, B.; Seo, J.; Kent, T.; Nguyen, T.-Q. *Appl. Phys. Lett.* **2009**, *94* (10), 103301.
- (42) Tamayo, A. B.; Walker, B.; Nguyen, T.-Q. *J. Phys. Chem. C* **2008**, *112* (30), 11545.
- (43) Wallquist, O.; Lenz, R. *Macromol. Symp.* **2002**, *187* (1), 617.
- (44) Hao, Z.; Iqbal, A. *Chem. Soc. Rev.* **1997**, *26* (3), 203.
- (45) Sun, Y.; Welch, G. C.; Leong, W. L.; Takacs, C. J.; Bazan, G. C.; Heeger, A. J. *Nat. Mater.* **2012**, *11* (1), 44.
- (46) Garcia, A.; Welch, G. C.; Ratcliff, E. L.; Ginley, D. S.; Bazan, G. C.; Olson, D. C. *Adv. Mater.* **2012**, *24* (39), 5368.
- (47) van der Poll, T. S.; Love, J. A.; Nguyen, T.-Q.; Bazan, G. C. *Adv. Mater.* **2012**, *24* (27), 3646.
- (48) Mukherjee, S.; Proctor, C. M.; Tumbleston, J. R.; Bazan, G. C.; Nguyen, T.-Q.; Ade, H. *Adv. Mater.* **2015**, *27* (6), 1105.
- (49) Love, J. A.; Nagao, I.; Huang, Y.; Kuik, M.; Gupta, V.; Takacs, C. J.; Coughlin, J. E.; Qi, L.; van der Poll, T. S.; Kramer, E. J.; Heeger, A. J.; Nguyen, T.-Q.; Bazan, G. C. *J. Am. Chem. Soc.* **2014**, *136* (9), 3597.
- (50) Lin, L.-Y.; Chen, Y.-H.; Huang, Z.-Y.; Lin, H.-W.; Chou, S.-H.; Lin, F.; Chen, C.-W.; Liu, Y.-H.; Wong, K.-T. *J. Am. Chem. Soc.* **2011**, *133* (40), 15822.

- (51) Fitzner, R.; Mena-Osteritz, E.; Mishra, A.; Schulz, G.; Reinold, E.; Weil, M.; Körner, C.; Ziehlke, H.; Elschner, C.; Leo, K.; Riede, M.; Pfeiffer, M.; Uhrich, C.; Bäuerle, P. *J. Am. Chem. Soc.* **2012**, *134* (27), 11064.
- (52) Liu, X.; Sun, Y.; Perez, L. A.; Wen, W.; Toney, M. F.; Heeger, A. J.; Bazan, G. C. *J. Am. Chem. Soc.* **2012**, *134* (51), 20609.
- (53) Huang, Y.; Liu, X.; Wang, C.; Rogers, J. T.; Su, G. M.; Chabynyc, M. L.; Kramer, E. J.; Bazan, G. C. *Adv. Energy Mater.* **2014**, *4* (10), n/a.
- (54) Proctor, C. M.; Kher, A. S.; Love, J. A.; Huang, Y.; Sharenko, A.; Bazan, G. C.; Nguyen, T.-Q. *Adv. Energy Mater.* **2016**, *6* (9), n/a.
- (55) Abdelsamie, M.; Treat, N. D.; Zhao, K.; McDowell, C.; Burgers, M. A.; Li, R.; Smilgies, D.-M.; Stingelin, N.; Bazan, G. C.; Amassian, A. *Adv. Mater.* **2015**, n/a.
- (56) Chen, X.; Liu, X.; Burgers, M. A.; Huang, Y.; Bazan, G. C. *Angew. Chem. Int. Ed.* **2014**, *53* (52), 14378.
- (57) Liu, X.; Hsu, B. B. Y.; Sun, Y.; Mai, C.-K.; Heeger, A. J.; Bazan, G. C. *J. Am. Chem. Soc.* **2014**, *136* (46), 16144.
- (58) Liu, X.; Burgers, M. A.; Hsu, B. B. Y.; Coughlin, J. E.; Perez, L. A.; Heeger, A. J.; Bazan, G. C. *RSC Adv.* **2015**, *5* (108), 89144.
- (59) Hoven, C. V.; Garcia, A.; Bazan, G. C.; Nguyen, T.-Q. *Adv. Mater.* **2008**, *20* (20), 3793.
- (60) Gaylord, B. S.; Heeger, A. J.; Bazan, G. C. *Proc. Natl. Acad. Sci.* **2002**, *99* (17), 10954.
- (61) Wang, D.; Gong, X.; Heeger, P. S.; Rininsland, F.; Bazan, G. C.; Heeger, A. J. *Proc. Natl. Acad. Sci.* **2002**, *99* (1), 49.
- (62) Mai, C.-K.; Schlitz, R. A.; Su, G. M.; Spitzer, D.; Wang, X.; Fronk, S. L.; Cahill, D. G.; Chabynyc, M. L.; Bazan, G. C. *J. Am. Chem. Soc.* **2014**, *136* (39), 13478.
- (63) Mai, C.-K.; Russ, B.; Fronk, S. L.; Hu, N.; Chan-Park, M. B.; Urban, J. J.; Segalman, R. A.; Chabynyc, M. L.; Bazan, G. C. *Energy Environ. Sci.* **2015**, *8* (8), 2341.
- (64) Seo, J. H.; Nguyen, T.-Q. *J. Am. Chem. Soc.* **2008**, *130* (31), 10042.
- (65) Seo, J. H.; Namdas, E. B.; Gutacker, A.; Heeger, A. J.; Bazan, G. C. *Adv. Funct. Mater.* **2011**, *21* (19), 3667.
- (66) Seo, J. H.; Namdas, E. B.; Gutacker, A.; Heeger, A. J.; Bazan, G. C. *Appl. Phys. Lett.* **2010**, *97* (4), 43303.

- (67) Yang, R.; Wu, H.; Cao, Y.; Bazan, G. C. *J. Am. Chem. Soc.* **2006**, *128* (45), 14422.
- (68) Oh, S.-H.; Na, S.-I.; Jo, J.; Lim, B.; Vak, D.; Kim, D.-Y. *Adv. Funct. Mater.* **2010**, *20* (12), 1977.
- (69) Zilberberg, K.; Behrendt, A.; Kraft, M.; Scherf, U.; Riedl, T. *Org. Electron.* **2013**, *14* (3), 951.
- (70) Yang, T.; Wang, M.; Duan, C.; Hu, X.; Huang, L.; Peng, J.; Huang, F.; Gong, X. *Energy Environ. Sci.* **2012**, *5* (8), 8208.
- (71) Zhou, Y.; Fuentes-Hernandez, C.; Shim, J.; Meyer, J.; Giordano, A. J.; Li, H.; Winget, P.; Papadopoulos, T.; Cheun, H.; Kim, J.; Fenoll, M.; Dindar, A.; Haske, W.; Najafabadi, E.; Khan, T. M.; Sojoudi, H.; Barlow, S.; Graham, S.; Brédas, J.-L.; Marder, S. R.; Kahn, A.; Kippelen, B. *Science* **2012**, *336* (6079), 327.
- (72) Sherman, J.; Chin, B.; Huibers, P. D. T.; Garcia-Valls, R.; Hatton, T. A. *Environ. Health Perspect.* **1998**, *106*, 253.
- (73) Beach, E. S.; Cui, Z.; Anastas, P. T. *Energy Environ. Sci.* **2009**, *2* (10), 1038.
- (74) Clark, J. H.; Budarin, V.; Deswarte, F. E. I.; Hardy, J. J. E.; Kerton, F. M.; Hunt, A. J.; Luque, R.; Macquarrie, D. J.; Milkowski, K.; Rodriguez, A.; Samuel, O.; Tavener, S. J.; White, R. J.; Wilson, A. J. *Green Chem.* **2006**, *8* (10), 853.
- (75) Ball, J. M.; Lee, M. M.; Hey, A.; Snaith, H. J. *Energy Environ. Sci.* **2013**, *6* (6), 1739.
- (76) Grätzel, M. *J. Photochem. Photobiol. C Photochem. Rev.* **2003**, *4* (2), 145.
- (77) Noel, N. K.; Stranks, S. D.; Abate, A.; Wehrenfennig, C.; Guarnera, S.; Haghighirad, A.-A.; Sadhanala, A.; Eperon, G. E.; Pathak, S. K.; Johnston, M. B.; Petrozza, A.; Herz, L. M.; Snaith, H. J. *Energy Environ. Sci.* **2014**, *7* (9), 3061.
- (78) Griffin, J.; Pearson, A. J.; Scarratt, N. W.; Wang, T.; Dunbar, A. D. F.; Yi, H.; Iraqi, A.; Buckley, A. R.; Lidzey, D. G. *Org. Electron.* **2015**, *21*, 216.
- (79) Davidson, M.; Feinleib, M. *Am. Heart J.* **1972**, *83* (1), 100.
- (80) Fu, B.; Wang, C.-Y.; Rose, B. D.; Jiang, Y.; Chang, M.; Chu, P.-H.; Yuan, Z.; Fuentes-Hernandez, C.; Kippelen, B.; Brédas, J.-L.; Collard, D. M.; Reichmanis, E. *Chem. Mater.* **2015**.
- (81) Aj, M. *IARC Sci. Publ.* **1987**, No. 85, 3.
- (82) Langman, J. M. *Pathology (Phila.)* **1994**, *26* (3), 301.
- (83) Kim, W.; Kim, J. K.; Kim, E.; Ahn, T. K.; Wang, D. H.; Park, J. H. *J. Phys. Chem. C* **2015**, *119* (11), 5954.

- (84) Kniepert, J.; Lange, I.; Heidbrink, J.; Kurpiers, J.; Brenner, T. J. K.; Koster, L. J. A.; Neher, D. *J. Phys. Chem. C* **2015**, *119* (15), 8310.
- (85) Sprau, C.; Buss, F.; Wagner, M.; Landerer, D.; Koppitz, M.; Schulz, A.; Bahro, D.; Schabel, W.; Scharfer, P.; Colsmann, A. *Energy Environ. Sci.* **2015**.
- (86) Gu, Y.; Jérôme, F. *Chem. Soc. Rev.* **2013**, *42* (24), 9550.
- (87) Pace, V.; Hoyos, P.; Castoldi, L.; Domínguez de María, P.; Alcántara, A. R. *ChemSusChem* **2012**, *5* (8), 1369.
- (88) Antonucci, V.; Coleman, J.; Ferry, J. B.; Johnson, N.; Mathe, M.; Scott, J. P.; Xu, J. *Org. Process Res. Dev.* **2011**, *15* (4), 939.
- (89) Henson, Z. B.; Zalar, P.; Chen, X.; Welch, G. C.; Nguyen, T.-Q.; Bazan, G. C. *J. Mater. Chem. A* **2013**, *1* (37), 11117.
- (90) Duan, C.; Cai, W.; Hsu, B. B. Y.; Zhong, C.; Zhang, K.; Liu, C.; Hu, Z.; Huang, F.; Bazan, G. C.; Heeger, A. J.; Cao, Y. *Energy Environ. Sci.* **2013**, *6* (10), 3022.
- (91) Kuik, M.; Wetzelaer, G.-J. A. H.; Nicolai, H. T.; Craciun, N. I.; De Leeuw, D. M.; Blom, P. W. M. *Adv. Mater.* **2014**, *26* (4), 512.
- (92) Eisenmenger, N. D.; Su, G. M.; Welch, G. C.; Takacs, C. J.; Bazan, G. C.; Kramer, E. J.; Chabinyk, M. L. *Chem. Mater.* **2013**, *25* (9), 1688.
- (93) Rivnay, J.; Mannsfeld, S. C. B.; Miller, C. E.; Salleo, A.; Toney, M. F. *Chem. Rev.* **2012**, *112* (10), 5488.
- (94) Nielsen, C. B.; Holliday, S.; Chen, H.-Y.; Cryer, S. J.; McCulloch, I. *Acc. Chem. Res.* **2015**, *48* (11), 2803.
- (95) Hwang, Y.-J.; Li, H.; Courtright, B. A. E.; Subramanian, S.; Jenekhe, S. A. *Adv. Mater.* **2015**, n/a.
- (96) Li, H.; Hwang, Y.-J.; Courtright, B. A. E.; Eberle, F. N.; Subramanian, S.; Jenekhe, S. A. *Adv. Mater.* **2015**, n/a.
- (97) Verreet, B.; Cnops, K.; Cheyins, D.; Heremans, P.; Stesmans, A.; Zango, G.; Claessens, C. G.; Torres, T.; Rand, B. P. *Adv. Energy Mater.* **2014**, n/a.
- (98) Zhao, J.; Li, Y.; Lin, H.; Liu, Y.; Jiang, K.; Mu, C.; Ma, T.; Lai, J. Y. L.; Hu, H.; Yu, D.; Yan, H. *Energy Environ. Sci.* **2015**, *8* (2), 520.
- (99) Holliday, S.; Ashraf, R. S.; Nielsen, C. B.; Kirkus, M.; Röhr, J. A.; Tan, C.-H.; Collado-Fregoso, E.; Knall, A.-C.; Durrant, J. R.; Nelson, J.; McCulloch, I. *J. Am. Chem. Soc.* **2015**, *137* (2), 898.
- (100) Shi, H.; Fu, W.; Shi, M.; Ling, J.; Chen, H. *J. Mater. Chem. A* **2015**, *3* (5), 1902.

- (101) Lin, Y.; Wang, J.; Zhang, Z.-G.; Bai, H.; Li, Y.; Zhu, D.; Zhan, X. *Adv. Mater.* **2015**, *27* (7), 1170.
- (102) Kwon, O. K.; Park, J.-H.; Kim, D. W.; Park, S. K.; Park, S. Y. *Adv. Mater.* **2015**, *27* (11), 1951.
- (103) Kim, Y.; Song, C. E.; Moon, S.-J.; Lim, E. *Chem. Commun.* **2014**, *50* (60), 8235.
- (104) Lin, Y.; Zhang, Z.-G.; Bai, H.; Wang, J.; Yao, Y.; Li, Y.; Zhu, D.; Zhan, X. *Energy Environ. Sci.* **2015**, *8* (2), 610.
- (105) Sun, Y.; Seo, J. H.; Takacs, C. J.; Seifert, J.; Heeger, A. J. *Adv. Mater.* **2011**, *23* (14), 1679.
- (106) Steim, R.; Kogler, F. R.; Brabec, C. J. *J. Mater. Chem.* **2010**, *20* (13), 2499.
- (107) Koster, L. J. A.; Mihailetschi, V. D.; Xie, H.; Blom, P. W. M. *Appl. Phys. Lett.* **2005**, *87* (20), 203502.
- (108) Blom, P. W. M.; Mihailetschi, V. D.; Koster, L. J. A.; Markov, D. E. *Adv. Mater.* **2007**, *19* (12), 1551.
- (109) Lenes, M.; Koster, L. J. A.; Mihailetschi, V. D.; Blom, P. W. M. *Appl. Phys. Lett.* **2006**, *88* (24), 243502.
- (110) Mühlbacher, D.; Scharber, M.; Morana, M.; Zhu, Z.; Waller, D.; Gaudiana, R.; Brabec, C. *Adv. Mater.* **2006**, *18* (21), 2884.

## **Chapter 2: Experimental Techniques**

### **2.1 Overview**

This chapter describes the general procedures used throughout this dissertation. This dissertation's main focus is the processing of organic photovoltaics from green solvents. Due to the need for high concentration solutions for processing, the solubility of many organic semiconductors had to be determined in 2-MeTHF. This method is outlined in section 2.2. The impact that processing conditions can have on device performance is closely tied to the film morphology, and a powerful tool for investigating the system's self-assembly is atomic force microscopy (AFM), described in section 2.3. While AFM is a powerful tool, it only can probe the surface morphology and only gives qualitative results regarding the film morphology, in order to gain quantitative results on structural order grazing incidence wide angle x-ray scattering will be done to further understand the effects of processing on self-assembly (section 2.4). Optical absorption can also show the effects of processing on structural order and is outlined in section 2.5.

In order to understand the impact of processing conditions on device performance, devices must be fabricated. Section 2.6 will go over the process of device fabrication focusing on thermal evaporation and spin casting. After the solar cells have been fabricated the testing and performance evaluation must be done, as described in section 2.7. If instead of solar cells, single carrier diodes were fabricated then the modified fabrication method, testing, and data work up process is outlined in section 2.8.

Several other, more specific forms of characterization were utilized in different experiments; however, these techniques are more niche and will instead be described in their respective chapters.

## **2.2 Solubility Testing**

The most important factor for making a solar cell is the ability to process the active layer. Since all of the materials used in these studies have varying levels of solubility in different solvents the solubility must be determined. This was done by creating several dilute solutions of known concentrations and measuring their absorption (section 2.5). Because of the linear relationship between solution concentration and absorbance, a calibration curve could be set. Once this was done, a saturated solution of the material in question was made and then filtered through a 0.45  $\mu\text{m}$  PVDF filter and diluted with a known amount of solvent until the absorbance fell within the calibration curve. The maximum concentration of the material was then back calculated using the diluted concentration determined from the calibration curve and the dilution factor.

## 2.3 Atomic Force Microscopy (AFM)

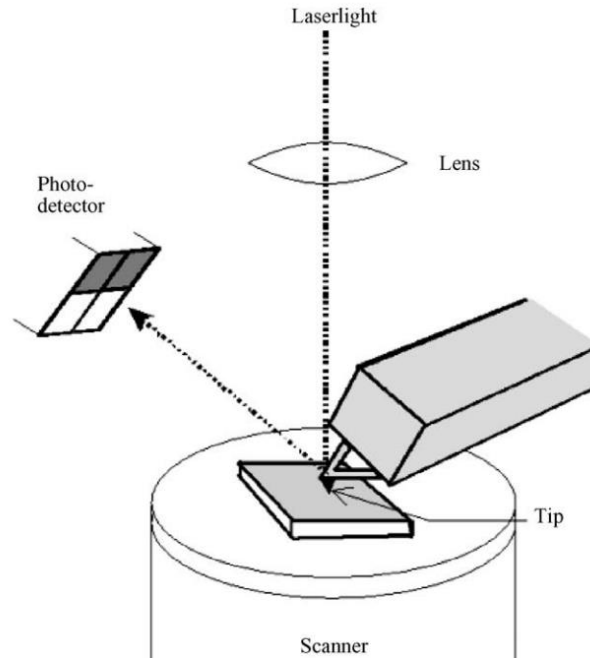


**Figure 1.** Schematic illustration of an AFM. Image used from reference 1.

Atomic force microscopy (AFM), although not being a quantitative, is a strong qualitative tool for investigating the surface morphology of thin film organic photovoltaics. Figure 2.1 shows a schematic of an AFM.<sup>1</sup> A sample, usually one of the devices that has been previously tested, is attached to a metal puck and is mounted on top of a piezoelectric motor. A reflective cantilever is placed in a holder above the sample and a laser beam is aligned to reflect off the tip. A photodiode is then aligned to maximize the amount of reflected light collected. As the tip scans along the surface deviations in the surface lead to deflections in the cantilever causing the reflected laser to move away from its aligned position on the photodiode. There are two modes for AFM, contact and tapping, in the case of this work only tapping mode was used.

Tapping mode is a variant of contact mode, where the tip oscillates near its resonant frequency by a driving signal. As the tip approached the sample, interactions between the tip and the surface effects the magnitude of the oscillations. The sample is moved back and forth in the X and Y plane and the height is controlled by piezo motor. Changes in the surface chemistry can also lead to changes in the oscillation of the tip, causing a phase shift between the driving signal and the photodiode. This allows for the imaging of changes in composition despite no change in surface topology. This is quite desirable for blend films, which have quite smooth layers, but varying composition. Unless otherwise noted, all AFM presented in this dissertation was done in tapping mode on an Innova scanning probe microscope with silicon tips.

## 2.4 Grazing Incidence Wide Angle X-Ray Scattering (GIWAXS)

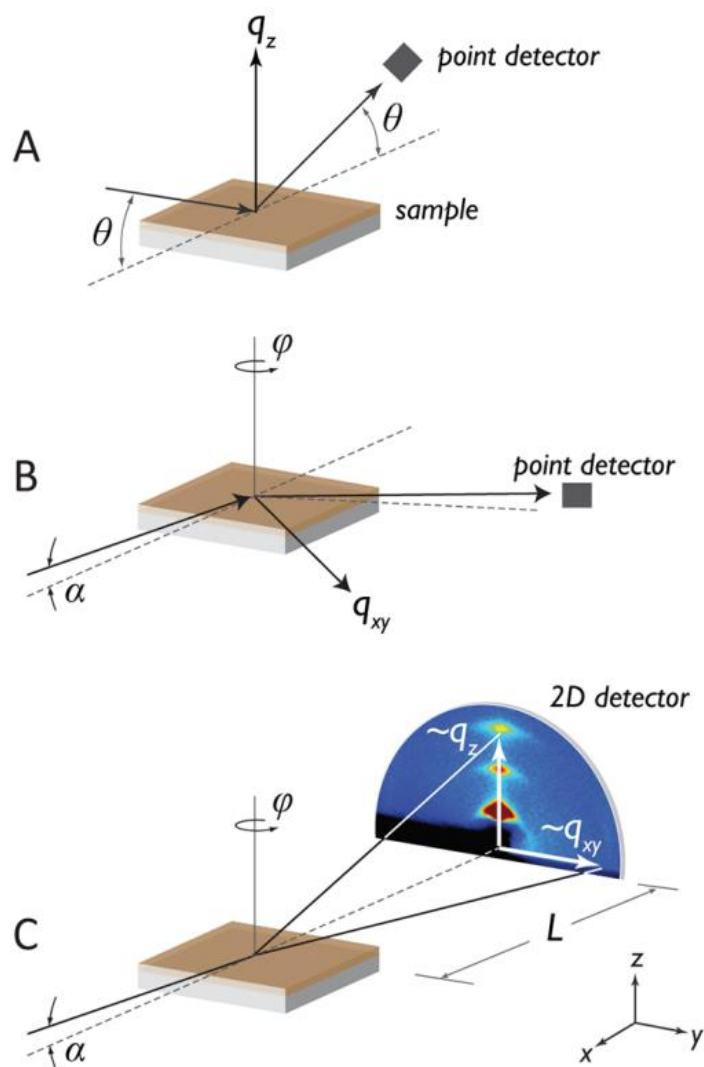


**Figure 2.2.** A comparison of the different types of detectors used for grazing incidence wide angle x-ray scattering, a) and b) show the use of 1-D or single point detector, while c) displays the use of a 2-D detector.

Similar to AFM, x-ray diffraction is a very strong tool for measuring the morphology and bulk film structural order for organic thin films. Unlike AFM, x-ray diffraction allows for both a qualitative and quantitative comparison of thin films.<sup>2</sup> Many organic

semiconductors tend to self-organize into regularly repeating patterns, also called crystal structures. This ability to self-assemble into ordered structures is a very desirable property allowing for decreased disorder of the electronic states and extended delocalization of orbitals across many sites, leading to improved phase separation, improved charge carrier mobility, and red-shifted/broadened absorption spectra improving the optical density. Having such a strong impact on the performance of organic semiconductors, being able to probe the degree of structural order is imperative for understanding the impact of morphology on device performance.

In grazing incidence wide angle x-ray scattering (GIWAXS) x-rays are incident on the sample at a shallow angle, in order to increase the amount of film probed, and a small portion of those x-rays are diffracted by the crystallites in the film. The angle of diffraction is related to the intermolecular spacing in the crystallite, and the direction of the diffracted beam is related to the molecular orientation. Figure 2.2 highlights the different types of detectors that can be used in GIWAXS. A, and B use point detectors, which give a small amount of information regarding the angle of diffraction, but require lower energy x-ray. When using a point detector if both in-plane and out-of-plane diffraction were to be measured then a large amount of time must be spent to collect diffraction at so many different angles of rotation. 2-D detectors are a much more powerful tool for gaining insight into the full diffraction pattern of the sample, but requires high energy x-rays generated at a synchrotron. All GIWAXS measurements done in this dissertation were done on 2-D detectors at either Stanford Linear Accelerator, or Lawrence Berkeley National Lab Advanced Light Source.

Work up for the data obtained was done as followed. Using proprietary software, the 2-D data was all converted into  $q_{xy}$ , and  $q_z$  space. Once converted, cake cuts were performed on both the in-plane and out-of-plane regions and a graph of signal intensity with respect to  $q$  was generated. Using peak fitting programs, the baseline was subtracted and the scattering peaks were analyzed. In order to obtain the intermolecular distance ( $d$ ) the center of the peak was found and converted from  $q$ -space to real space using the Bragg equation (below).<sup>2</sup>

$$q = \frac{2\pi}{d}$$

Using the same peak fitting analysis, the crystalline correlation length (CCL), a measure of crystallite size and quality, can be determined. By obtaining the full width at half max for the peak and using the Scherrer equation to convert to real space will yield the CCL for the sample. This is a powerful tool for comparing the impact different processing conditions have on the morphology of the films.

Samples for GIWAXS were prepared in the same manner as device fabrication and were spin coated on silicon substrates with a thin native oxide layer. Substrates were cleaned by sonication in Soapy water for 15 minutes, followed sonication in deionized water for 10 min, then sonication in an acetone and isopropyl alcohol bath for 30 min each. After sonication, substrates were placed in a petri dish in a drying over for overnight. Directly before spin coating of the active layer, the silicon substrates were treated with UV/Ozone for 30 min.

## 2.5 UV/Vis Absorption

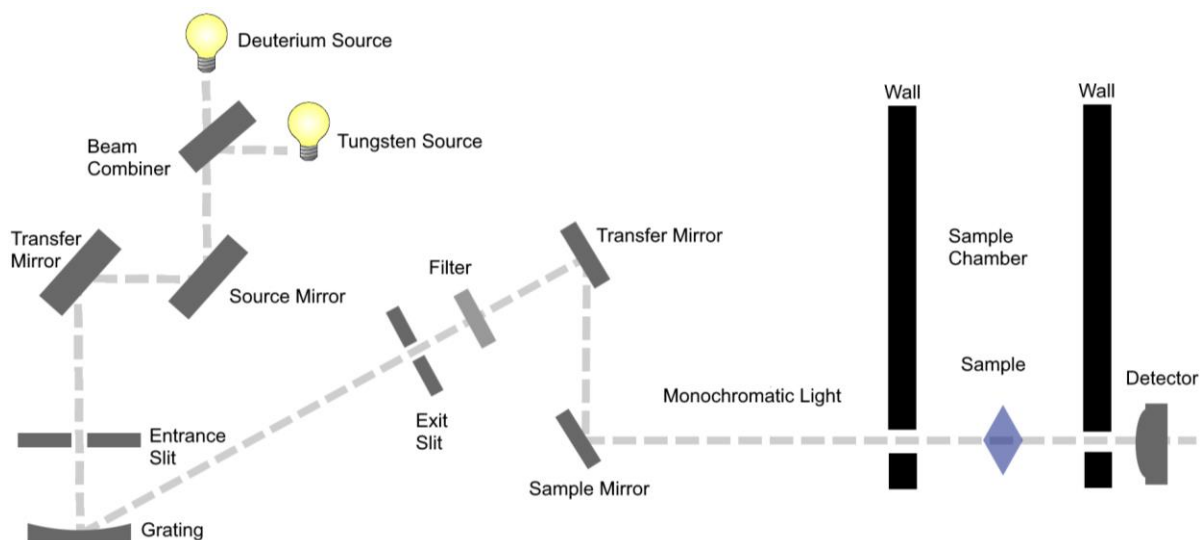


**Figure 2.3.** Schematic diagram illustrating the components of the Beckman Coulter DU800 Spectrophotometer.

There are many properties required of a semiconductor to make a high performance photovoltaic, but the important property of any semiconductor related to solar cell performance is the ability to absorb light that does not get filtered by the ozone layer. This unfiltered range of light is essentially the visible spectrum, and the ability of a compound to absorb visible light is characterized by a UV-Vis absorption spectrum. Absorption is characterized by the excitation of an electron from the HOMO to the LUMO of the molecule, and for that excitation to occur light of an energy equal to or greater than the energy gap between the HOMO and LUMO must be incident on the molecule. This HOMO-LUMO gap can effectively be called the band gap. This optical bandgap can be calculated using the onset of absorption and converting the wavelength in nanometers to energy in electron volts.

In UV/Vis spectrophotometer, UV light is generated using a deuterium lamp and visible light is generated using a tungsten filament lamp. The generated light is then combined and passed through a slit. After passing through the slit, the light is then split into all component wavelengths and a single wavelength can be selected using the diffraction grating. The monochromatic light is then passed through another slit and a filter, before finally being passed through the sample and collected at the detector. Before passing through the sample, the beam is split and detected at another detector to compensate for fluctuations in light intensity. The sample can either be a solution in a cuvette, or a thin film on glass or quartz substrate. Before the samples are measured, a background is run using the cuvette and solvent, or blank substrate. In this dissertation, all absorption spectra were run on a Beckman Coulter DU800 spectrophotometer, and samples run on quartz were compared to actual solar cell devices that were fabricated on glass and indium tin oxide.

## 2.6 Solar Cell Fabrication

The process for fabrication of thin film organic electronics is quite simple in explanation, but rather difficult to achieve high performances. Fabrication begins with glass substrates patterned with ~150 nm of indium tin oxide (ITO), a transparent and rather conductive electrode commonly used in optoelectronic research, purchased from commercial suppliers. The ITO substrates are clearly marked on the glass side with a diamond scribe etching pen for the sake of book keeping, then placed in a Teflon holder and sonicated in soapy water for 15-20 minutes. The substrates are then taken out of the sonicator and scrubbed for 2 minutes for each substrate. The scrubbing allows for the removal of any contaminants as well as helps to smooth out the rather rough ITO surface, decreasing the probability of shorts and reducing the leakage current. After scrubbing the ITO substrates are then sonicated for 5-10 minutes to help remove any residual soap, Substrates are then subsequently sonicated in acetone and isopropanol for 30 minutes each, after sonication substrates are blown dry using nitrogen and immediately put in a drying oven for 5-10 minutes to drive off residual solvent. After dried, the ITO substrates are then put in a UV/ozone cleaner for 30 minutes, or an O<sub>2</sub> plasma cleaner for 5 minutes.

The next step changes depending on the material or type of device being fabricated, for single carrier diodes see section 2.8. The bottom contact must be applied on top of the ITO; this helps to lower the work function allowing for more ohmic contacts. When using a molecule or polymer that contains the pyridyl thiadiazole moiety a 9 nm thick molybdenum oxide (MoO<sub>x</sub>) layer is thermally evaporated through a shadow mask at a pressure of 10<sup>-6</sup> torr. When working with most other polymers or molecules a buffer layer of PEDOT:PSS is

spin coated at 2500 RPM for 40 sec and then heated to 150 °C to drive off water and thermally anneal the layer.

After the bottom contact is deposited, the devices are then transferred to a processing glovebox containing a spin coater in an inert nitrogen atmosphere. When using MoO<sub>x</sub> as a bottom contact, the substrates are transferred using a device transfer chamber keeping the substrates in an inert atmosphere for transfer outside of the glovebox. Devices are placed on the spin coater and the desired deposition RPM and time is set, and the substrate is given a small blast of nitrogen from a nitrogen gun to remove any potential dust. Approximately 20 µl of solution are pulled up using a micropipette and deposited on the substrate. Once the solution had been deposited on the substrate, the spin coater is started and allowed to run for the allotted time. After spin coating is finished the devices then sit for approximately 20 min to allow for slow drying, and after that thermally annealed if the procedure calls for it.

Once active layer deposition and post-deposition treatment is completed, the devices are then scratched on one side to allow for contact to be made with the electrode, and placed in the evaporation chamber. The top contact usually a 15 nm thick layer of Calcium followed by a 100 nm thick layer of Aluminum are deposited through a patterned shadow mask of known area at 10<sup>-6</sup> torr, for single carrier diode contacts see section 2.8. In this dissertation the vast majority of solar cells use a bottom contact of MoO<sub>x</sub> and a top contact of Ca/Al unless otherwise noted.

The night before devices are fabricated, the active layer solution must be made. Using a balance accurate to the 0.01 mg, the active layer components are weighed out individually to their desired blend ratio and carefully transferred to a cleaned glass vial with a Teflon sealed cap. A cleaned stir bar is then placed in the vial and carefully transferred

into the processing glovebox. Once in the glovebox, the solution is then made using the desired solvents at the desired concentration, and a solution never had a volume of less than 250  $\mu$ l. Devices made from solutions lower than that volume tended to have a wide variance in performances. After the solvent was added the vials were tightly capped and then placed on a hotplate at a desired temperature and stir rate over night. On the day of device fabrication, 1 hour before active layer deposition, the solutions are taken off the hotplate and allowed to rest and any material that has stuck to the vial walls is washed back down.

It is extremely important that great care is taken in every step of fabrication to ensure the highest level of reproducibility. Any minor mistake in device fabrication can lead to poor performances and inconsistent results.

## 2.7 Solar Cell Characterization

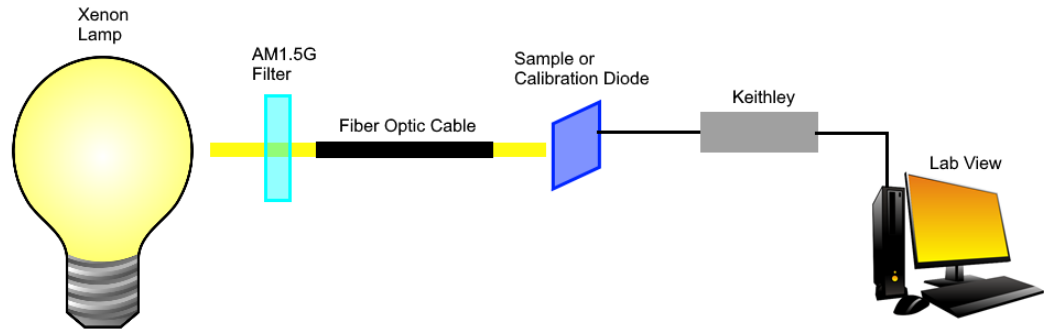


**Figure 2.4.** Schematic illustrating the equipment setup for measuring J-V characteristics of fabricated solar cells under simulated sunlight.

Solar cell characterization involved two forms of characterization. First the current voltage (J-V) characteristics were collected under simulated solar irradiation and in the dark. The photo-generated current was then measured of a few of the higher performing devices using monochromatic to quantify the incident photon-to-electron conversion efficiency (IPCE) or more commonly called external quantum efficiency (EQE).

J-V measurements were carried out on a Keithley 2400 source measure unit (SMU), the unit was controlled by a Lab View program allowing for hysteresis voltage sweeps. Using a 300 W Xenon arc lamp solar light was simulated by passing through an AM1.5G global filter, focused with a fiber optic cable. Light intensity was calibrated before testing each batch of devices using an NREL certified photodiode. Figure 2.4 illustrates the layout used to measure the J-V characteristics of solar cells.

EQE measurements on the same devices used white light generated using 75 W Xenon arc lamp that was modulated into an oscillating signal by using a chopper and a chopper controller connected to a function generator set to 138 Hz. The chopped white light is then passed through a monochromator and focused into two fiber optic cables, one going

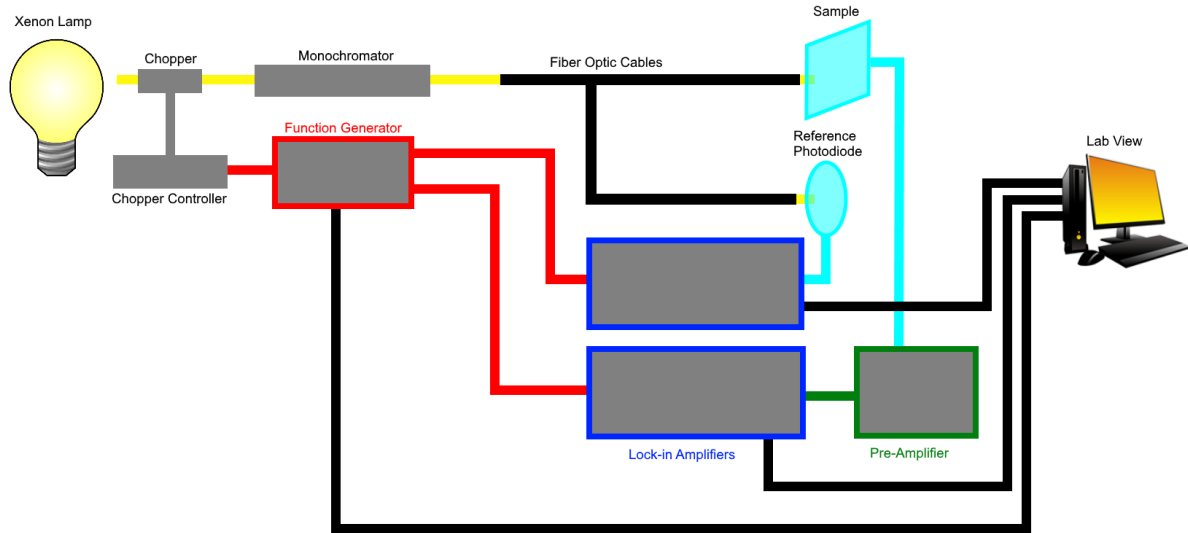


**Figure 2.5.** Schematic illustrating the equipment setup for measuring the external quantum efficiency (EQE) of fabricated solar cells.

to the sample and the other to a reference diode. The photocurrent produced are measured by a lock-in amplifier receiving the same 138 Hz signal from the function generator filtering out all other signal not in phase. The voltage produced from the sample is compared to the reference ( $V_{\text{samp}}/V_{\text{ref}}$ ) for each wavelength. In order to obtain the EQE, these same measurements are run on a NIST calibration diode and put into the equation below.

$$EQE = \frac{V_{\text{samp}}}{V_{\text{ref}}} \frac{V_{\text{ref}}}{V_{\text{calib}}} EQE_{\text{calib}}$$

The generated EQE can then be integrated over the spectrum measured and should yield have good agreement with the  $J_{sc}$  measured in the J-V scans. This is a powerful tool as the measurements are independent of device area or illumination area, and if there is a mismatch between the J-V measured  $J_{sc}$  and the EQE measured  $J_{sc}$  then the device area used was incorrect, or the light calibration was done incorrectly. Figure 2.5 shows an illustration of the setup used for measuring EQE of fabricated solar cells.

## 2.8 Single Carrier Diodes for Space Charge Limited Current (SCLC) Mobilities

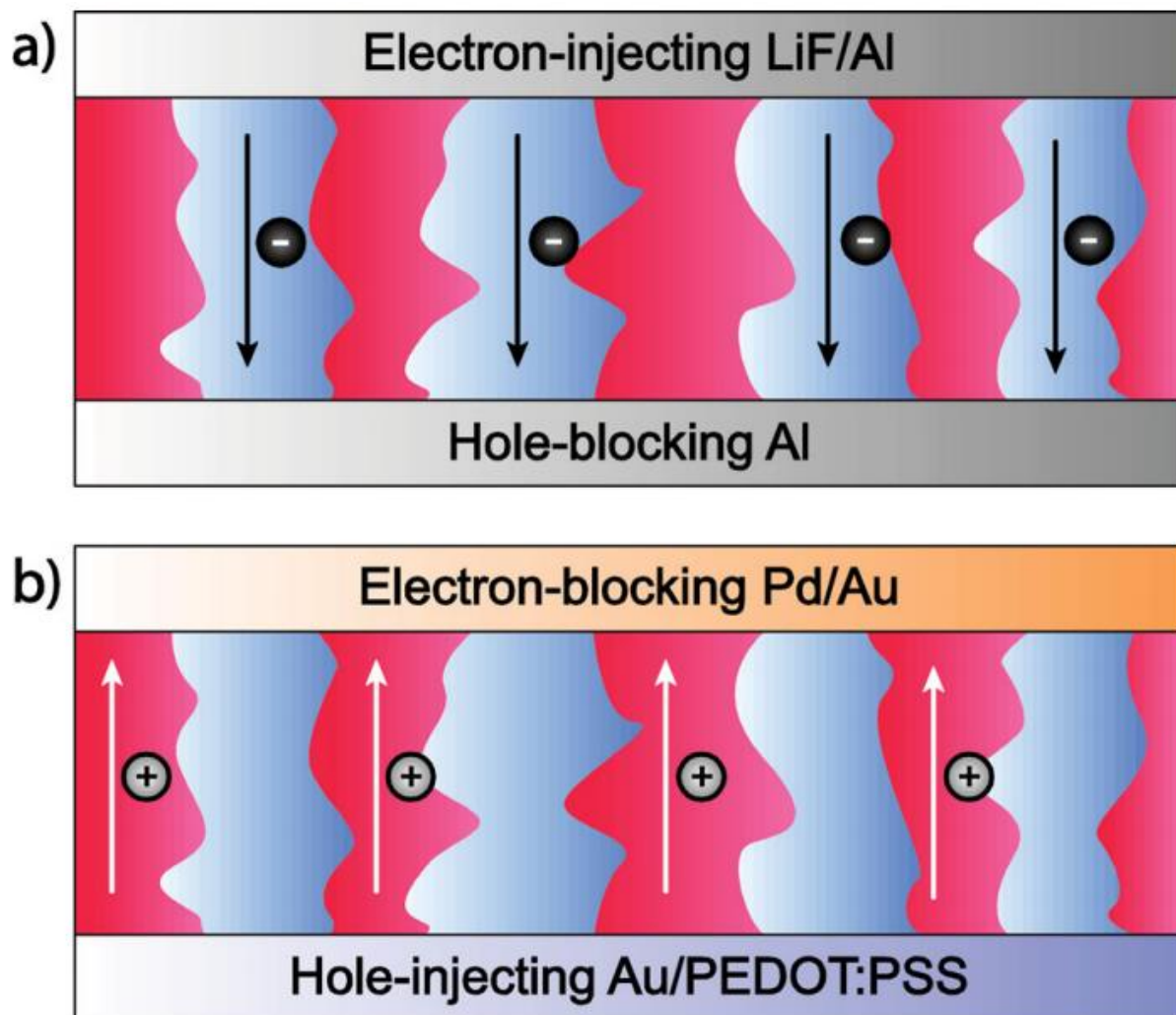


**Figure 2.6.** Schematic illustrating the two types of single carrier diodes: a) electron only diodes, b) hole only diodes. A forward bias is applied across the device and the charges travel in directions depicted. Reproduced from reference 7.

Charge carrier mobility ( $\mu$ ) describes how quickly a charge can move through a certain material. Several techniques can be used to measure charge carrier mobilities of a certain material, field effect transistors,<sup>3</sup> time-of-flight measurements of photo generated

charges,<sup>4</sup> or measuring the space charge limited current (SCLC) of a single carrier diode.<sup>5-7</sup> Of the three techniques SCLC measurements are the most related to organic solar cells, as they exhibit similar architectures and operate in the same carrier density regime. The direction of charge transport in single carrier diodes is also perpendicular to the plane film, the same direction of transport for organic solar cells. As they use a similar architecture as organic solar cells, the facilities required to fabricate and characterize them are the same.

To measure SCLC mobilities a single carrier diode must be fabricated. This is done by properly choosing your injection and extraction contacts. For hole only diodes, the electrodes must have a work function that is deeper than the HOMO of your P-type semiconductor to ensure an ohmic contact. If the contacts do not have an ohmic nature, then instead of SCLC, the single carrier diodes will exhibit Contact Limited Current (CLC). This is commonly done by depositing gold, MoOx or PEDOT:PSS on ITO. In this dissertation all hole only diodes were fabricated using a 9 nm thick layer of MoOx, thermally evaporated through a patterned shadow mask at  $10^{-6}$  torr. This method is exactly the same as the deposition of MoOx as described in section 2.6, as such the devices were subjected to the same cleaning routine. After the active layer was deposited and treated according to the procedure the top contacts were evaporated. In this dissertation the top contact used was either gold (100 nm), or MoOx (5 nm) then gold (100 nm) all deposited by thermal evaporation through a patterned shadow mask at  $10^{-6}$  torr. This sufficiently blocked electron injection from the LUMO and allowed for SCLC hole mobility to be measured. Similarly, when fabricating electron only diodes, the contacts must be higher than the LUMO of the n-type semiconductor to achieve ohmic contact. In this dissertation this is achieved by evaporating ~20 nm of Aluminum on the glass side of a cleaned ITO substrate, then spin

coating of the active layer. After spin coating and post deposition treatments Calcium (15 nm) and then Aluminum (100 nm) were deposited by thermal evaporation through a patterned shadow mask at  $10^{-6}$  torr.

Once the devices have been fabricated they are measured using the same Keithely 2400 Source Measure Unit (SMU) as the solar cells; however, the single carrier diodes require measurement in the dark to reduce any contribution from photo generated charges. Once the electric field has been applied, one charge carrier is injected into the organic material. Since the injected charge carriers can only travel at the rate of charge mobility, a region of charge will build up in the film dominating the current measured through the device that is proportional to the applied bias squared, shown in the equation below.<sup>6</sup>

$$J = \frac{9}{8} \epsilon \epsilon_0 \mu \frac{V^2}{L^3}$$

In the SCLC equation  $\epsilon$  is the dielectric constant of the material, for organic semiconductors this is generally 3.4-4,  $\epsilon_0$  is the vacuum permittivity,  $\mu$  is the charge carrier mobility we are determining,  $L$  is the film thickness, and  $V$  is the applied bias. There is one more factor in this equation that must be taken into account. When using electrodes of different work functions, there is an energy level alignment across the device, leading to an inherent electric field equal to the difference in work functions, this field is called the built in field ( $V_{bi}$ ) and must be corrected for in the equation giving the modified equation below.

$$J = \frac{9}{8} \epsilon \epsilon_0 \mu \frac{(V - V_{bi})^2}{L^3}$$

Using this equation and the current measured the mobility can be solved for by simple curve modeling. This is a very powerful tool for understanding the impact of morphology on device performance. As stated in section 2.4, improving the crystallinity in a

film will also help to improve the charge transport in the film by developing more efficient transport pathways, improving the overall performance of the devices.<sup>8,9</sup> Using this method of charge carrier mobility measurements, this can be confirmed as well as quantified, giving a better insight to the impact of processing conditions on solar cell performance.

## 2.9 References

- (1) Butt, H.-J.; Cappella, B.; Kappl, M. *Surf. Sci. Rep.* **2005**, *59* (1–6), 1.
- (2) Rivnay, J.; Mannsfeld, S. C. B.; Miller, C. E.; Salleo, A.; Toney, M. F. *Chem. Rev.* **2012**, *112* (10), 5488.
- (3) Braga, D.; Horowitz, G. *Adv. Mater.* **2009**, *21* (14–15), 1473.
- (4) Campbell, I. H.; Smith, D. L.; Neef, C. J.; Ferraris, J. P. *Appl. Phys. Lett.* **1999**, *74* (19), 2809.
- (5) Mark, P.; Helfrich, W. *J. Appl. Phys.* **1962**, *33* (1), 205.
- (6) Kuik, M.; Wetzelaer, G.-J. A. H.; Nicolai, H. T.; Craciun, N. I.; De Leeuw, D. M.; Blom, P. W. M. *Adv. Mater.* **2014**, *26* (4), 512.
- (7) Wetzelaer, G.-J. A. H.; Van der Kaap, N. J.; Koster, L. J. A.; Blom, P. W. M. *Adv. Energy Mater.* **2013**, n/a.
- (8) Andersson, L. M.; Müller, C.; Badada, B. H.; Zhang, F.; Würfel, U.; Inganäs, O. *J. Appl. Phys.* **2011**, *110* (2), 24509.
- (9) Bartelt, J. A.; Lam, D.; Burke, T. M.; Sweetnam, S. M.; McGehee, M. D. *Adv. Energy Mater.* **2015**, n/a.

## **Chapter 3: Application of Conjugated Polyelectrolyte Interlayers in Small Molecule Solar Cells and the Impact of Methanol Treatment**

### **3.1 Introduction**

Bulk Heterojunction (BHJ) solar cells comprising of conjugated polymer or small molecule donors and fullerene acceptors have received considerable attention due to their potential for light weight and flexible devices with relatively low-cost of fabrication. Thanks to considerable efforts made in the fields of materials design,<sup>1,2</sup> morphology control,<sup>3,4</sup> operational understanding,<sup>5-7</sup> and interface engineering<sup>8,9</sup> power conversion efficiencies (PCE) have broken the 10% threshold.<sup>9-11</sup> Interface engineering in particular has received a large amount of attention because of the issue of contact resistance between the electrodes and the active layer, and to minimize this resistance the interface between the semiconducting layer and the electrode must be more ohmic in nature.<sup>12,13</sup> This push towards a reduction in contact resistance has led to new innovations in interface engineering such as polar solvent treatment,<sup>14,15</sup> quantum dot buffer layers, and conjugated polyelectrolyte interlayers.<sup>8,16</sup>

Conjugated polyelectrolytes (CPEs) are polymers with pi-conjugated backbones with ionically functionalized pendant groups affording solubility in polar solvents, such as water and methanol.<sup>17</sup> This interesting class of material has a wide array of applications in the field of organic electronics, from thermoelectrics<sup>18,19</sup> to work function modifiers.<sup>20</sup> This property of work function modification is quite beneficial, when a sufficiently thin CPE layer is used as an electrode interlayer the ionic pendant group causes an interfacial dipole and leads to a vacuum level shift of the metal electrode, reducing the injection barrier and making a more ohmic contact with the electrode.<sup>8,21</sup> CPEs solubility in highly polar solvents also allows for

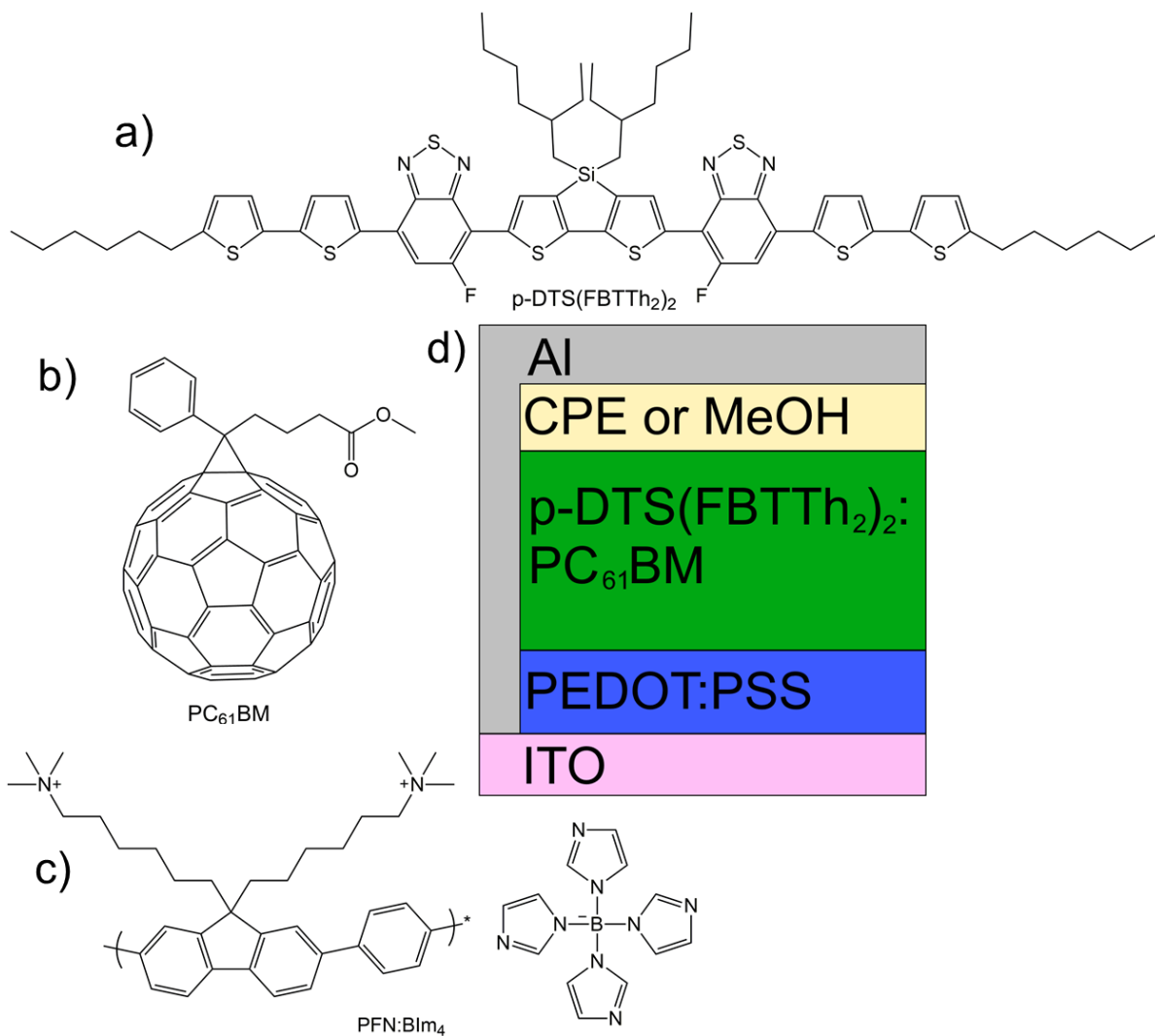


**Figure 3.1.** Molecular structures of the a) donor, b) acceptor, and c) conjugated polyelectrolyte used in device fabrication. d) Device architecture used for the solar cells in this study.

the fabrication of multilayered devices without disturbing the morphology of the organic active layer which is typically only soluble in halogenated and/or aromatic solvents.

Advances in materials design have led to the development of several high performance small molecule donor materials, with an interesting modular architecture.<sup>1,2,22</sup>

These materials have exhibited relatively good open circuit voltages thanks to a reduction in the HOMO. Interestingly, Sun et al. did not fabricate their devices on the commonly used anode buffer layer, PEDOT:PSS, due to protonation of the pyridyl nitrogen in the molecule.<sup>23</sup> Instead devices were fabricated using MoOx,<sup>1</sup> a material with a deep work function (5.4 eV). By using the fluorinated benzothiadiazole group instead of a pyridyl thiadiazole, the issue of protonation was solved and could be processed on PEDOT:PSS, improving ease of processing.<sup>22</sup> In this contribution we demonstrate the deposition of a CPE cathode interlayer on top of p-DTS(FBTTh<sub>2</sub>)<sub>2</sub>:PC<sub>71</sub>BM (figure 3.1), as well as show the impact of just treatment with polar solvent, and provide further insight into the mechanism by which polar solvents can help to improve device performance.

## 3.2 Results and discussion

### 3.2.1 Device Properties

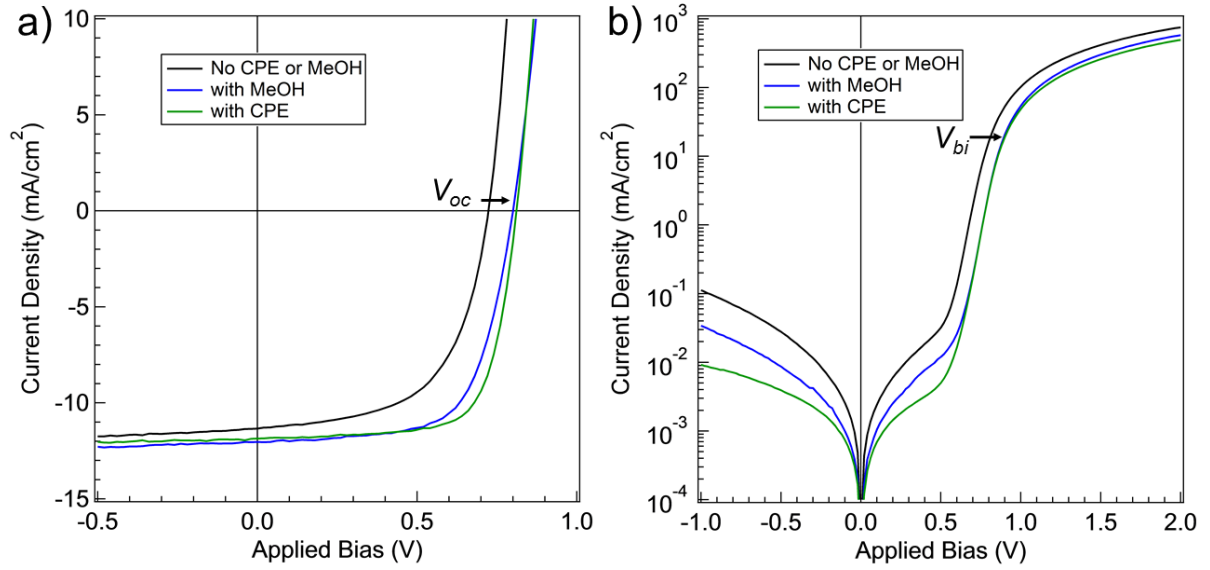


**Figure 3.2.** JV characteristics of p-DTS(FBTTh<sub>2</sub>)<sub>2</sub>:PC<sub>61</sub>BM devices with no treatment (black), with methanol spin treatment (blue), and with PFN:BIm<sub>4</sub> interlayer (green) a) under illumination of solar simulated light, and b) in the dark. The arrow in a) indicates the increase in  $V_{oc}$ . The arrow in b) indicates the increase in the built in voltage.

J-V scans in the dark and under illumination for the best devices are shown in figure 3.2 and the device performance parameters are summarized in table 3.1. Compared to the controlled devices, there is little change in the  $J_{sc}$  after methanol treatment, changing from 11.3 mA/cm<sup>2</sup> to 11.9 mA/cm<sup>2</sup>, and after the introduction of the CPE interlayer increasing to 12.1 mA/cm<sup>2</sup>. This was quite different for the case of the  $V_{oc}$ , where treatment with methanol increased the open circuit voltage from 710 mV to 790 mV, and after introduction of the CPE interlayer there is a further increase in the  $V_{oc}$  to 810 mV. This increase in  $V_{oc}$  is highlighted in figure 3.2a by the black arrow. Similarly, the  $FF$  exhibited a substantial

**Table 3.1.** Summary of device performance parameters of p-DTS(FBTTh<sub>2</sub>)<sub>2</sub>:PC<sub>61</sub>BM solar cells without any treatment, with methanol treatment, and with a CPE interlayer.

<b>Treatment</b>	<b><math>J_{sc}</math> (mA/cm<sup>2</sup>)</b>	<b><math>V_{oc}</math> (mV)</b>	<b><math>FF</math> (%)</b>	<b>PCE (%) Avg. Best</b>	
no treatment	11.3±0.1	710±10	57±1	4.6	4.8
with MeOH	11.9±0.5	790±20	64±1	6.0	6.4
with CPE	12.1±0.2	800±10	71±1	6.9	7.0

increase from 57% for the control devices, to 65% and 71% for the methanol treated and CPE interlayer devices respectively. From dark current JV measurements, figure 3.2b, there is an interesting shift that occurs in the built in voltage  $V_{bi}$ , after methanol treatment and insertion of the CPE interlayer, which appears to have a similar order of improvement as the  $V_{oc}$ . An increase in the built in voltage indicates a shift in the work function of either the bottom or the top contact.<sup>24</sup> Introducing a CPE as a cathode interlayer has been shown to modify the work function of the top contact by the formation of an interfacial dipole;<sup>8,20</sup> however, little is known as to how methanol can modify an electrodes work function, or which work function it would modify.

### 3.2.2 Contact Angle Measurements

To confirm the presence of the CPE layer, measurements of the water contact angle were performed on the surface of all three different layers, and the images were collected with a digital camera shown in figure 3.3. The p-DTS(FBTTh<sub>2</sub>)<sub>2</sub>:PC<sub>61</sub>BM surface was quite hydrophobic with a contact angle of  $\theta = \sim 100^\circ$ , and remained just as hydrophobic after the

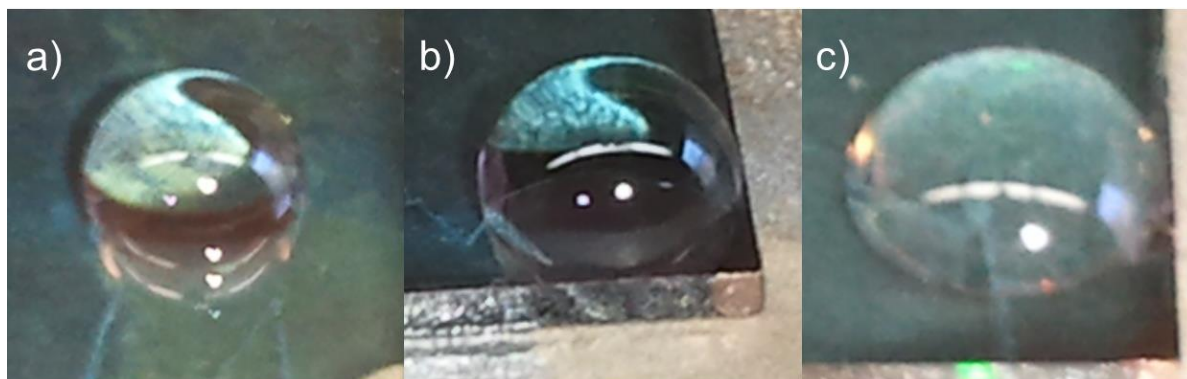


**Figure 3.3.** Photos of water droplets on the surfaces of a) p-DTS(FBTTh<sub>2</sub>)<sub>2</sub>:PC<sub>61</sub>BM, b) p-DTS(FBTTh<sub>2</sub>)<sub>2</sub>:PC<sub>61</sub>BM after methanol spin casting, and c) PFN:BIm<sub>4</sub> spin coated on p-DTS(FBTTh<sub>2</sub>)<sub>2</sub>:PC<sub>61</sub>BM

methanol treatment. The surface with the thin layer of PFN:BIm<sub>4</sub> was significantly less hydrophobic with a contact angle of  $\theta = \sim 50^\circ$ , which would indicate the presence of the ionic pendant groups of PFN:BIm<sub>4</sub> at the surface of the film, in agreement with previous work.<sup>8</sup>

### 3.2.3 Contact Potential Measurements

Figure 3.4 shows the surface morphology measured by AFM, and the surface potential map measured by scanning kelvin probe microscopy the p-DTS(FBTTh<sub>2</sub>)<sub>2</sub>:PC<sub>61</sub>BM films with no treatment, and with the PFN:BIm<sub>4</sub> interlayer. Surface of both the non-treated film, and the CPE treated film are quite smooth and homogeneous, but little more information cannot be discerned from the topographical measurements. The scanning kelvin probe microscopy (SKPM) measurements are quite different showing a change in surface potential for the CPE treated films. Despite this difference in surface potential the CPE does not appear to have full coverage of the p-

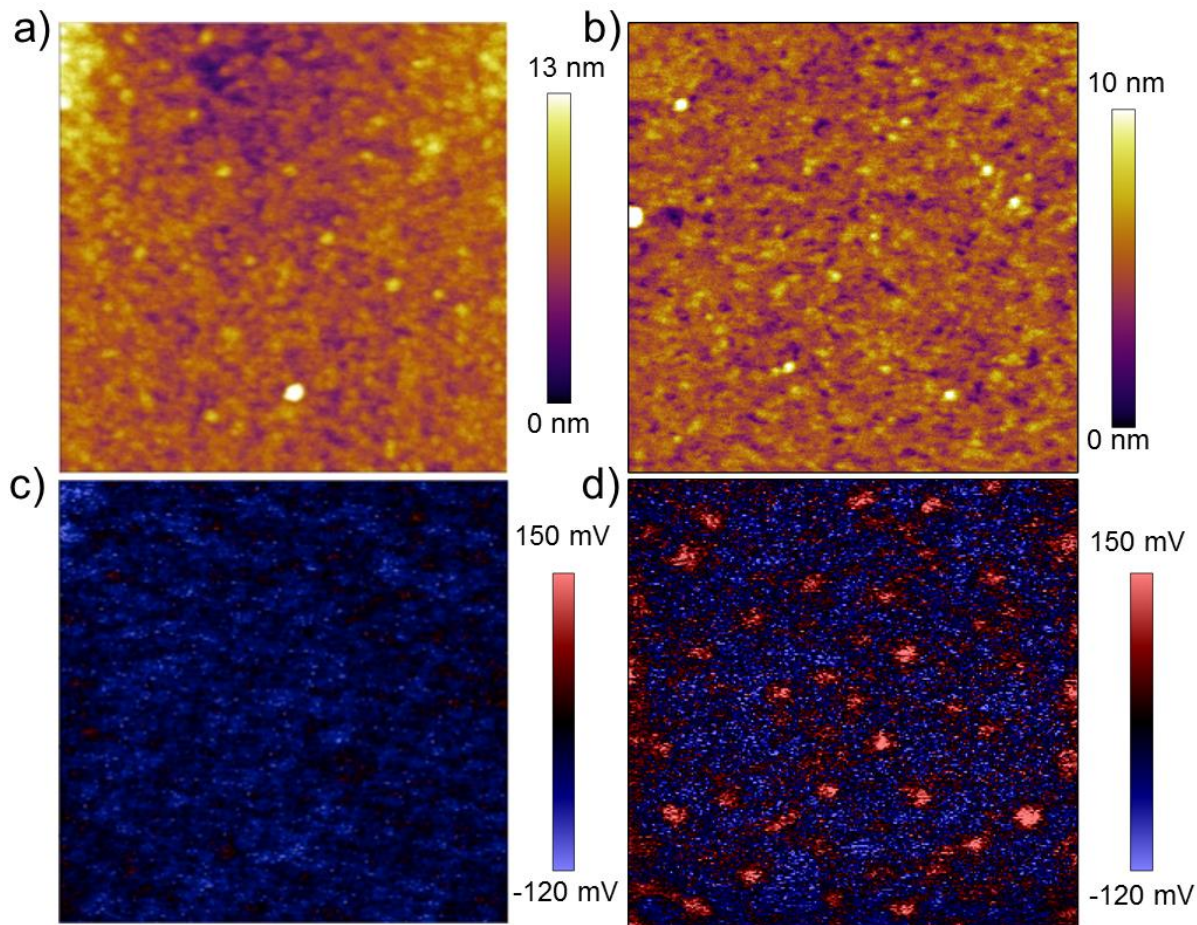


**Figure 3.4.** Surface morphology AFM images of a) p-DTS(FBTTh<sub>2</sub>)<sub>2</sub>:PC<sub>61</sub>BM film, and b) PFN:BIm<sub>4</sub> film spin coated on top of the p-DTS(FBTTh<sub>2</sub>)<sub>2</sub>:PC<sub>61</sub>BM. Surface potential maps of c) p-DTS(FBTTh<sub>2</sub>)<sub>2</sub>:PC<sub>61</sub>BM film, and d) PFN:BIm<sub>4</sub> film on p-DTS(FBTTh<sub>2</sub>)<sub>2</sub>:PC<sub>61</sub>BM obtained by scanning kelvin probe microscopy.

DTS(FTTh<sub>2</sub>)<sub>2</sub>:PC<sub>61</sub>BM film, but forms aggregated islands. The lack of change in the roughness between the p-DTS(FTTh<sub>2</sub>)<sub>2</sub>:PC<sub>61</sub>BM film and the CPE treated films, but the presence of the higher energy islands in the scanning kelvin probe micrograph is consistent with an ultrathin layer (<10 nm) of PFN:BIm<sub>4</sub>. The bulk surface potentials were measured

**Table 3.2** Summarized kelvin probe measurements, and surface work functions for the untreated films, methanol films, and films with PFN:BI<sub>m</sub><sub>4</sub> spin coated on top.

<b>Treatment</b>	<b>CPD (mV)</b>	<b>Work Function (eV)</b>
No Treatment	-114±6	-5.05
w/ MeOH	-112±7	-5.05
w/ PFN:BI <sub>m</sub> <sub>4</sub>	198±5	-4.74

using contact potential difference measurements and were compared to what was observed for the scanning kelvin probe measurements. The bulk surface potential for the p-DTS(FBTTh<sub>2</sub>)<sub>2</sub>:PC<sub>61</sub>BM film is in agreement with what was observed from the SKPM measurements. The bulk surface potential measurements for the PFN:BI<sub>m</sub><sub>4</sub> coated film is slightly higher than what was observed in the SKPM measurements, but the direction of the contact potential difference (CPD) is still the same. This significant change in (CPD) compared to the untreated film further confirms the presence of the CPE at the surface, and the presence of an interfacial dipole caused by the ionic pendant groups, in agreement with the water contact angle measurements. Interestingly, the methanol treated films exhibited no change in the surface potential or work function compared to the untreated samples, despite the changes in  $V_{oc}$ ,  $V_{bi}$ , and  $FF$  that were observed in the J-V scans for the devices. This lack of change in the surface potential would indicate that the methanol is altering the interface between the PEDOT:PSS and the active layer, which is in agreement with what has been observed in the literature.<sup>15</sup>

### 3.2.5 Methanol Penetration Measurements

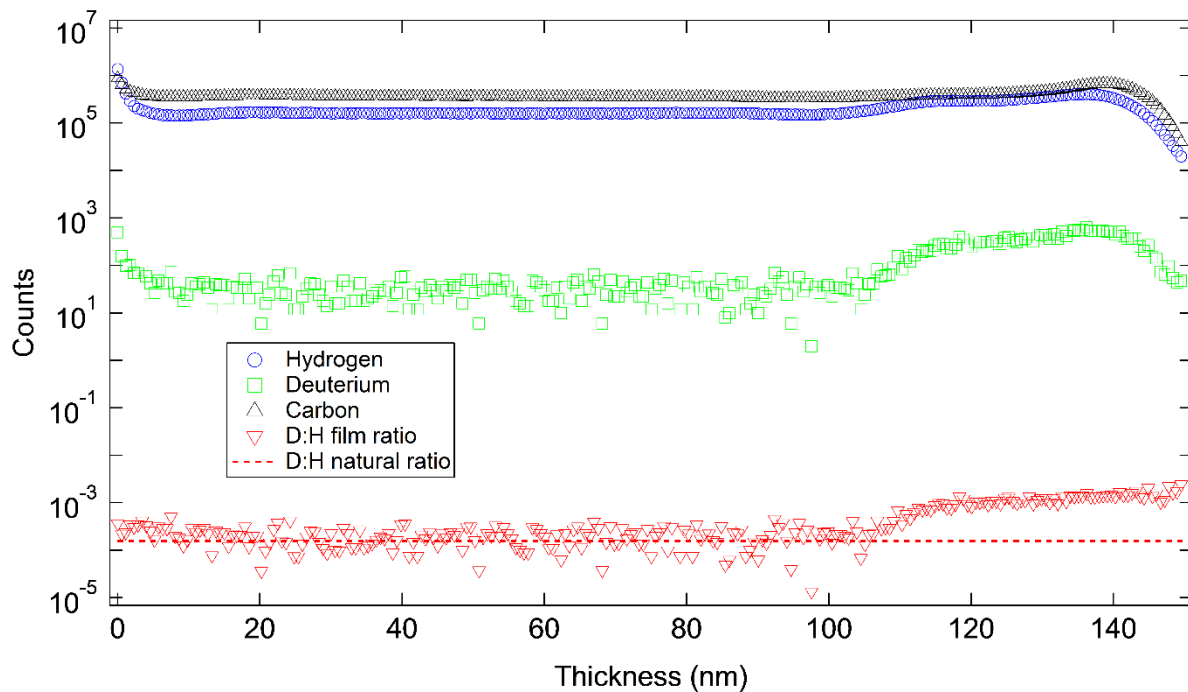


**Figure 3.5.** Elemental depth profile of p-DTS(FBTTh<sub>2</sub>)<sub>2</sub>:PC<sub>61</sub>BM films treated with deuterated methanol.

To confirm that the methanol is in fact altering the interface between the PEDOT:PSS and the active layer, the penetration depth of the methanol was determined using dynamic secondary ion mass spectrometry (DSIMS). By taking the ratio of deuterium atoms to hydrogen atoms in the film, and comparing it to the naturally occurring ratio of deuterium to hydrogen, and idea of how deep the methanol penetrates the film and where it resides can be determined. For the majority of the depth the films deuterium to hydrogen ratio does not deviate much from the naturally occurring ratio but after 105 nm there appears to be an increase by nearly an order of magnitude for the films ratio compared to the

naturally occurring ratio and then plateaus for the next 40 to 50 nm. The resolution of DSIMS is approximately 5 nm which means that the methanol penetrates to a depth of 100 to 110 nm and then remains nearly homogeneously dispersed for the next 40 to 50 nm. The standard thickness of the p-DTS(FBTTh<sub>2</sub>)<sub>2</sub>:PC<sub>61</sub>BM and PEDOT:PSS films are approximately 110 nm and 50 nm respectively. These results confirm that when spin coating methanol on the film, the methanol penetrates the entire active layer and then resides in the PEDOT:PSS film. It is likely that thanks to the retained methanol, an interfacial dipole develops at the bottom contact due to the high polarity of the methanol, which would be in agreement with the literature.<sup>15</sup>

### 3.3 Conclusions

In conclusion we have demonstrated that by incorporating a conjugated polyelectrolyte interlayer, device performance can be significantly improved, from 4.5% to 7%. The main performance increases come from improvement in the  $V_{oc}$  and  $FF$ , both of which are likely caused by the noticeable increase in the built in voltage across the device. It is likely that the further improved  $V_{oc}$  and  $FF$  for the CPE containing devices, compared to the methanol treated, is caused by an increase in the Al work function caused by the interfacial dipole, a function of the ionic groups in the CPE. The presence of the CPE layer was confirmed using water contact angle measurements and surface potential measurements. Interestingly it appears that when using methanol, the solvent will penetrate the entirety of the hydrophobic active layer, and be retained in the PEDOT:PSS layer. It is likely that the retained methanol is what causes the formation of an interfacial dipole at the PEDOT:PSS active layer interface, forming a more ohmic contact. It is likely that the overall improvement observed when incorporating a CPE interlayer is a multifaceted effect caused by both the CPE affecting the cathode interface, and the methanol affecting the anode interface.

### 3.4 Experimental

*Materials Used:* Poly[9,9'-bis[6''-(*N,N,N*-trimethylammonium)-hexyl]fluorine-*alt-co*-phenylene] with tetrakis(imidazolyl)-borate counterion, PFN-BIm4, was synthesized according to the literature.<sup>25,26</sup> p-DTS(FBTTh<sub>2</sub>)<sub>2</sub> was purchased from 1-material, PC<sub>61</sub>BM was purchased from Solenne BV, Chlorobenzene, diiodooctane and anhydrous methanol were purchased from Sigma Aldrich. All chemicals were used as received.

*Device Fabrication:* Solar cells devices were fabricated on cleaned, UV/ozone treated Corning 1737 glass patterned with 150 nm ITO. Active layers were spun at 1750 RPM for 60sec from a solution of p-DTS(FBTTh<sub>2</sub>)<sub>2</sub> and PC<sub>61</sub>BM at a weight ratio of 60:40 in chlorobenzene with 0.4% v/v% DIO, at an overall concentration of 35 mg/ml. Solutions were heated overnight and residual solids were filtered prior to casting at 90 °C. Films were allowed to dry for 30 minutes then heated at 70 °C for 10 minutes to drive off residual solvent. PFN-BIm4 solutions were prepared using anhydrous methanol in an inert atmosphere at a concentration of 1 mg/ml and were deposited on top of the active layer via spin coating at 2500 RPM for 60 seconds. Cathodes were deposited by thermal evaporation of 100 nm of Al through a shadow mask at less than 10<sup>-6</sup> torr. Device performances were tested using a Keithly 2602 system Source Meter under illumination by a simulated 100 mW cm<sup>-2</sup> AM 1.5G light source using a 300 W Xe arc lamp with an AM 1.5 global filter. Solar-simulator irradiance was calibrated using standard silicon photovoltaic with a protective KG1 filter calibrated by the National Renewable Energy Laboratory.

*Water Contact Angle & DSIMS:* Samples for water contact angle measurements and DSIMS were prepared in the exact same way as the devices except no electrode was

thermally evaporated, but the films were still placed under vacuum at  $10^{-6}$  torr to simulate device conditions.

### 3.5 References

- (1) Sun, Y.; Welch, G. C.; Leong, W. L.; Takacs, C. J.; Bazan, G. C.; Heeger, A. J. *Nat. Mater.* **2012**, *11* (1), 44.
- (2) Eisenmenger, N. D.; Su, G. M.; Welch, G. C.; Takacs, C. J.; Bazan, G. C.; Kramer, E. J.; Chabinyk, M. L. *Chem. Mater.* **2013**, *25* (9), 1688.
- (3) Peet, J.; Kim, J. Y.; Coates, N. E.; Ma, W. L.; Moses, D.; Heeger, A. J.; Bazan, G. C. *Nat. Mater.* **2007**, *6* (7), 497.
- (4) Liao, H.-C.; Ho, C.-C.; Chang, C.-Y.; Jao, M.-H.; Darling, S. B.; Su, W.-F. *Mater. Today* **2013**, *16* (9), 326.
- (5) Bartelt, J. A.; Lam, D.; Burke, T. M.; Sweetnam, S. M.; McGehee, M. D. *Adv. Energy Mater.* **2015**, n/a.
- (6) Proctor, C. M.; Kuik, M.; Nguyen, T.-Q. *Prog. Polym. Sci.* **2013**, *38* (12), 1941.
- (7) Wetzelaer, G.-J. A. H.; Kuik, M.; Blom, P. W. M. *Adv. Energy Mater.* **2012**, *2* (10), 1232.
- (8) Seo, J. H.; Gutacker, A.; Sun, Y.; Wu, H.; Huang, F.; Cao, Y.; Scherf, U.; Heeger, A. J.; Bazan, G. C. *J. Am. Chem. Soc.* **2011**, *133* (22), 8416.
- (9) Nam, S.; Seo, J.; Woo, S.; Kim, W. H.; Kim, H.; Bradley, D. D. C.; Kim, Y. *Nat. Commun.* **2015**, *6*, 8929.
- (10) He, Z.; Xiao, B.; Liu, F.; Wu, H.; Yang, Y.; Xiao, S.; Wang, C.; Russell, T. P.; Cao, Y. *Nat. Photonics* **2015**, *9* (3), 174.
- (11) Liu, Y.; Zhao, J.; Li, Z.; Mu, C.; Ma, W.; Hu, H.; Jiang, K.; Lin, H.; Ade, H.; Yan, H. *Nat. Commun.* **2014**, *5*, 5293.
- (12) Dennler, G.; Scharber, M. C.; Brabec, C. J. *Adv. Mater.* **2009**, *21* (13), 1323.
- (13) Blom, P. W. M.; Mihailetschi, V. D.; Koster, L. J. A.; Markov, D. E. *Adv. Mater.* **2007**, *19* (12), 1551.
- (14) Liu, X.; Wen, W.; Bazan, G. C. *Adv. Mater.* **2012**, *24* (33), 4505.
- (15) Tan, Z.-K.; Vaynzof, Y.; Credgington, D.; Li, C.; Casford, M. T. L.; Sepe, A.; Huettner, S.; Nikolka, M.; Paulus, F.; Yang, L.; Sirringhaus, H.; Greenham, N. C.; Friend, R. H. *Adv. Funct. Mater.* **2014**, n/a.
- (16) He, Z.; Zhong, C.; Su, S.; Xu, M.; Wu, H.; Cao, Y. *Nat. Photonics* **2012**, *6* (9), 591.
- (17) Lee, W.; Seo, J. H.; Woo, H. Y. *Polymer* **2013**, *54* (19), 5104.

- (18) Mai, C.-K.; Schlitz, R. A.; Su, G. M.; Spitzer, D.; Wang, X.; Fronk, S. L.; Cahill, D. G.; Chabinyk, M. L.; Bazan, G. C. *J. Am. Chem. Soc.* **2014**, *136* (39), 13478.
- (19) Mai, C.-K.; Russ, B.; Fronk, S. L.; Hu, N.; Chan-Park, M. B.; Urban, J. J.; Segalman, R. A.; Chabinyk, M. L.; Bazan, G. C. *Energy Environ. Sci.* **2015**, *8* (8), 2341.
- (20) Seo, J. H.; Nguyen, T.-Q. *J. Am. Chem. Soc.* **2008**, *130* (31), 10042.
- (21) Zilberberg, K.; Behrendt, A.; Kraft, M.; Scherf, U.; Riedl, T. *Org. Electron.* **2013**, *14* (3), 951.
- (22) van der Poll, T. S.; Love, J. A.; Nguyen, T.-Q.; Bazan, G. C. *Adv. Mater.* **2012**, *24* (27), 3646.
- (23) Garcia, A.; Welch, G. C.; Ratcliff, E. L.; Ginley, D. S.; Bazan, G. C.; Olson, D. C. *Adv. Mater.* **2012**, *24* (39), 5368.
- (24) Kuik, M.; Wetzelaer, G.-J. A. H.; Nicolai, H. T.; Craciun, N. I.; De Leeuw, D. M.; Blom, P. W. M. *Adv. Mater.* **2014**, *26* (4), 512.
- (25) Stork, M.; Gaylord, B. s.; Heeger, A. j.; Bazan, G. c. *Adv. Mater.* **2002**, *14* (5), 361.
- (26) Yang, R.; Wu, H.; Cao, Y.; Bazan, G. C. *J. Am. Chem. Soc.* **2006**, *128* (45), 14422.

## Chapter 4: Towards Green Solvent Processing of Organic Solar

### Cells

#### 4.1 Introduction

Organic Photovoltaics (OPVs) have received a large amount of interest due to the possibility of large area, low cost, light weight, and flexible devices. Thanks to development of novel narrow bandgap polymers and small molecules, as well as the use of solvent additives and temperature dependent processing for control over bulk heterojunction morphology, OPVs have seen a meteoric increase in power conversion efficiencies over the last few years.<sup>1-7</sup> Although these results are very promising, one issue relevant for consideration regarding the fabrication of OPVs has received relatively little attention, namely the toxicity and sustainability of processing solvents.<sup>8</sup>

Currently, all highly efficient devices are processed using halogenated solvents (e.g. chlorobenzene, chloroform dichlorobenzene) and halogenated solvent additives (e.g. diiodooctane, chloronappthalene). These solvents have varying levels of toxicities and carcinogenic properties, as well as readily contaminate ground water.<sup>9-14</sup> With this in mind, more environmentally benign solvents must be investigated in order to make OPV a more sustainable and environmentally friendly form of alternative energy.

A few groups have achieved good results using non-halogenated aromatics as processing solvents (e.g. xylenes, toluene, trimethylbenzene);<sup>15,16</sup> however, these solvents have well documented long term carcinogenic properties and at their core are not sustainable.<sup>17,18</sup> Griffin et al. have reported 6.6% efficiencies using binary a binary solvent blend containing no halogenated or aromatic solvents; however, the binary solvent system is acetone and CS<sub>2</sub>.<sup>19</sup> While the efficiencies are very promising, the processing blend uses CS<sub>2</sub>,

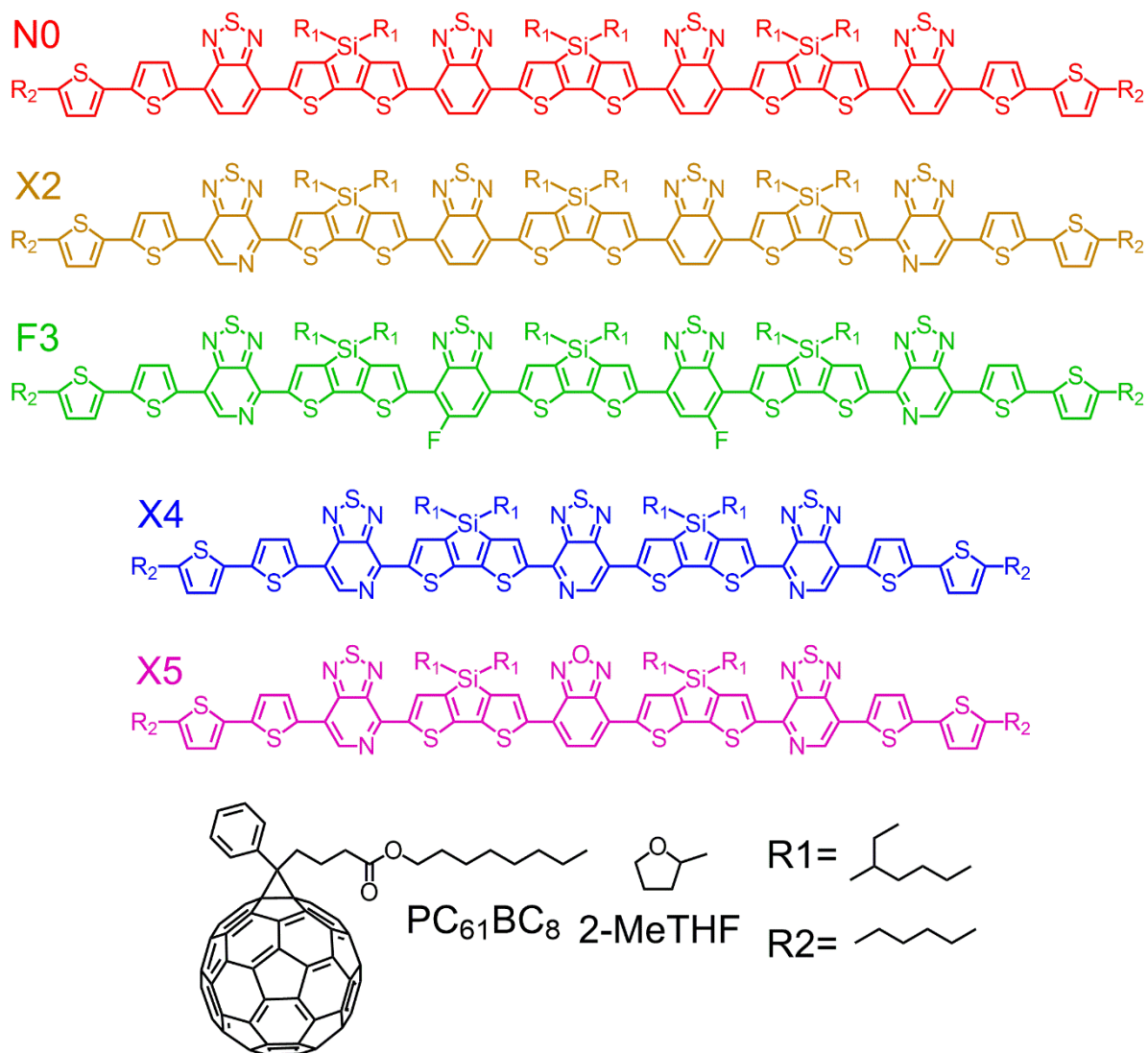


**Figure 4.1.** Chemical structures of molecular donors, acceptor and solvent used in the following investigation.

a chemical that is just as, or even more toxic than commonly used halogenated processing solvents,<sup>20</sup> and so is incompatible with a future goal of sustainability.

Recently, the use of 2-methyltetrahydrofuran (2-MeTHF) as a processing solvent for OPV active layers yielding efficient devices has been reported.<sup>21,22</sup> 2-MeTHF can be

synthesized from agricultural by-products, and has a much reduced toxicity when compared to commonly used halogenated and aromatic solvents.<sup>23-27</sup> These beneficial properties allow it to be classified as a green solvent.

From our previous studies it was apparent that switching from  $\text{CHCl}_3$  to 2-MeTHF had no negative impact on device performance and in fact led to a slight increase in PCE.<sup>21</sup> With the success that was obtained from the use of the extended chromophore molecular donor, **X2**, and fullerene derivative  $\text{PC}_{61}\text{BC}_8$ , it seemed reasonable to examine molecular donors that exhibit similar molecular and bulk properties to **X2** (see figure 4.1 for molecular structures).

The materials used in this study all exhibit relatively high thermal stabilities and crystallinities, as well as exceptional photovoltaic performance ranging from 5.5% to 7.4% when blended with PCBM without the use of solvent additives or thermal annealing.<sup>28-32</sup> Also worth noting is that while **X4**, and **X5** need thermal annealing when blended with PCBM to achieve optimal performance, **X2** and **F3** have no such requirement. Interestingly all materials do exhibit a decrease in PCE when blended with  $\text{PC}_{61}\text{BC}_8$  compared to the PCBM systems caused by a decrease in- short circuit current ( $J_{sc}$ ) and fill factor ( $FF$ ). This is likely due to the increased miscibility of the fullerene in the donor phase caused by the octyl ester chain in comparison to the methyl ester. This increase in fullerene miscibility is likely increasing the size of the “mixed phase” region. Recently, the development of a mixed phase, and fullerene miscibility in the donor phase have received a large amount of attention;<sup>33-36</sup> however, it has been stressed that if the fullerene is too miscible then the mixed region would become too large and the system would be subjected to more charge

carrier recombination.<sup>37-39</sup> This would mean that control over the fullerene and donor miscibility and phase purity would be crucial to achieve high performance.

## 4.2 Results and Discussion

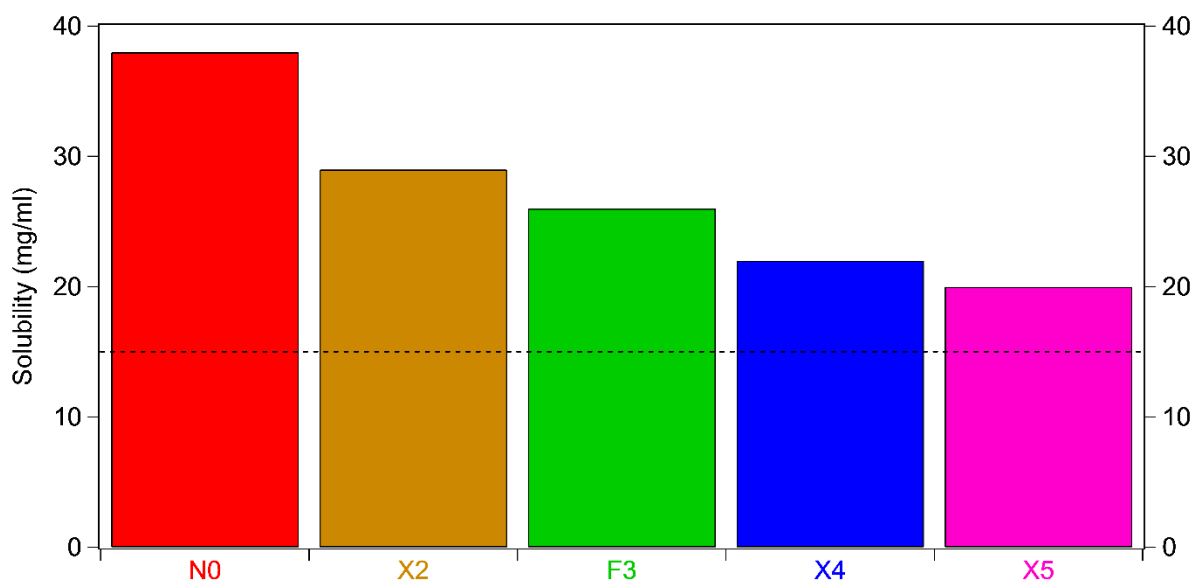


**Figure 4.2.** Solubility table of molecular donors used in the experiment. The dashed line at 15 mg/ml represents the minimum solubility for processing good films from 2-MeTHF

Initial solubility test indicates that all materials have solubility greater than 20 mg/mL in 2-MeTHF (figure 4.2), a necessity for obtaining thick active layers and high photocurrent. These materials also fall into a class of molecular semiconductors that exhibit an excellent performance tolerance to blend ratio.<sup>31</sup> Here we examine the applicability of 2-MeTHF as the processing solvent for an array of molecular semiconductor donors together with PC<sub>61</sub>BC<sub>8</sub> yielding a range of efficiencies from 3.6% to 5.6% with no solvent additives. The only exception is compound **X6** which was unable to form films from 2-MeTHF, despite having good solubility. BHJ devices for all materials were fabricated and characterized in Parallel to accurately investigate photovoltaic properties. A literature examination of the materials led us to process from a weight ratio of 1:1 (donor: acceptor) with a total solid concentration of 20 mg/ml.<sup>28</sup> Due to the large number of materials containing the acceptor

moiety, pyridylthiodiazole, the following device architecture was adopted, ITO/MoO<sub>x</sub>/active layer/Ca/Al, to avoid protonation of the slightly basic pyridyl nitrogen by acidic PEDOT:PSS.<sup>40</sup>

#### 4.2.1 Solar Cell Performance

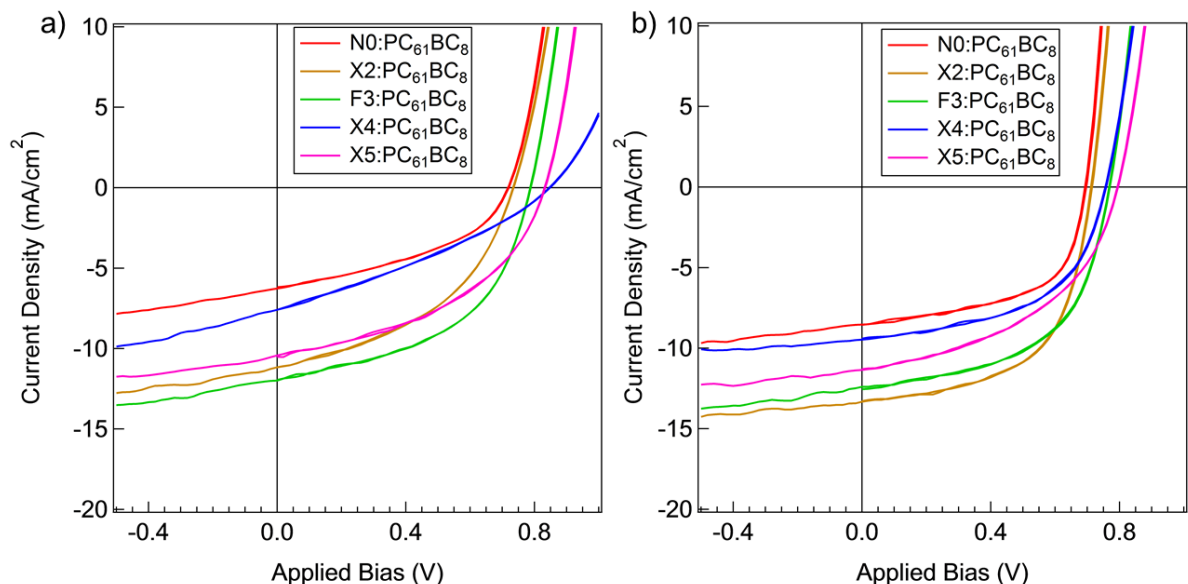


**Figure 4.3.** J-V curves for the highest performing a) as cast, and b) annealed devices under illumination.

Figure 4.3 shows the J-V scans for the as cast and annealed systems, and Table 4.1 summarizes relevant device characteristics for both the as cast and annealed systems. There is a noticeable increase in device performance for all the annealed systems over the as-cast counterparts. **N0** and **X4** show very similar performance increases from 1.6% to 3.4% and 1.9% to 3.3% after annealing respectively. **N0** and **X4** display an increase in  $J_{sc}$  and a substantial increase in  $FF$ . These improvements are offset by an open circuit voltage ( $V_{oc}$ ) decrease of ~20 mV for **N0** and a rather substantial ~70 mV decrease for **X4**. **X5** shows very

**Table 4.1.** Summarized J-V characteristics for the as cast and annealed devices

processed from 2-MeTHF.

Material	Condition	$J_{sc}$ (mA/cm <sup>2</sup> )	$V_{oc}$ (mV)	FF (%)	PCE (%)	
					Avg.	Best
N0	As Cast	5.6±0.7	720±5	39±2	1.6	1.9
	Annealed	8.3±0.3	700±5	58±1	3.4	3.6
X2	As Cast	9.6±1.1	730±10	43±3	3.0	3.6
	Annealed	12.7±0.5	710±5	59±2	5.3	5.5
F3	As Cast	11.3±0.5	780±10	51±4	4.5	4.9
	Annealed	11.9±0.5	770±5	57±2	5.3	5.6
X4	As Cast	6.9±0.3	830±20	31±1	1.8	2.0
	Annealed	8.6±0.4	760±10	52±4	3.3	3.8
X5	As Cast	9.8±0.3	830±5	45±1	3.7	3.8
	Annealed	10.5±0.4	790±5	47±1	3.9	4.2

little change in performance from 3.7% to 3.9% when subjected to thermal annealing, despite having a  $J_{sc}$  of ~10 mA/cm<sup>2</sup> the system suffers from a low  $FF$  (<50%). **F3** exhibits a slight performance improvement, 4.5% to 5.3%, when subjected to thermal annealing. Small improvements in  $J_{sc}$  and  $FF$  coupled with a very small, less than 10 mV, decrease in  $V_{oc}$  leads to a noticeable increase in device performance. **X2** shows the largest improvement after annealing, going from 3.0% to 5.3% with an increase in  $FF$  from 43% to 59% and a remarkable increase in  $J_{sc}$  from 9.6 mA/cm<sup>2</sup> to 12.7 mA/cm<sup>2</sup>. From the data it is apparent that the thermal annealing is driving phase separation and crystallization of the BHJ and donor phases respectively. This would explain the increase in fill factor as well as the increase in  $J_{sc}$ . When comparing these results to the what has been previously reported for

these donors when blended with PCBM, it is clear that these systems have a lower  $J_{sc}$ , and  $FF$ , but give a higher  $V_{oc}$ .

#### 4.2.2 Charge Carrier Mobility

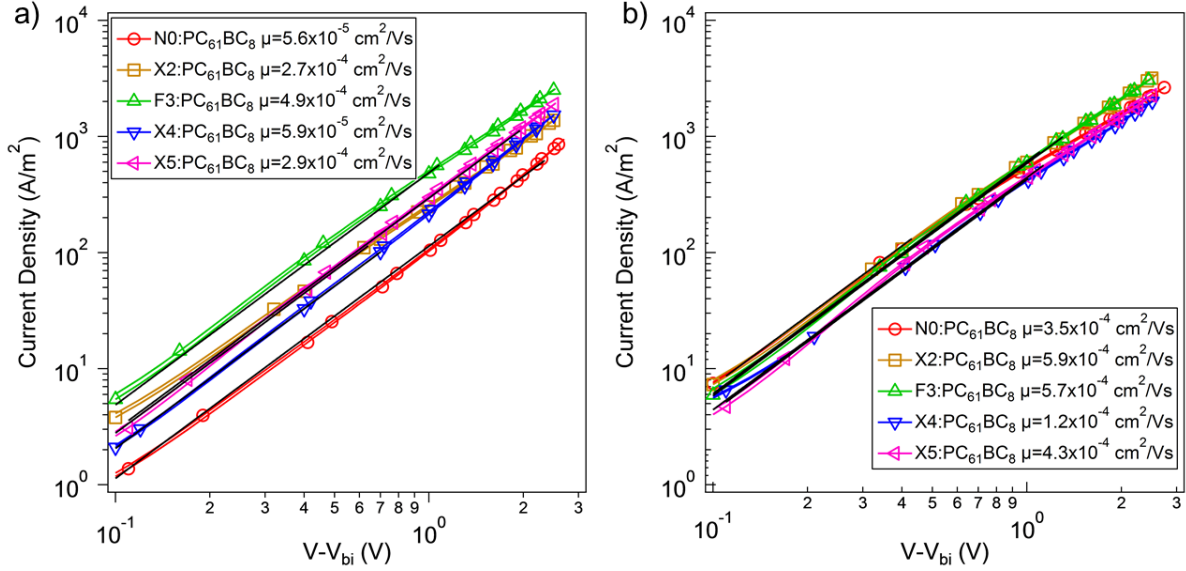


**Figure 4.4.** Single carrier diodes used to measure the SCLC hole mobilities for the a) as-cast and b) annealed systems processed from 2-MeTHF.

It is well established that higher and balanced charge carrier mobilities are required to obtain better fill factors,<sup>41–45</sup> highlighted in figure 4.5 b). To help understand the origin of the increase in fill factor after thermal annealing single carrier diodes were fabricated by adopting the architecture ITO/MoOx/Active Layer/Au to selectively inject and collect holes. Using the Mott-Gurney law for space charge limited current,<sup>46,47</sup> the hole mobilities were obtained for the as cast and annealed devices (figure 4.4). The difference in hole mobility between the as cast and the annealed devices is compared to the difference in as cast and annealed fill factors in Figure 4.5 b), and the relationship between hole mobility and fill factor is shown in figure 4.5 b). **N0**, **X2**, and **X4** all exhibit nearly an order of magnitude

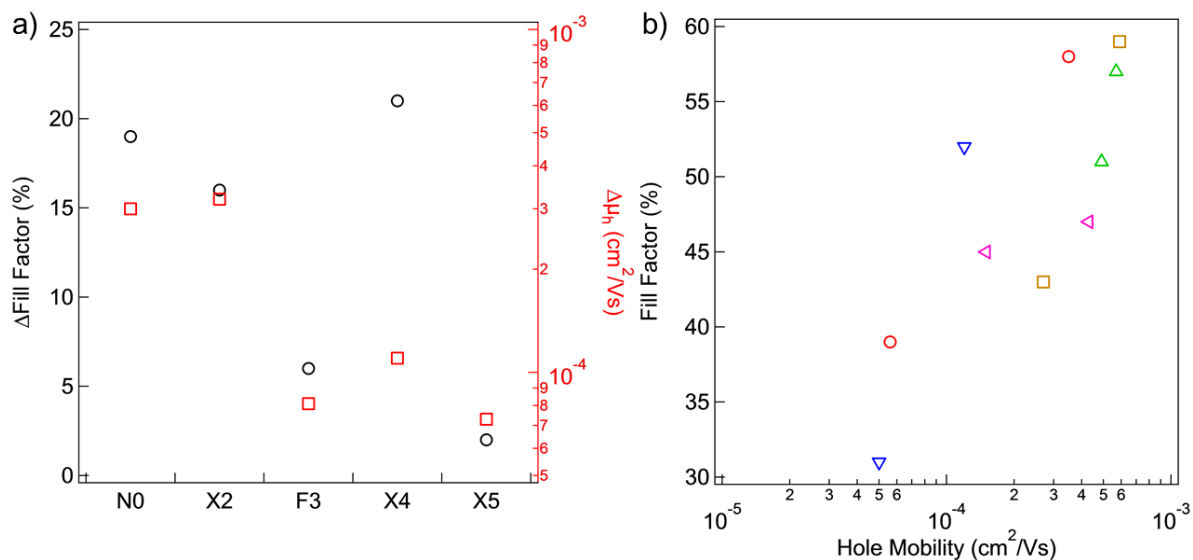


**Figure 4.5** a) Change in mobility between as cast and annealed devices compared to the change in fill factor for the as cast and annealed devices. b) plot highlighting the relationship between the hole mobility of the blend and the fill factor of the devices.

increase in hole mobility, but **X4** did not improve as much as the previous two. This is likely due to the lower annealed fill factor for **X4**, 52% compared to the 58% and 59% fill factors for **N0** and **X2** respectively. All these systems saw a greater than 15% increase in fill factor with **N0** increasing by 19%, **X2** increasing by 16% and **X4** increasing by 21%. **F3** and **X5** both exhibit essentially no increase in hole mobility and only a miniscule increase in fill factor, 6% for **F3** and 2% for **X5**. From these results it is quite clear that the increased fill factors for **N0** and **X2** are due to the development of more efficient charge transport pathways being formed caused by thermal annealing. The overall lack of change in charge transport for **F3** and **X5** is also in agreement with the minor increase in observed fill factor, meaning that these two molecules form efficient pathways for hole transport without any need of post treatment.

### 4.2.3 EQE and UV/Vis

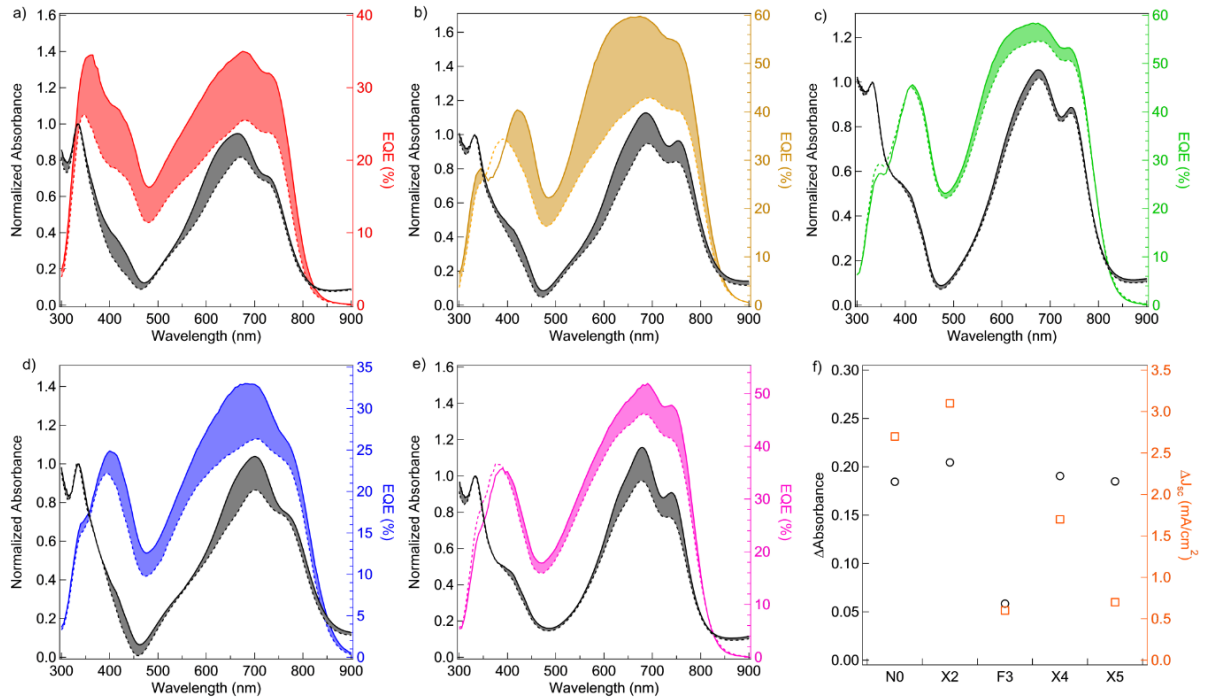


**Figure 4.6.** Absorbance (black) and EQE (colored) for the as cast and annealed devices processed from 2-MeTHF of a) N0:PC<sub>61</sub>BC<sub>8</sub>, b) X2:PC<sub>61</sub>BC<sub>8</sub>, c) F3:PC<sub>61</sub>BC<sub>8</sub>, d) X4:PC<sub>61</sub>BC<sub>8</sub>, and e) X5:PC<sub>61</sub>BC<sub>8</sub>. The difference between the as cast (dotted line) and annealed (solid line) absorbance and EQE is highlighted by the shaded area. A comparison between the difference in as cast and annealed absorption at  $\lambda_{\text{max}}$  and the measure  $J_{sc}$  is shown in f).

External quantum efficiency (EQE) of the as cast and annealed devices were measured and are plotted in color in Figure 4.6. **N0** and **X4** both exhibit very low EQE, not even reaching over 40% after annealing. **X2** shows, by far the most significant improvement in EQE with an as cast peak of less than 44% and an annealed peak of ~60%. **F3** and **X5** both show promising as cast EQE of ~54% and ~46% respectively, but after annealing both

showed very little improvement in EQE increasing to ~58% and ~52% respectively. This was what was observed in the J-V measurements and the hole mobility measurements.

With the observed increases in  $J_{sc}$  from both the J-V measurements and the EQE measurements, the question of is this increase in current a function of the better phase separation after annealing, or does the annealing also affect the absorption properties of the system? To probe this effect UV/Vis absorption was performed on each system and plotted in with black lines in Figure 4.6. When normalized to the  $\pi$ - $\pi^*$  transition (~330 nm) a significant increase in oscillator strength at the intramolecular charge transfer band was observed for **N0**, **X2**, **X4** and **X5**; however, **F3** exhibited very little increase in oscillator strength. Interestingly, **X5** exhibits a noticeable increase in oscillator strength, this is in contrast to the results observed in the solar cell performance studies and the hole mobility studies. A thermal response of this level implies significant reorganization of the donor phase and BHJ morphology. Furthermore, the apparent lack of any thermal sensitivity for **F3** supports the idea that this system creates more optimally organized as cast system, which has also been observed in the literature.<sup>28,48</sup>

Upon seeing the increase in absorption, EQE, and  $J_{sc}$  caused by thermal treatment, the question then arises, how much is the increased absorption leading to the increase in  $J_{sc}$ ? The difference in absorbance at  $\lambda_{max}$  between the as cast and annealed films was compared to the difference between as cast and annealed device  $J_{sc}$  in Figure 4.6 f). There appears to be good agreement with the observed changes in absorption and  $J_{sc}$  for all of the materials except **X5**. This could likely be attributed to the lack of increase in hole mobility, meaning that the optimal transport pathway for the material has already been achieved pre-annealing

but there is still further structural organization occurring and that leads to the increase in absorption.

#### 4.2.4 Probing the Structural Order

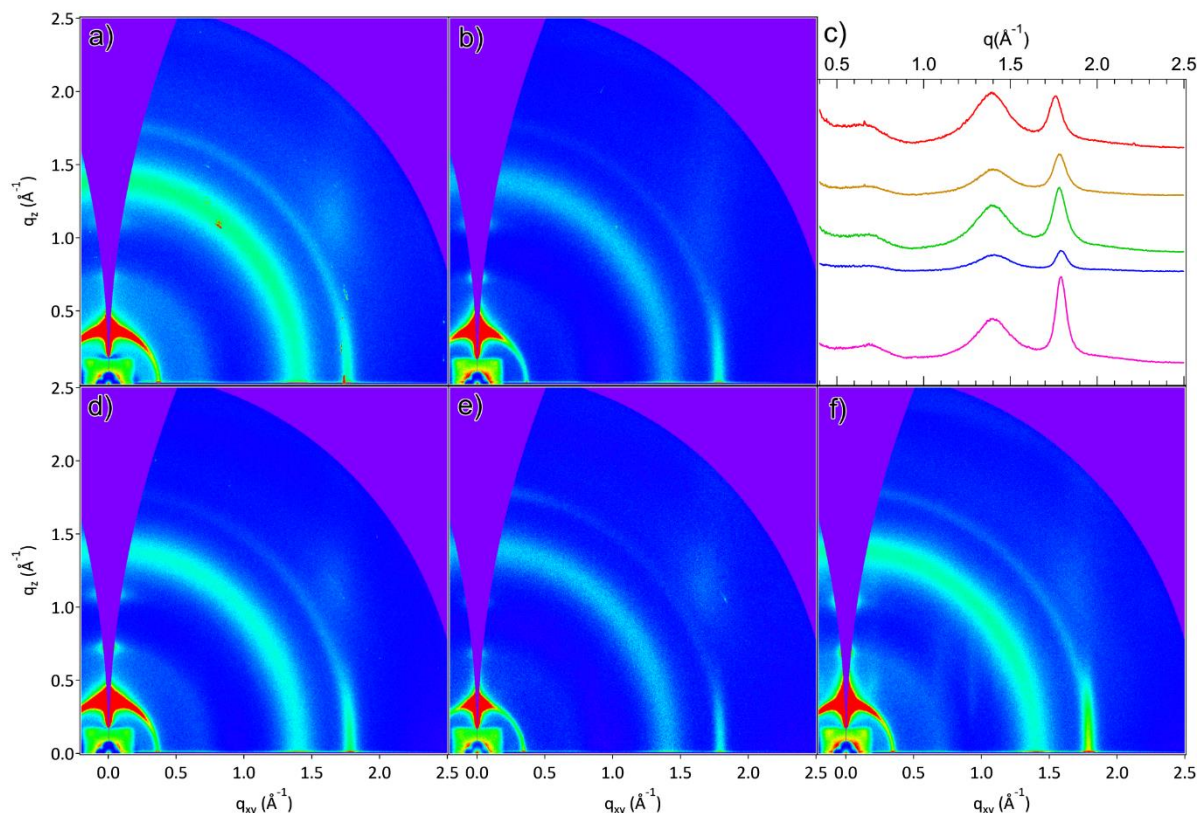


**Figure 4.7.** 2D GIWAXS plots for a) N0:PC<sub>61</sub>BC<sub>8</sub>, b) X2:PC<sub>61</sub>BC<sub>8</sub>, d) F3:PC<sub>61</sub>BC<sub>8</sub>, e) X4:PC<sub>61</sub>BC<sub>8</sub>, and f) X5:PC<sub>61</sub>BC<sub>8</sub>. c) shows the line cuts in the in plane direction highlighting the  $\pi$ - $\pi$ stacking peak for N0:PC<sub>61</sub>BC<sub>8</sub> (red) X2:PC<sub>61</sub>BC<sub>8</sub> (gold), F3:PC<sub>61</sub>BC<sub>8</sub> (green), X4:PC<sub>61</sub>BC<sub>8</sub> (blue), X4:PC<sub>61</sub>BC<sub>8</sub> (purple).

Despite AFM showing that the film quality is good when cast from green solvents, there is no way to quantify the difference in structural order between the as cast and annealed systems when using this measurement method. For measuring quantitative difference in

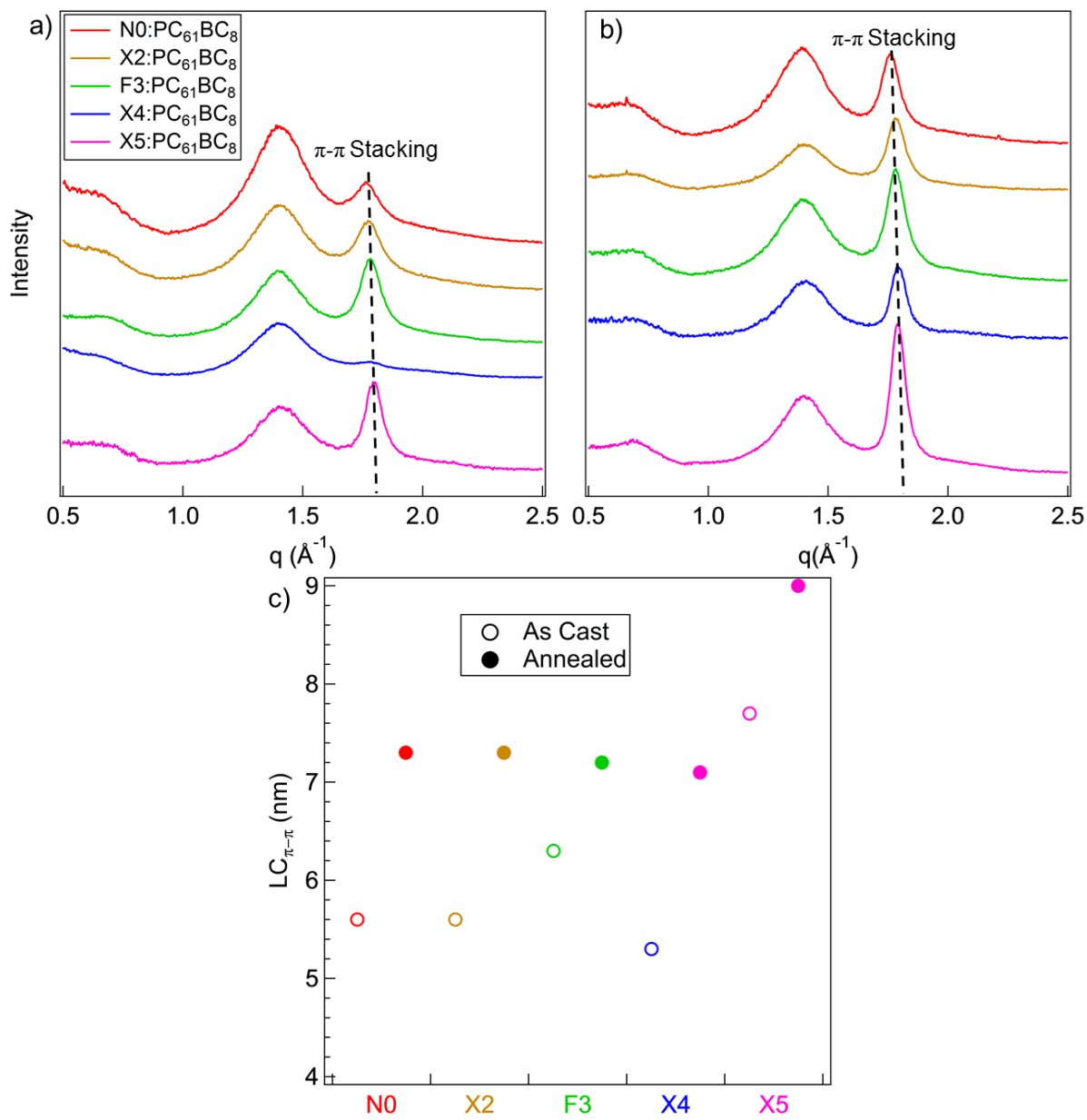


**Figure 4.8.** In-Plane line cuts of the 2D GIWAXS plots of a) as cast, and b) annealed devices, the dashed lines on the two plots indicate the location of the  $\pi$ - $\pi$  stacking peak. C) A summary of the  $\pi$ - $\pi$  crystalline correlations lengths calculated using the in plane line cuts. structural order grazing incidence wide angle X-ray scattering (GIWAXS) was used. The two dimensional GIWAXS plots for the annealed systems are shown in figure 4.7. From the scattering patterns all systems exhibit alky stacking in the out-of-plane direction and the  $\pi$ - $\pi$

stacking in the in-plane direction. There is very little difference in the  $\pi$ - $\pi$  spacing between as cast and annealed systems, 3.5 - 3.6 Å, but there is a huge difference in the crystalline correlation length (CCL) shown in figure 4.8. **N0** and **X2** have CCL of 5.6 nm for the as cast system, and both increase to 7.3 nm for their annealed systems. **X4** has a slightly smaller as cast CCL of 5.3 nm but nearly the same annealed CCL of 7.1 nm. **F3** has a much higher as cast CCL of 6.3 and after annealing sees a subsequent increase to 7.2 nm. **X5** has a 7.7nm as cast CCL, much greater than all other materials, and after annealing sees an increase to 9.0 nm. These observed really help explain everything that has been observed in previous measurements. **N0**, **X2**, and **X4** all exhibit a very large increase in the CCL when annealed. **F3** has a similar annealed CCL, but has a much higher as cast CCL when compared to the previous materials, which really helps to explain the lack of difference in all other measurements. **X5** has a large difference in CCL after annealing, but the as cast material is already so crystalline that the observed increase in crystallite quality and size had no major influence on the system. Most importantly, switching from chlorinated solvents to the green solvent 2-MeTHF does not inhibit crystallite formation.

#### 4.2.5 Surface Morphology

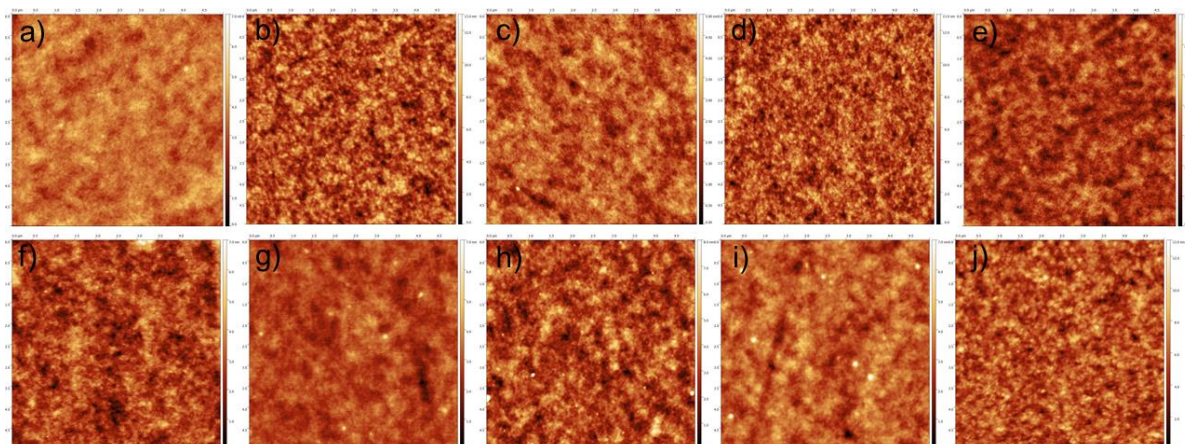


**Figure 4.7.** As cast AFM for a) N0:PC<sub>61</sub>BC<sub>8</sub>, c) X2:PC<sub>61</sub>BC<sub>8</sub>, e) F3:PC<sub>61</sub>BC<sub>8</sub>, g) X4:PC<sub>61</sub>BC<sub>8</sub>, and i) X5:PC<sub>61</sub>BC<sub>8</sub> devices processed from 2-MeTHF. Annealed AFM b) N0:PC<sub>61</sub>BC<sub>8</sub>, d) X2:PC<sub>61</sub>BC<sub>8</sub>, f) F3:PC<sub>61</sub>BC<sub>8</sub>, h) X4:PC<sub>61</sub>BC<sub>8</sub>, j) X5:PC<sub>61</sub>BC<sub>8</sub> devices processed from 2-MeTHF

In order to investigate the effect processing from green solvent as well as annealing the devices would have on the morphology, AFM was performed on the devices, figure 4.8. All films are extremely smooth, except for **X4** and **X5** most likely due to the lower solubility of these two materials in 2-MeTHF, with roughness ranging from 0.4 nm to 1.6 nm. The AFMs are reminiscent of other small molecule donor systems, showing that the processing from 2-MeTHF leads to no adverse effects on film quality. When looking at the features in the AFM it appears that annealing is inducing crystallization and phase separation. This becomes obvious when comparing the RMS roughness for each system. **N0** as cast has a roughness of 0.5 nm and after annealing roughness goes up to 1.6 nm. **X2**, similar to **N0**, has an as cast roughness of 0.5 nm and after annealing has a roughness of 1.4 nm. **F3** shows a very similar response to annealing in this study as it did to all previous studies having an as

cast roughness of 0.6 nm and an annealed roughness of 0.7 nm. **X4**, unlike in previous studies, also showed resilience to annealing with an as cast roughness of 0.5 nm and an annealed roughness of 0.9 nm. Following a similar trend as **X4**, **X5** also broke its previous trend of resistance to annealing and showed an increase in roughness from 0.6 nm, as cast, to 1.3 nm annealed. From looking at the AFMs it is quite apparent that the annealing has a substantial impact on the morphology, but processing from green solvent does not.

### 4.3 Conclusion

Throughout this study a few things have become clearer regarding processing from 2-MeTHF, and here we present a few notes to keep in mind when fabricating solar cells from a green solvent. Obviously solubility in desired green solvent is the most crucial characteristic, though is not the only necessity to make good films. **X6** exhibited a solubility in 2-MeTHF that was greater than 20 mg/ml, however was not able form films, despite considerable effort, when spin cast from 2-MeTHF. Many tricky processing methods currently exist such as solvent additives and heated substrates.<sup>1,2</sup> Due to the toxic nature of the solvent additives these are undesirable when processing from a green solvent, as it goes against the goal of sustainability, also the boiling point of 2-MeTHF is substantially lower than chlorobenzene, so heated substrates will possibly lead to problems with accelerated drying. This class of extended length donor material has shown have resistant morphology to blend ratio. This is possibly what has led to the ease of processing from 2-MeTHF that was observed for the systems.

We have shown that an array of molecular donors when blended with blended with the more soluble fullerene derivative, PC<sub>61</sub>BC<sub>8</sub>, can be processed from the green solvent, 2-MeTHF, yielding devices with power conversion efficiencies greater than 5.5%. These materials also avoid the use of toxic solvent additives such as 1, 8-diodooctane, and only require simple thermal annealing. The increased performance after annealing is attributed to the overall increase in structural order, which was confirmed by GIWAXS. This increase in structural order allowed for an increase in oscillator strength for the systems, as well as an increase in charge carrier mobility. The only system where thermal annealing did not lead to any significant increase in performance was **F3**. This is most likely due to a higher driving

force for phase separation caused by the fluorinated benzothiadiazole group in the molecule. The results show that a multitude of molecular donors of varying chemical structure and dimension can be processed from 2-MeTHF and further opens the door to mass produced, environmentally friendly, solution processed organic solar cells and other organic optoelectronic devices. It further highlights that 2-MeTHF can effectively function as a green solvent replacement for a variety of organic semiconductors in comparison to commonly used toxic halogenated and aromatic solvents.

#### 4.4 Experimental

*Materials:* N0, X2, F3, X4, and X5 were all synthesized according to the literature.<sup>28–30</sup> PC<sub>61</sub>BC<sub>8</sub> was purchased from Solenne BV company, Anhydrous 2-MeTHF was purchased from Sigma Aldrich. All Materials were used as received.

*Device Fabrication:* Solar cells devices were fabricated on cleaned, UV/ozone treated Corning 1737 glass patterned with 150 nm ITO. MoOx films (9 nm) were thermally evaporated on top of ITO substrates at a rate of 0.1 Å/s under vacuum below 10<sup>-6</sup> torr. The organic films were prepared from solutions with a total solids concentration of 20 mg/mL with D:A ratio of 50:50, wt/wt by spin-coating at 2000 rpm for 60 seconds. Samples that were thermally annealed were done so at 100 °C for 10 min then allowed to cool to room temperature for 10 minutes. Finally, cathodes were deposited by sequential thermal evaporation of calcium (~15 nm) followed by aluminum (~100 nm) through a shadow mask by thermal evaporation under a vacuum of about 3 x 10<sup>-7</sup> torr. An aperture with area of 0.045 cm<sup>2</sup> was used during the measurement. Device performances were tested using a Keithly 2602 system Source Meter under illumination by a simulated 100 mW cm<sup>-2</sup> AM 1.5G light source using a 300 W Xe arc lamp with an AM 1.5 global filter. Solar-simulator irradiance was calibrated using standard silicon photovoltaic with a protective KG1 filter calibrated by the National Renewable Energy Laboratory.

*UV/Vis Absorption Spectroscopy:* Absorption measurements were performed using a Beckman Coulter U800 UV/Vis spectrophotometer. Thin films were prepared by spin-coating on top of MoOx covered ITO substrates (same condition as device fabrication) at a spin speed of 2000 rpm.

*EQE Measurements:* External quantum efficiencies were measured using a 75 W Xe source, monochromator, optical chopper, lock-in amplifier, and a NIST calibrated silicon photodiode was used for power-density calibration.

*Hole Only Diode Measurements:* Hole only devices were fabricated on cleaned, UV/ozone treated Corning 1737 glass patterned with 140 nm Indium Tin Oxide. Molybdenum oxide (MoOx) was chosen as the bottom contact since it has a deeper work function, 5.5 eV, than the HOMO energy of all donors used. MoOx was thermally evaporated as a bottom contact at a rate of 0.2 Å/s with a thickness of 9 nm. The active layer was spin cast at 2000 rpm for 60 seconds at a 5:5 blend ratio with a total concentration of 20 mg/ml. In order to sufficiently reduce electron injection, gold top contacts were thermally evaporated at 0.2 Å/s with a final thickness of approximately 50 nm. Since the work function of gold, 5.1 eV, is deeper than the LUMO of PC<sub>61</sub>BC<sub>8</sub>, 4.2 eV, there will be non-ohmic electron injection yielding electron current several orders of magnitude lower than the hole current. Devices were measured in the dark using a Keithly 2602 system Source Meter and the Mott-Gurney law for the space-charge-limited-current (SCLC)<sup>46,47</sup> was used to determine the zero field mobility of the layer according to the following equation:

$$J = \frac{9}{8} \epsilon \epsilon_0 \mu \frac{V^2}{L^3}$$

where  $\epsilon$  is the material's dielectric constant,  $\epsilon_0$  is the permittivity of vacuum,  $V$  is the applied bias,  $L$  is the film thickness,  $J$  is the measured current density and  $\mu$  is the charge carrier mobility of the material.

*GIWAXS Measurements:* GIWAXS patterns were collected at the Stanford Synchrotron Radiation Lightsource (SSRL) beamline 11-3 with an X-ray wavelength of 0.9752 Å, at a 40 cm sample detector distance at an incident angle of 0.12°. Samples were

probed under a helium environment to minimize beam damage and reduce diffuse scattering. The measurements were calibrated using a LaB<sub>6</sub> standard. The crystalline correlation length (CCL) values, which provide an estimation of crystallite size and quality, were calculated using the Scherrer equation.

## 4.5 References

- (1) Liu, Y.; Zhao, J.; Li, Z.; Mu, C.; Ma, W.; Hu, H.; Jiang, K.; Lin, H.; Ade, H.; Yan, H. *Nat. Commun.* **2014**, *5*, 5293.
- (2) Peet, J.; Kim, J. Y.; Coates, N. E.; Ma, W. L.; Moses, D.; Heeger, A. J.; Bazan, G. C. *Nat. Mater.* **2007**, *6* (7), 497.
- (3) You, J.; Dou, L.; Yoshimura, K.; Kato, T.; Ohya, K.; Moriarty, T.; Emery, K.; Chen, C.-C.; Gao, J.; Li, G.; Yang, Y. *Nat. Commun.* **2013**, *4*, 1446.
- (4) van der Poll, T. S.; Love, J. A.; Nguyen, T.-Q.; Bazan, G. C. *Adv. Mater.* **2012**, *24* (27), 3646.
- (5) Zhang, Q.; Kan, B.; Liu, F.; Long, G.; Wan, X.; Chen, X.; Zuo, Y.; Ni, W.; Zhang, H.; Li, M.; Hu, Z.; Huang, F.; Cao, Y.; Liang, Z.; Zhang, M.; Russell, T. P.; Chen, Y. *Nat. Photonics* **2014**, advance online publication.
- (6) van Franeker, J. J.; Heintges, G. H. L.; Schaefer, C.; Portale, G.; Li, W.; Wienk, M. M.; van der Schoot, P.; Janssen, R. A. J. *J. Am. Chem. Soc.* **2015**, *137* (36), 11783.
- (7) He, Z.; Xiao, B.; Liu, F.; Wu, H.; Yang, Y.; Xiao, S.; Wang, C.; Russell, T. P.; Cao, Y. *Nat. Photonics* **2015**, *9* (3), 174.
- (8) Duan, C.; Cai, W.; Hsu, B. B. Y.; Zhong, C.; Zhang, K.; Liu, C.; Hu, Z.; Huang, F.; Bazan, G. C.; Heeger, A. J.; Cao, Y. *Energy Environ. Sci.* **2013**, *6* (10), 3022.
- (9) Calamari, D.; Galassi, S.; Setti, F.; Vighi, M. *Chemosphere* **1983**, *12* (2), 253.
- (10) Clemens, T. L.; Hill, R. N.; Bullock, L. P.; Dean Johnson, W.; Sultatos, L. G.; Vesell, E. S. *Toxicol. Appl. Pharmacol.* **1979**, *48* (1, Part 1), 117.
- (11) Heitmuller, P. T.; Hollister, T. A.; Parrish, P. R. *Bull. Environ. Contam. Toxicol.* **1981**, *27* (1), 596.
- (12) MD, R. D. K. *Arch. Environ. Health Int. J.* **1972**, *25* (2), 125.
- (13) Sullivan, T. M.; Born, C. S.; Carlson, G. P.; Kessler, W. V. *Toxicol. Appl. Pharmacol.* **1983**, *71* (2), 194.
- (14) Van Hoogen, G.; Opperhuizen, A. *Environ. Toxicol. Chem.* **1988**, *7* (3), 213.
- (15) Sprau, C.; Buss, F.; Wagner, M.; Landerer, D.; Koppitz, M.; Schulz, A.; Bahro, D.; Schabel, W.; Scharfer, P.; Colsmann, A. *Energy Environ. Sci.* **2015**.
- (16) Susanna, G.; Salamandra, L.; Ciceroni, C.; Mura, F.; Brown, T. M.; Reale, A.; Rossi, M.; Di Carlo, A.; Brunetti, F. *Sol. Energy Mater. Sol. Cells* **2015**, *134*, 194.
- (17) Aj, M. *IARC Sci. Publ.* **1987**, No. 85, 3.

- (18) Langman, J. M. *Pathology (Phila.)* **1994**, 26 (3), 301.
- (19) Griffin, J.; Pearson, A. J.; Scarratt, N. W.; Wang, T.; Dunbar, A. D. F.; Yi, H.; Iraqi, A.; Buckley, A. R.; Lidzey, D. G. *Org. Electron.* **2015**, 21, 216.
- (20) Davidson, M.; Feinleib, M. *Am. Heart J.* **1972**, 83 (1), 100.
- (21) Chen, X.; Liu, X.; Burgers, M. A.; Huang, Y.; Bazan, G. C. *Angew. Chem. Int. Ed.* **2014**, 53 (52), 14378.
- (22) Chen, Y.; Cui, Y.; Zhang, S.; Hou, J. *Polym. Chem.* **2015**, 6 (22), 4089.
- (23) Pace, V.; Hoyos, P.; Castoldi, L.; Domínguez de María, P.; Alcántara, A. R. *ChemSusChem* **2012**, 5 (8), 1369.
- (24) Clark, J. H.; Pfaltzgraff, L. A.; Budarin, V. L.; Hunt, A. J.; Gronnow, M.; Matharu, A. S.; Macquarrie, D. J.; Sherwood, J. R. *Pure Appl. Chem.* **2013**, 85 (8), 1625.
- (25) Sherman, J.; Chin, B.; Huibers, P. D. T.; Garcia-Valls, R.; Hatton, T. A. *Environ. Health Perspect.* **1998**, 106, 253.
- (26) Antonucci, V.; Coleman, J.; Ferry, J. B.; Johnson, N.; Mathe, M.; Scott, J. P.; Xu, J. *Org. Process Res. Dev.* **2011**, 15 (4), 939.
- (27) Gu, Y.; Jérôme, F. *Chem. Soc. Rev.* **2013**, 42 (24), 9550.
- (28) Liu, X.; Sun, Y.; Hsu, B. B. Y.; Lorbach, A.; Qi, L.; Heeger, A. J.; Bazan, G. C. *J. Am. Chem. Soc.* **2014**, 136 (15), 5697.
- (29) Liu, X.; Sun, Y.; Perez, L. A.; Wen, W.; Toney, M. F.; Heeger, A. J.; Bazan, G. C. *J. Am. Chem. Soc.* **2012**, 134 (51), 20609.
- (30) Liu, X.; Burgers, M. A.; Hsu, B. B. Y.; Coughlin, J. E.; Perez, L. A.; Heeger, A. J.; Bazan, G. C. *RSC Adv.* **2015**, 5 (108), 89144.
- (31) Huang, Y.; Liu, X.; Wang, C.; Rogers, J. T.; Su, G. M.; Chabiny, M. L.; Kramer, E. J.; Bazan, G. C. *Adv. Energy Mater.* **2014**, 4 (10), n/a.
- (32) Abdelsamie, M.; Treat, N. D.; Zhao, K.; McDowell, C.; Burgers, M. A.; Li, R.; Smilgies, D.-M.; Stingelin, N.; Bazan, G. C.; Amassian, A. *Adv. Mater.* **2015**, n/a.
- (33) Treat, N. D.; Brady, M. A.; Smith, G.; Toney, M. F.; Kramer, E. J.; Hawker, C. J.; Chabiny, M. L. *Adv. Energy Mater.* **2011**, 1 (1), 82.
- (34) Treat, N. D.; Varotto, A.; Takacs, C. J.; Batara, N.; Al-Hashimi, M.; Heeney, M. J.; Heeger, A. J.; Wudl, F.; Hawker, C. J.; Chabiny, M. L. *J. Am. Chem. Soc.* **2012**, 134 (38), 15869.

- (35) Treat, N. D.; Mates, T. E.; Hawker, C. J.; Kramer, E. J.; Chabynyc, M. L. *Macromolecules* **2013**, *46* (3), 1002.
- (36) Bartelt, J. A.; Beiley, Z. M.; Hoke, E. T.; Mateker, W. R.; Douglas, J. D.; Collins, B. A.; Tumbleston, J. R.; Graham, K. R.; Amassian, A.; Ade, H.; Fréchet, J. M. J.; Toney, M. F.; McGehee, M. D. *Adv. Energy Mater.* **2013**, *3* (3), 364.
- (37) Li, M.; Liu, F.; Wan, X.; Ni, W.; Kan, B.; Feng, H.; Zhang, Q.; Yang, X.; Wang, Y.; Zhang, Y.; Shen, Y.; Russell, T. P.; Chen, Y. *Adv. Mater.* **2015**, n/a.
- (38) Ma, W.; Tumbleston, J. R.; Ye, L.; Wang, C.; Hou, J.; Ade, H. *Adv. Mater.* **2014**, n/a.
- (39) Mukherjee, S.; Proctor, C. M.; Tumbleston, J. R.; Bazan, G. C.; Nguyen, T.-Q.; Ade, H. *Adv. Mater.* **2014**, n/a.
- (40) Garcia, A.; Welch, G. C.; Ratcliff, E. L.; Ginley, D. S.; Bazan, G. C.; Olson, D. C. *Adv. Mater.* **2012**, *24* (39), 5368.
- (41) Bartelt, J. A.; Lam, D.; Burke, T. M.; Sweetnam, S. M.; McGehee, M. D. *Adv. Energy Mater.* **2015**, n/a.
- (42) Love, J. A.; Nagao, I.; Huang, Y.; Kuik, M.; Gupta, V.; Takacs, C. J.; Coughlin, J. E.; Qi, L.; van der Poll, T. S.; Kramer, E. J.; Heeger, A. J.; Nguyen, T.-Q.; Bazan, G. C. *J. Am. Chem. Soc.* **2014**, *136* (9), 3597.
- (43) Mihailetchi, V. D.; Wildeman, J.; Blom, P. W. M. *Phys. Rev. Lett.* **2005**, *94* (12), 126602.
- (44) Di Nuzzo, D.; van Reenen, S.; Janssen, R. A. J.; Kemerink, M.; Meskers, S. C. J. *Phys. Rev. B* **2013**, *87* (8), 85207.
- (45) Proctor, C. M.; Love, J. A.; Nguyen, T.-Q. *Adv. Mater.* **2014**, *26* (34), 5957.
- (46) Kuik, M.; Wetzelaer, G.-J. A. H.; Nicolai, H. T.; Craciun, N. I.; De Leeuw, D. M.; Blom, P. W. M. *Adv. Mater.* **2014**, *26* (4), 512.
- (47) Coropceanu, V.; Cornil, J.; da Silva Filho, D. A.; Olivier, Y.; Silbey, R.; Brédas, J.-L. *Chem. Rev.* **2007**, *107* (4), 926.
- (48) Liu, X.; Hsu, B. B. Y.; Sun, Y.; Mai, C.-K.; Heeger, A. J.; Bazan, G. C. *J. Am. Chem. Soc.* **2014**, *136* (46), 16144.

## **Chapter 5: High Efficiency Non-Fullerene Based Small Molecule Organic Solar Cells Processed from Green Solvents**

### **5.1 Introduction**

Organic photovoltaics (OPVs) have been extensively studied for the past 20 years, with significant attention going towards the development of novel photoactive polymers and small molecules.<sup>1-3</sup> The majority of material design was focused on the development of high performance donor materials to be matched with fullerene based electron acceptors and recently achieving efficiencies greater than 10%.<sup>3-5</sup> Despite the wide variety of electron donor materials, the field of high performance electron acceptor materials has been dominated by fullerene derivatives such as PCBM.

This domination by fullerenes is thanks to their highly favorable electron acceptor properties such as their high electron mobility, three-dimensional electron accepting and transporting properties thanks to the LUMO being delocalized across the whole molecule, and three stable/reversible electrochemical reductions.<sup>6</sup> Despite these highly favorable electron accepting properties, fullerenes do have their limitations. These limitations include costly synthesis, difficult purification, little to no absorption in the UV/Vis spectrum severely limiting their contribution to photocurrent, also limiting the tunability of their absorption, and energy levels. With these limitations of fullerenes, research has shifted towards the development of non-fullerene based electron acceptors, such as perylene diimides, or other fused ring systems receiving the most attention.<sup>7-11</sup> Another class of non-fullerene acceptor (NFA) that has begun to receive more attention recently are calamitic molecules, which utilize the push-pull chromophore design strategy from the development of narrow bandgap donor materials.<sup>12</sup> This modular design strategy affords greater synthetic

flexibility, and more control over the optical and electronic properties of the molecule, and has seen a fair amount of success.<sup>13-18</sup> Despite all of these great improvements in the development of donors and NFAs, one major aspect has been overlooked, the toxicity and environmental impact of the processing solvents used in device fabrication.

The vast majority of solar cells being reported in the literature use highly toxic halogenated solvents (e.g. chlorobenzene, chloroform, dichlorobenzene) and require the use of halogenated high boiling point solvent additives (e.g. diiodooctane, chloronaphthalene). These solvents have rather well documented toxicities and carcinogenic properties, as well as the synthesis of these solvents requires the use of toxic halogen gasses, and dangerous byproducts (HCl). With this in mind, more environmentally benign solvents must be investigated to form a more sustainable and environmentally friendly future for the OPV field.

A few groups have begun to investigate the use of non-halogenated solvents such as xylenes, toluene and trimethylbenzene.<sup>19,20</sup> While these results are a good step in the right direction they still utilize highly carcinogenic solvents that are unsustainable.<sup>21,22</sup> The question must be asked; what solvent would fall under a sustainable solvent? Well the solvent in question must be an environmentally friendly solvent or biosolvent, it must have a low toxicity and have no carcinogenic properties, degrade to a naturally occurring or reusable product, and most importantly it must be obtained from a renewable resource, such as agricultural waste.<sup>23,24</sup> 2-methyltetrahydrofuran is such a solvent, being synthesized from agricultural by-products, and has a much reduced toxicity when compared to commonly used halogenated and aromatic solvents.<sup>23-28</sup> These environmentally friendly properties of 2-MeTHF allow it to be classified as a green solvent. The use of the green solvent, 2-MeTHF,

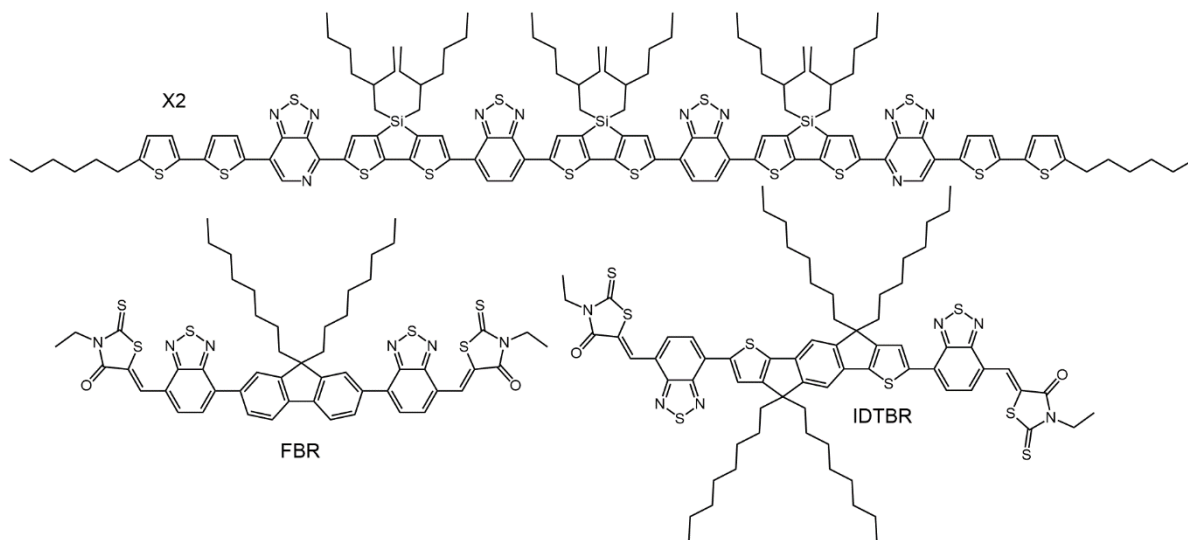


**Figure 5.1.** Chemical structures of the donor and non-fullerene acceptors used in this investigation.

for processing of OPV active layers resulting in efficient devices has been reported in the literature.<sup>29,30</sup>

From our previous studies, it was apparent that there was no negative impact on morphology and performance when switching from  $\text{CHCl}_3$  to 2-MeTHF.<sup>29</sup> With the substantial amount of success that was achieved using a series of extended molecular length donors, it seemed reasonable to examine one of these donors in the context of a non-fullerene acceptor. Of these extended chromophores, **X2** has received the most attention for its blend ratio tolerant morphology,<sup>31</sup> its simple processing conditions to achieve high performances,<sup>32,33</sup> high thermal stability,<sup>34</sup> and well documented self-assembly.<sup>35,36</sup> When determining the best non-fullerene acceptor to match with **X2**, the modular nature of calamitic molecules came to mind, and in this class of molecules, **FBR** and **IDTBR** have some interesting properties that would match nicely with **X2** (Figure 5.1).<sup>13,37</sup>

## 5.2 Results and Discussion

### 5.2.1 UV/Vis & Energy Levels

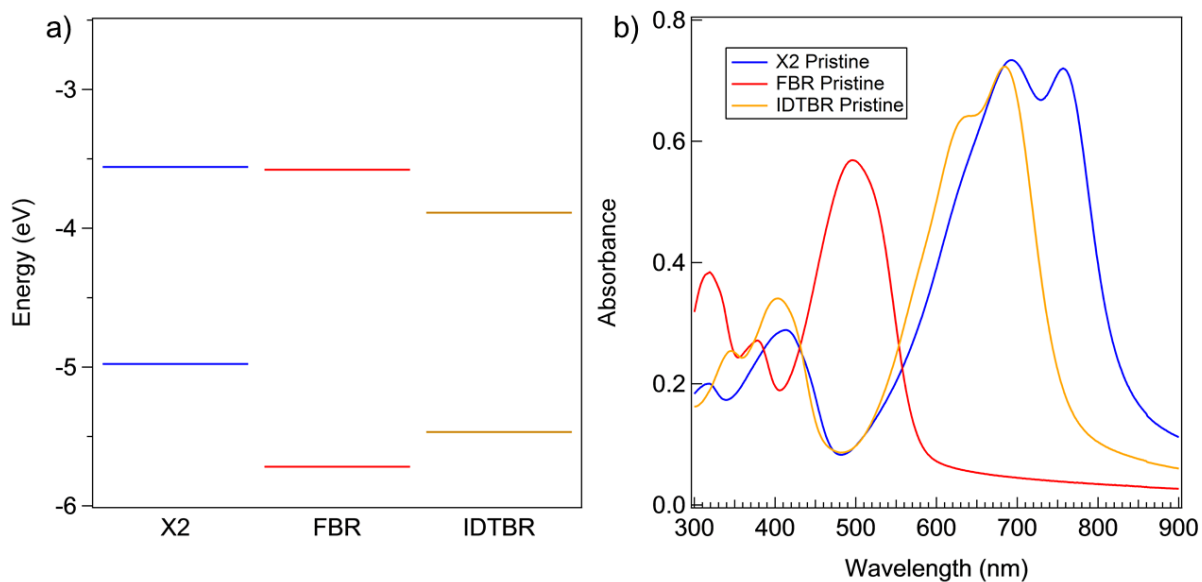


**Figure 5.2.** a) energy levels, and b) pristine film UV/Vis absorption for **X2**, **FBR**, and

### **IDTBR**

**FBR** and **IDTBR** have quite favorable optical and electronic properties when compared to **X2** (figure 5.2). **FBR** has good complimentary optical absorption compared to **X2**, leading to a larger range of the visible spectrum will be absorbed. The LUMO-LUMO offset between the two materials is quite small though, possibly leading to lower driving force for charge separation reducing the number of photogenerated charges. Unlike **FBR**, **IDTBR** has overlapping absorption with **X2**, possibly causing competing absorption events; however, there is a much more significant LUMO-LUMO offset meaning a greater driving force for charge separation. The presence of the shoulder peak in the **IDTBR** absorption at ~700 nm is also indicative of a more crystalline compound possibly leading to a greater

degree of phase separation reducing recombination and possibly leading to a more optimal morphology.

### 5.2.2 Device Performances

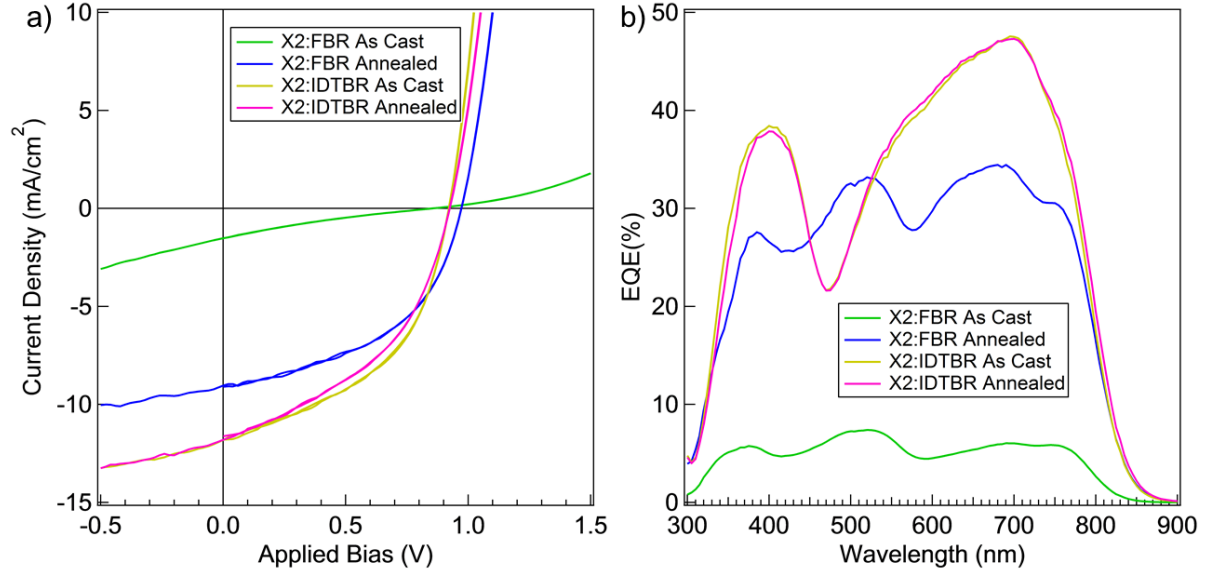


**Figure 5.3.** a) JV characteristics and b) EQE spectra for as cast and annealed devices of **X2:FBR** and **X2:IDTBR**.

Figure 5.3 shows both the as cast and annealed JV characteristics, and EQE measurements for **X2:FBR** and **X2:IDTBR**, and table 5.1 summarize the device parameters. The **X2:FBR** system when tested as cast shows essentially no photovoltaic response, but after thermal annealing the  $J_{sc}$  has a drastic increase by nearly 5 times the as cast condition, and the fill factor also sees an impressive increase of nearly 50%. Even the  $V_{oc}$  had an increase of greater than 100 mV, yielding an overall 10 times performance increase, from 0.4% to 4.3%. It is worth mentioning that the EQE is nearly level across the entire visible spectrum, and shows a significant improvement after thermal annealing as well. This is likely due to a lack of structural order, or phase separation before thermal annealing, and

**Table 5.1.** Summarized device parameters for the as cast and annealed conditions of **X2:FBR**, and **X2:IDTBR**.

<b>Acceptor</b>	$J_{sc}$ (mA/cm <sup>2</sup> )	$V_{oc}$ (mV)	<i>FF</i> (%)	<b>PCE (%)</b> Avg. Best	
FBR As Cast	1.7±0.3	860±20	20±1	0.3	0.4
FBR Annealed	8.9±0.3	980±10	48±1	4.1	4.3
IDTBR As Cast	12.0±0.7	920±10	48±1	5.3	5.6
IDTBR Annealed	11.7±0.7	930±10	47±1	5.0	5.3

after thermal annealing the two phases crystallize driving phase separation. There is also a likely chance that the low LUMO-LUMO offset is in fact preventing charge separation. The **IDTBR** system is a very different story, thanks to the improved crystallinity afforded by the indacenodithiophene core, the most optimal condition for the **X2:IDTBR** blend is the as cast condition barely out performing the annealed system. When comparing the **FBR** system to the **IDTBR** system, it is apparent that the **IDTBR** has a much higher  $J_{sc}$ , greater than 3 mA/cm<sup>2</sup>, despite having competitive absorption events. When comparing the JV characteristics in the dark, it is apparent that there is a significant difference between the as cast **X2:FBR** devices and all other devices by nearly an order of magnitude. The current density here is related to the double carrier mobility in the device, which is related to the non-geminate recombination in the device.<sup>38</sup> This could be cause by the improved LUMO-LUMO offset, giving a much higher driving force for charge separation, or by the more optical morphology that is formed allowing for reduced recombination.

### 5.2.3 Blend UV/Vis & Photoluminescence Quenching

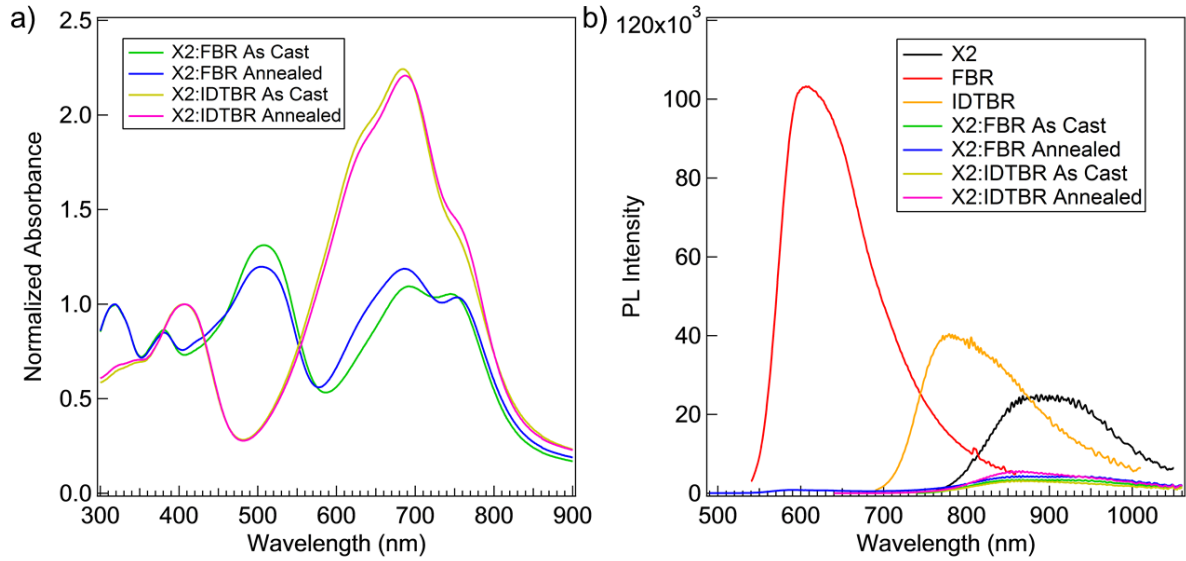


**Figure 5.4.** a) UV/Vis absorption for the as cast and annealed **X2:FBR**, and **X2:IDTBR** films. b) photoluminescence measurements of the pristine and blend as cast and annealed films.

The absorption profile for the as cast and annealed blends were measured using UV/Vis absorption. The **X2:FBR** blend shows good absorption across the whole spectrum in agreement with the EQE measurements. Interestingly, the **FBR** oscillator strength decreases after thermal annealing, which is not expected; however, the **X2** oscillator strength increases bringing their absorption peaks essentially equal. It is worth noting that the as cast films exhibit a reddish color, while the annealed films are black. The **X2:IDTBR** films exhibit very strong absorption near 700 nm which is to expected since both materials exhibited similar  $\lambda_{\max}$  in that region. Similarly to the **X2:FBR** blend, it appears that the **IDTBR** contribution decreases after thermal annealing, and the **X2** contribution has a slight increase.

To investigate the degree of electron transfer between **X2** and the two acceptors the photoluminescence of the pristine films were compared to the as cast and annealed blend films (figure 5.4b). It appears that there is efficient driving force for electron transfer between the **X2** and the **FBR**, ruling that out as the cause of the reduce  $J_{sc}$  relative to the **IDTBR** system. It is worth mentioning that the highest and lowest degree of quenching measured was from the **X2:IDTBR** as cast and annealed films, respectively.

### 5.2.4 Structural Order Effects

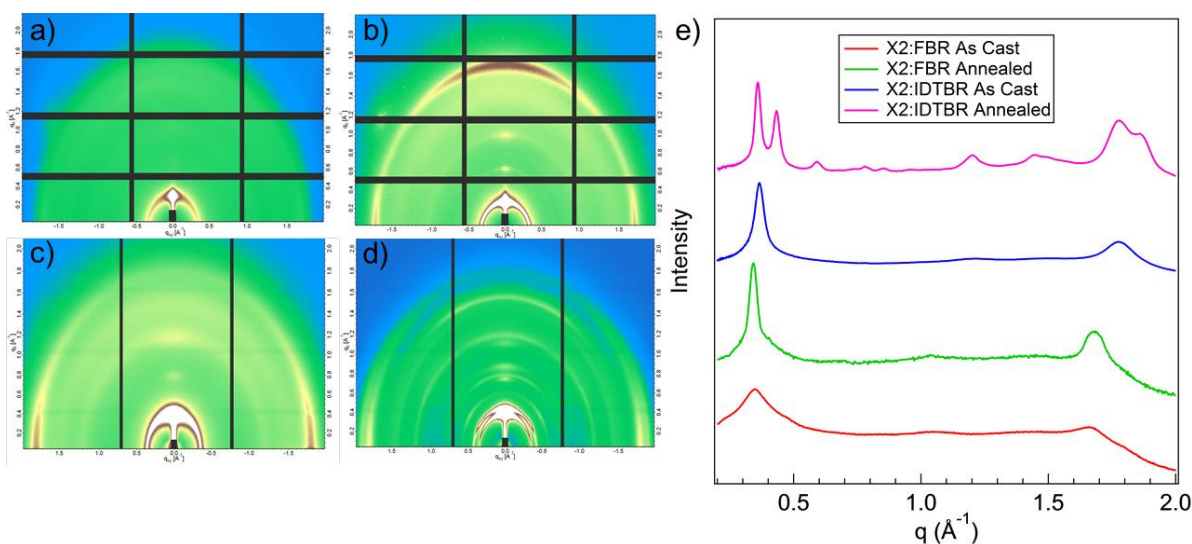


**Figure 5.5.** 2-D GIWAXS plots for the **X2:FBR** a) as cast, and b) annealed films, and for the **X2:IDTBR** c) as cast, and d) annealed films. e) in-plane line cuts for the shown 2-D GIWAXS to further probe the  $\pi$ - $\pi$  stacking.

After thermal annealing there is a significant improvement in the **X2:FBR** system, while the **X2:IDTBR** system has little change after thermal annealing. The lack of planarity in the **FBR** molecule reduces the crystallinity when cast and in fact could be inhibiting the crystallization of the **X2**. In contrast, the highly planar indacenodithiophene core in **IDTBR** leads to a much higher crystallinity, increasing the molecules propensity to phase separate

and form well-ordered domains. To probe the structural order of the different materials, and how the processing conditions impact their morphology, GIWAXS was performed (Figure 5.5). From the 2-D GIWAXS plots, it appears that the FBR is in fact inhibiting the crystallization of the **X2**, and this is further confirmed by the line cuts in the in-plane direction. Before annealing, the crystalline correlation length (CCL) for the as cast **X2:FBR** system was 4.7 nm, but after annealing increased to 7.1 nm. This confirms that the presence of the **FBR** does in fact inhibit the crystallization of **X2** significantly impacting the initial degree of phase separation, and presence of efficient transport domains. Conversely, the **IDTBR** has very little impact on the crystallization of **X2** yielding an as cast CCL of 6.3 nm, and after thermal annealing increasing to 8.2 nm. After thermal annealing, the presence of **IDTBR**  $\pi$ - $\pi$  stacking peak can actually be resolved in the in-plane line cuts. It has been well established that the presence of mixed domains is important for good performance in OPVs,<sup>39</sup> and it is possible that the thermal annealing of the **X2:IDTBR** system reduced the size of the mixed phase too much.

### 5.2.5 Charge Carrier Mobility

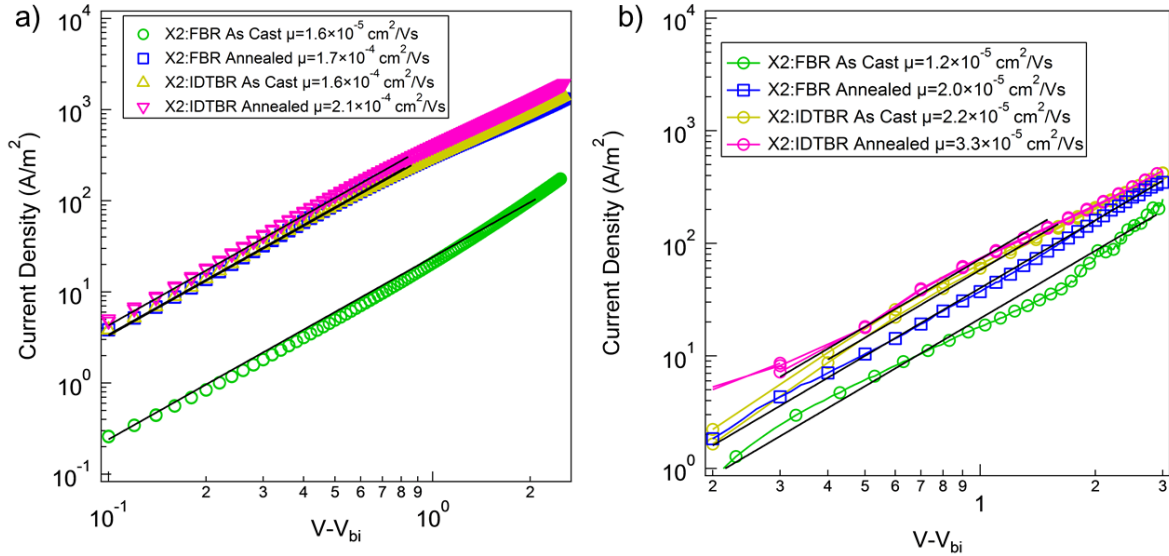


**Figure 5.6.** a) hole mobility, and b) electron mobility measurements for as cast and annealed **X2:FBR**, and **X2:IDTBR** obtained by SCLC diode measurements. Mobility values are summarized in the legends.

If the **FBR** is in fact inhibiting the crystallization of the **X2**, then the development of efficient charge transport pathways will be significantly impacted, and this can be confirmed by SCLC mobility measurements (figure 5.6). The hole transport for **X2** is significantly reduced when blended with **FBR**; however, the mobility increases by an order of magnitude after thermal annealing confirming that **FBR** does inhibit the crystallization of **X2** when cast reducing the amount of efficient hole transport pathways. In agreement with the GIWAXS measurements, the **IDTBR** does not prevent the crystallization of **X2** allowing for good charge carrier mobility when as cast, and after thermal annealing there is virtually no change. Interestingly, it appears that thermal annealing has little to any effect on the electron mobilities for **FBR** and **IDTBR**. It is worth noting these electron mobilities are rather low

compared to fullerenes, which tend to have two orders of magnitude higher mobility, this might help to explain the relatively low fill factors, <50%, for these systems despite the hole mobilities being equivalent to other high performance small molecule solar cells.<sup>40,41</sup>

### 5.3 Conclusions

In Conclusion, two different non-fullerene acceptors were blended with a molecular donor of intermediate length and processed from a green solvent. The devices fabricated are comparable, if not better than what has previously been reported for this donor when processed from 2-MeTHF. Despite exhibiting complimentary absorption to X2, FBR based devices were lower performing due to the inhibited X2 crystallization. This decreased crystallization reduced phase separation, and prevented the development of efficient hole transport pathways. After subjected to thermal annealing, the X2 crystallinity was restored and produce efficient devices, but still under performed due to a low  $J_{sc}$ . The introduction of the indacenodithiophene core enhanced the crystallinity of the acceptor, but red shifted the absorption causing an overlap with X2. Despite this overlap, the enhanced crystallinity of the IDTBR, drove phase separation when cast and did not inhibit the crystallization of X2. This led to an optimized device morphology without any form of post treatment (e.g. thermal annealing, solvent annealing, solvent additives), which is rather rare. Interestingly, the electron mobility for the two acceptors is rather low, two orders of magnitude lower than fullerene. This significantly reduced electron mobility is likely the cause of the low fill factors for the devices, less than 50%. These results show the potential that processing of non-fullerene acceptors from green solvents can compete with fullerene based green solvent processed solar cells. More importantly, that green solvent processed non-fullerene based solar cells can compete with the halogenated solvent processed counter parts, and further highlights the progression of a more sustainable future for organic photovoltaics.

## 5.4 Experimental

*Materials:* X2, FBR, IDTBR, and PFN:BIm<sub>4</sub> were all synthesized according to the literature.<sup>13,32,37,42</sup> Anhydrous 2-MeTHF was purchased from Sigma Aldrich. All Materials were used as received.

*Device Fabrication:* Solar cells devices were fabricated on cleaned, UV/ozone treated Corning 1737 glass patterned with 150 nm ITO. MoO<sub>x</sub> films (9 nm) were thermally evaporated on top of ITO substrates at a rate of 0.1 Å/s under vacuum below 10<sup>-6</sup> torr. The organic films were prepared from solutions with a total solids concentration of 20 mg/mL with D:A ratio of 1:1, wt/wt by spin-coating at 2000 rpm for 60 seconds. Samples that were thermally annealed were done so at 100 °C for 10 min then allowed to cool to room temperature for 10 minutes. After cooling, a thin layer of PFN:BIm<sub>4</sub> was spin coated on top from a 1 mg/ml solution in methanol at a spin speed of 2500 RPM for 60 seconds. Finally, cathodes were deposited by sequential thermal evaporation of calcium (~15 nm) followed by aluminum (~100 nm) through a shadow mask by thermal evaporation under a vacuum of about 3 x 10<sup>-7</sup> torr. An aperture with area of 0.045 cm<sup>2</sup> was used during the measurement. Device performances were tested using a Keithly 2602 system Source Meter under illumination by a simulated 100 mW cm<sup>-2</sup> AM 1.5G light source using a 300 W Xe arc lamp with an AM 1.5 global filter. Solar-simulator irradiance was calibrated using standard silicon photovoltaic with a protective KG1 filter calibrated by the National Renewable Energy Laboratory.

*UV/Vis Absorption Spectroscopy:* Absorption measurements were performed using a Beckman Coulter U800 UV/Vis spectrophotometer. Thin films were prepared by spin-

coating on top of MoOx covered ITO substrates (same condition as device fabrication) at a spin speed of 2000 rpm.

*EQE Measurements:* External quantum efficiencies were measured using a 75 W Xe source, monochromator, optical chopper, lock-in amplifier, and a NIST calibrated silicon photodiode was used for power-density calibration.

*Hole Only Diode Measurements:* Hole only devices were fabricated on cleaned, UV/ozone treated Corning 1737 glass patterned with 140 nm Indium Tin Oxide. Molybdenum oxide (MoOx) was chosen as the bottom contact since it has a deeper work function, 5.5 eV, than the HOMO energy of X2. MoOx was thermally evaporated as a bottom contact at a rate of 0.2 Å/s with a thickness of 9 nm. The active layer was spin cast at 2000 rpm for 60 seconds at a 1:1 blend ratio with a total concentration of 20 mg/ml. In order to sufficiently reduce electron injection, gold top contacts were thermally evaporated at 0.2 Å/s with a final thickness of approximately 50 nm. Since the work function of gold, 5.1 eV, is deeper than the LUMO of FBR and IDTBR, there will be non-ohmic electron injection yielding electron current several orders of magnitude lower than the hole current. The electron only diodes were fabricated first by evaporating 20 nm of Aluminum on top of 9 nm of MoOx. Active layers were then spin coated at 2000 RPM for 60 seconds form a 1:1 blend ratio with a total concentration of 20 mg/ml, then Calcium (15 nm) and Aluminum (100 nm) top contacts were thermally evaporated. Devices were measured in the dark using a Keithly 2602 system Source Meter and the Mott-Gurney law for the space-charge-limited-current (SCLC)<sup>43,44</sup> was used to determine the zero field mobility of the layer according to the following equation:

$$J = \frac{9}{8} \epsilon \epsilon_0 \mu \frac{V^2}{L^3}$$

where  $\epsilon$  is the material's dielectric constant,  $\epsilon_0$  is the permittivity of vacuum,  $V$  is the applied bias,  $L$  is the film thickness,  $J$  is the measured current density and  $\mu$  is the charge carrier mobility of the material.

*GIWAXS Measurements:* GIWAXS patterns were collected at the Lawrence Berkeley National Lab Advanced Light Source (ALS). Samples were probed under a helium environment to minimize beam damage and reduce diffuse scattering. The measurements were calibrated using a LaB6 standard. The crystalline correlation length (CCL) values, which provide an estimation of crystallite size and quality, were calculated using the Scherrer equation.

## 5.5 References

- (1) Shaheen, S. E.; Brabec, C. J.; Sariciftci, N. S.; Padinger, F.; Fromherz, T.; Hummelen, J. C. *Appl. Phys. Lett.* **2001**, *78* (6), 841.
- (2) Lin, L.-Y.; Chen, Y.-H.; Huang, Z.-Y.; Lin, H.-W.; Chou, S.-H.; Lin, F.; Chen, C.-W.; Liu, Y.-H.; Wong, K.-T. *J. Am. Chem. Soc.* **2011**, *133* (40), 15822.
- (3) Liu, Y.; Zhao, J.; Li, Z.; Mu, C.; Ma, W.; Hu, H.; Jiang, K.; Lin, H.; Ade, H.; Yan, H. *Nat. Commun.* **2014**, *5*, 5293.
- (4) He, Z.; Xiao, B.; Liu, F.; Wu, H.; Yang, Y.; Xiao, S.; Wang, C.; Russell, T. P.; Cao, Y. *Nat. Photonics* **2015**, *9* (3), 174.
- (5) Nam, S.; Seo, J.; Woo, S.; Kim, W. H.; Kim, H.; Bradley, D. D. C.; Kim, Y. *Nat. Commun.* **2015**, *6*, 8929.
- (6) Yu, G.; Gao, J.; Hummelen, J. C.; Wudl, F.; Heeger, A. J. *Science* **1995**, *270* (5243), 1789.
- (7) Hwang, Y.-J.; Li, H.; Courtright, B. A. E.; Subramaniyan, S.; Jenekhe, S. A. *Adv. Mater.* **2015**, n/a.
- (8) Li, H.; Hwang, Y.-J.; Courtright, B. A. E.; Eberle, F. N.; Subramaniyan, S.; Jenekhe, S. A. *Adv. Mater.* **2015**, n/a.
- (9) Sharenko, A.; Proctor, C. M.; van der Poll, T. S.; Henson, Z. B.; Nguyen, T.-Q.; Bazan, G. C. *Adv. Mater.* **2013**, 4403.
- (10) Zhao, J.; Li, Y.; Lin, H.; Liu, Y.; Jiang, K.; Mu, C.; Ma, T.; Lai, J. Y. L.; Hu, H.; Yu, D.; Yan, H. *Energy Environ. Sci.* **2015**, *8* (2), 520.
- (11) Zang, Y.; Li, C.-Z.; Chueh, C.-C.; Williams, S. T.; Jiang, W.; Wang, Z.-H.; Yu, J.-S.; Jen, A. K.-Y. *Adv. Mater.* **2014**, *26* (32), 5708.
- (12) Nielsen, C. B.; Holliday, S.; Chen, H.-Y.; Cryer, S. J.; McCulloch, I. *Acc. Chem. Res.* **2015**, *48* (11), 2803.
- (13) Holliday, S.; Ashraf, R. S.; Nielsen, C. B.; Kirkus, M.; Röhr, J. A.; Tan, C.-H.; Collado-Fregoso, E.; Knall, A.-C.; Durrant, J. R.; Nelson, J.; McCulloch, I. *J. Am. Chem. Soc.* **2015**, *137* (2), 898.
- (14) Shi, H.; Fu, W.; Shi, M.; Ling, J.; Chen, H. *J. Mater. Chem. A* **2015**, *3* (5), 1902.
- (15) Lin, Y.; Wang, J.; Zhang, Z.-G.; Bai, H.; Li, Y.; Zhu, D.; Zhan, X. *Adv. Mater.* **2015**, *27* (7), 1170.

- (16) Kwon, O. K.; Park, J.-H.; Kim, D. W.; Park, S. K.; Park, S. Y. *Adv. Mater.* **2015**, 27 (11), 1951.
- (17) Lin, Y.; Zhang, Z.-G.; Bai, H.; Wang, J.; Yao, Y.; Li, Y.; Zhu, D.; Zhan, X. *Energy Environ. Sci.* **2015**, 8 (2), 610.
- (18) Kim, Y.; Song, C. E.; Moon, S.-J.; Lim, E. *Chem. Commun.* **2014**, 50 (60), 8235.
- (19) Sprau, C.; Buss, F.; Wagner, M.; Landerer, D.; Koppitz, M.; Schulz, A.; Bahro, D.; Schabel, W.; Scharfer, P.; Colsmann, A. *Energy Environ. Sci.* **2015**.
- (20) Susanna, G.; Salamandra, L.; Ciceroni, C.; Mura, F.; Brown, T. M.; Reale, A.; Rossi, M.; Di Carlo, A.; Brunetti, F. *Sol. Energy Mater. Sol. Cells* **2015**, 134, 194.
- (21) Aj, M. *IARC Sci. Publ.* **1987**, No. 85, 3.
- (22) Langman, J. M. *Pathology (Phila.)* **1994**, 26 (3), 301.
- (23) Sherman, J.; Chin, B.; Huibers, P. D. T.; Garcia-Valls, R.; Hatton, T. A. *Environ. Health Perspect.* **1998**, 106, 253.
- (24) Gu, Y.; Jérôme, F. *Chem. Soc. Rev.* **2013**, 42 (24), 9550.
- (25) Antonucci, V.; Coleman, J.; Ferry, J. B.; Johnson, N.; Mathe, M.; Scott, J. P.; Xu, J. *Org. Process Res. Dev.* **2011**, 15 (4), 939.
- (26) Pace, V.; Hoyos, P.; Castoldi, L.; Domínguez de María, P.; Alcántara, A. R. *ChemSusChem* **2012**, 5 (8), 1369.
- (27) Clark, J. H.; Pfaltzgraff, L. A.; Budarin, V. L.; Hunt, A. J.; Gronnow, M.; Matharu, A. S.; Macquarrie, D. J.; Sherwood, J. R. *Pure Appl. Chem.* **2013**, 85 (8), 1625.
- (28) Clark, J. H.; Budarin, V.; Deswarte, F. E. I.; Hardy, J. J. E.; Kerton, F. M.; Hunt, A. J.; Luque, R.; Macquarrie, D. J.; Milkowski, K.; Rodriguez, A.; Samuel, O.; Tavener, S. J.; White, R. J.; Wilson, A. J. *Green Chem.* **2006**, 8 (10), 853.
- (29) Chen, X.; Liu, X.; Burgers, M. A.; Huang, Y.; Bazan, G. C. *Angew. Chem. Int. Ed.* **2014**, 53 (52), 14378.
- (30) Chen, Y.; Cui, Y.; Zhang, S.; Hou, J. *Polym. Chem.* **2015**, 6 (22), 4089.
- (31) Huang, Y.; Liu, X.; Wang, C.; Rogers, J. T.; Su, G. M.; Chabinyk, M. L.; Kramer, E. J.; Bazan, G. C. *Adv. Energy Mater.* **2014**, 4 (10), n/a.
- (32) Liu, X.; Sun, Y.; Perez, L. A.; Wen, W.; Toney, M. F.; Heeger, A. J.; Bazan, G. C. *J. Am. Chem. Soc.* **2012**, 134 (51), 20609.
- (33) Liu, X.; Sun, Y.; Hsu, B. B. Y.; Lorbach, A.; Qi, L.; Heeger, A. J.; Bazan, G. C. *J. Am. Chem. Soc.* **2014**, 136 (15), 5697.

- (34) Liu, X.; Hsu, B. B. Y.; Sun, Y.; Mai, C.-K.; Heeger, A. J.; Bazan, G. C. *J. Am. Chem. Soc.* **2014**, *136* (46), 16144.
- (35) Abdelsamie, M.; Treat, N. D.; Zhao, K.; McDowell, C.; Burgers, M. A.; Li, R.; Smilgies, D.-M.; Stingelin, N.; Bazan, G. C.; Amassian, A. *Adv. Mater.* **2015**, n/a.
- (36) Liu, X.; Burgers, M. A.; Hsu, B. B. Y.; Coughlin, J. E.; Perez, L. A.; Heeger, A. J.; Bazan, G. C. *RSC Adv.* **2015**, *5* (108), 89144.
- (37) Holliday, S.; Ashraf, R. S.; Wadsworth, A.; Baran, D.; Yousaf, S. A.; Nielsen, C. B.; Tan, C.-H.; Dimitrov, S. D.; Shang, Z.; Gasparini, N.; Alamoudi, M.; Laquai, F.; Brabec, C. J.; Salleo, A.; Durrant, J. R.; McCulloch, I. *Nat. Commun.* **2016**, *7*, 11585.
- (38) Wetzelaer, G.-J. A. H.; Van der Kaap, N. J.; Koster, L. J. A.; Blom, P. W. M. *Adv. Energy Mater.* **2013**, n/a.
- (39) Bartelt, J. A.; Beiley, Z. M.; Hoke, E. T.; Mateker, W. R.; Douglas, J. D.; Collins, B. A.; Tumbleston, J. R.; Graham, K. R.; Amassian, A.; Ade, H.; Fréchet, J. M. J.; Toney, M. F.; McGehee, M. D. *Adv. Energy Mater.* **2013**, *3* (3), 364.
- (40) Proctor, C. M.; Love, J. A.; Nguyen, T.-Q. *Adv. Mater.* **2014**, *26* (34), 5957.
- (41) Bartelt, J. A.; Lam, D.; Burke, T. M.; Sweetnam, S. M.; McGehee, M. D. *Adv. Energy Mater.* **2015**, n/a.
- (42) Yang, R.; Wu, H.; Cao, Y.; Bazan, G. C. *J. Am. Chem. Soc.* **2006**, *128* (45), 14422.
- (43) Kuik, M.; Wetzelaer, G.-J. A. H.; Nicolai, H. T.; Craciun, N. I.; De Leeuw, D. M.; Blom, P. W. M. *Adv. Mater.* **2014**, *26* (4), 512.
- (44) Coropceanu, V.; Cornil, J.; da Silva Filho, D. A.; Olivier, Y.; Silbey, R.; Brédas, J.-L. *Chem. Rev.* **2007**, *107* (4), 926.

## Chapter 6: Summary and Outlook

In this dissertation, we explored the processing organic solar cells from environmentally friendly, green solvents, and investigated the impact on device morphology and performance. We first began by expanding our understanding of green solvent processing, by investigating a wide array of molecular donors blended with PC<sub>61</sub>BC<sub>8</sub>. We found that out of the 5 molecular semiconductors **X2**, and **F3** have the most promise for further studies in green solvent processing. **X2**, while requiring thermal annealing to achieve optimal conditions, was able to achieve an efficiency of 5.5%. **F3** on the other hand, appears to form a more robust and thermally stable morphology brought about by the improved phase separation afforded by the fluorinated benthothiadiazole group. Despite this, the devices still performed lower than what has been reported in the literature when blended with PC<sub>61</sub>BM, perhaps indicating that the addition of the octyl chain on the fullerene is somehow decreasing performance. The hole mobilities of the green solvent processed devices are comparable to what has been reported for other high performance small molecule devices, indicating the octylester derivative to be the likely culprit for the decrease in device performance. If solar cells processed from 2-MeTHF are to rival their halogenated/aromatic processed counter parts, the origin of this performance decrease must be determined.

Next, we investigated two new non-fullerene acceptors blended with the high performance donor molecule, **X2**, and determined the feasibility of processing from 2-MeTHF. Despite having complimentary absorption to **X2**, **FBR** device performed rather poorly. This was caused by the **FBR** inhibiting the **X2** crystallization, significantly reducing

phase separation and development of efficient transport pathways. By switching the fluorene core with a more planar indacenodithiophene core, the crystallinity of the acceptor was significantly improved, at the cost of complimentary absorption. The improved crystallinity of **IDTBR** did not inhibit **X2** crystallization and in fact developed an optimized, and thermally stable morphology when cast. This improved morphology better facilitated charge separation, yielding a higher  $J_{sc}$  despite not having the complimentary absorption that the **X2:FBR** system had. The results obtained here show the promise that both non-fullerene acceptors and green solvent processing have to bring greater sustainability to OPVs.

Although this concludes the green solvent research covered in this dissertation, the field of green solvent processing has been opened up, and many groups have begun to focus their efforts on this important field. If organic photovoltaics are ever to become a commercially viable product, then environmentally friendly solvents must become the norm. Perhaps, large scale production through inkjet printing and roll-to-roll processing using 2-MeTHF, will someday be commercially available.